Spontaneous ordering of nanostructures on crystal surfaces

Vitaliy A. Shchukin* and Dieter Bimberg

Technische Universität Berlin, Institut für Festkörperphysik, Berlin D-10623, Germany

A review is given of theoretical concepts and experimental results on spontaneous formation of periodically ordered nanometer-scale structures on crystal surfaces. Thermodynamic theory is reviewed for various classes of spontaneously ordered nanostructures, namely, for periodically faceted surfaces, for periodic surface structures of planar domains, and for ordered arrays of three-dimensional coherently strained islands. All these structures are described as equilibrium structures of elastic domains. Despite the fact that driving forces of the instability of a homogeneous phase are different in each case, the common driving force for the long-range ordering of the inhomogeneous phase is the elastic interaction. The theory of the formation of multisheet structures of islands is reviewed, which is governed by both equilibrium ordering and kinetic-controlled ordering. For the islands of the first sheet, an equilibrium structure is formed, and for the next sheets, the structure of the surface islands meets the equilibrium under the constraint of the fixed structures of the buried islands. The experimental situation for the fabrication technology of ordered arrays of semiconductor quantum dots is analyzed, including a discussion of both single-sheet and multiple-sheet ordered arrays. [S0034-6861(99)01304-5]

CONTENTS

I. Introduction 1125
II. Periodically Faceted Surfaces 1127
A. Equilibrium crystal shape: Two distinct formulations of the problem 1127
B. Intrinsic surface stress of a solid 1128
C. Capillarity phenomena on solid surfaces 1129
D. Periodically faceted surfaces 1130
E. Periodic arrays of macroscopic step bunches 1131
F. Formation of quantum wires on faceted surfaces 1132
III. Surface Structures of Planar Domains; Heteroepitaxial Systems at Submonolayer Coverage 1133
IV. Ordered Arrays of Three-Dimensional Coherently Strained Islands 1135
A. General morphology of lattice-mismatched systems 1135
B. Energetics of a heteroepitaxial system 1138
C. Dilute array of islands 1139
D. Ordering of islands in shape 1141
E. Ordering of islands in size versus Ostwald ripening 1142
F. Lateral arrangement of islands 1143
G. Phase diagram of 2D array of islands 1145
H. Equilibrium thickness of the wetting layer 1147
I. Two exact theorems on shape-versus-volume dependence for 3D islands 1148
J. Kinetic theories of ordering 1151
K. Experimental techniques 1152
1. Direct imaging methods 1152
2. Diffraction methods 1154
3. Optical methods 1154
L. Experimental studies of 3D islands in lattice-mismatched heteroepitaxial systems 1154
1. Effect of growth interruption on the morphology of InAs/GaAs systems 1155
2. Reversible 3D-to-2D transitions in heteroepitaxial systems 1155
3. Transition from an ordered array of InAs quantum dots to Ostwald ripening 1156
4. Other materials systems 1158
5. Discussion 1158
V. Multisheet Arrays of Three-Dimensional Islands 1160
VI. Multisheet Arrays of Two-Dimensional Islands 1161
A. Interaction of an array of surface islands and an array of buried islands 1162
B. Experiments on multisheets of 2D islands 1164
VII. Summary 1166
Acknowledgments 1166
Appendix 1166
References 1167

I. INTRODUCTION

Spontaneous formation of periodic domain structures with a macroscopic periodicity is a common phenomenon in solids known for several decades (see, for example, Landau and Lifshits, 1960). In recent years, the formation of macroscopic periodically ordered structures *on crystal surfaces* has become a subject of intense experimental and theoretical study. There are two main reasons for a rapidly growing interest in the phenomenon. First, the progress in precise experimental techniques, such as transmission electron microscopy, scanning tunnelling microscopy, and atomic force microscopy, allows reliable and accurate investigation of surface structures with the characteristic periodicity 1–100 nm. Second, the formation of periodically ordered structures on semiconductor surfaces offers the possibility of direct fabrication of *semiconductor quantum nanostructures* in which a narrow-gap material is embedded into the matrix of a wide-gap material. This provides a confinement potential for electrons in the conduction band and for holes in the valence band. Periodic structures of such inclusions create a superlattice comprising quantum wells, quantum wires, or quantum dots.

Particular interest in *quantum dots* is due to their electronic properties typical of zero-dimensional systems which differ drastically from those of the bulk system. The electronic density of states of the quantum dot con-

*Permanent address: A.F. Ioffe Physical Technical Institute, St. Petersburg 194021, Russia. Electronic address: shchukin@sol.physik.TU-Berlin.DE

 ©1999 The American Physical Society

sists of delta peaks, in contrast to the continuous spectrum of the bulk. Thus the electronic spectrum of the dot is sometimes referred to as an atomlike spectrum, and the dot is called a "superatom," although it contains from $\approx 10^5$ to $\approx 10^6$ atoms.

To act as a quantum dot, the size of the inclusion has to lie within a certain range. On the one hand, the confinement potential has to have at least one localized state, which implies a lower size limit. On the other hand, the inclusions should not exceed a certain size, at which the energy-level spacing becomes too small and thermal smearing and evaporation of carriers from the dot will destroy the desired quantum dot properties. The particular size limits depend on the material, e.g., for InAs quantum dots in a GaAs matrix Ledentsov (1996) estimated the dot size to be within the range 4–20 nm.

Such small structures are difficult to prepare by standard lithography techniques. Recent breakthroughs in fabrication of quantum dots and quantum wires have been achieved by using the effects of spontaneous formation of ordered nanostructures on semiconductor surfaces. Quantum dots having an atomlike electronic spectrum have become a fascinating object both for basic research and for device applications, for example, as an active medium of semiconductor lasers (Kirstaedter *et al.*, 1994; Alferov, 1996; Bimberg, Ledentsov *et al.*, 1996; Ledentsov, Grundmann, *et al.*, 1996; Bimberg, Kirstaedter *et al.*, 1997; Ustinov *et al.*, 1997), in which they improve the laser performance. Fabrication of quantum dots even allows one to construct new kinds of devices, e.g., single-electron transistors (Kastner, 1996), cellular automata (Chen and Porod, 1995), or lasers based on the resonant waveguiding effect (Ledentsov, Krestnikov, *et al.*, 1996, 1997; Krestnikov, Ivanov, *et al.*, 1998).

In the present article we review the physical mechanisms which govern spontaneous formation of nanostructures on crystal surfaces. The discussion includes five classes of spontaneously formed nanostructures shown in Fig. 1. These nanostructures are periodically faceted surfaces [Fig. 1(a)], periodic structures of planar domains, e.g., monolayer high islands [Fig. 1(b)], ordered arrays of three-dimensional coherently strained islands in lattice-mismatched heteroepitaxial systems [Fig. 1(c)], multisheet arrays of two-dimensional islands [Fig. 1(d)], and multisheet arrays of three-dimensional islands [Fig. 1(e)].

Despite the fact that the geometry of the five classes is different, there exist common features for all the nanostructures. The main one is that the driving force of the periodic ordering is *long-range elastic interaction*. The elastic strain field is created due to the discontinuity of the intrinsic surface stress tensor τ_{ij} on domain boundaries and/or by the lattice mismatch between two materials composing the heteroepitaxial system.

The first three classes depicted in Figs. 1(a)–1(c), are described as equilibrium structures. We concentrate on structures that are observed upon annealing of the crystal, or upon interruption of the crystal growth. In our general approach we consider them as equilibrium structures of elastic domains (Shchukin, 1996; Shchukin, Ledentsov, *et al.*, 1997; Bimberg, Ipatova *et al.*, 1997).

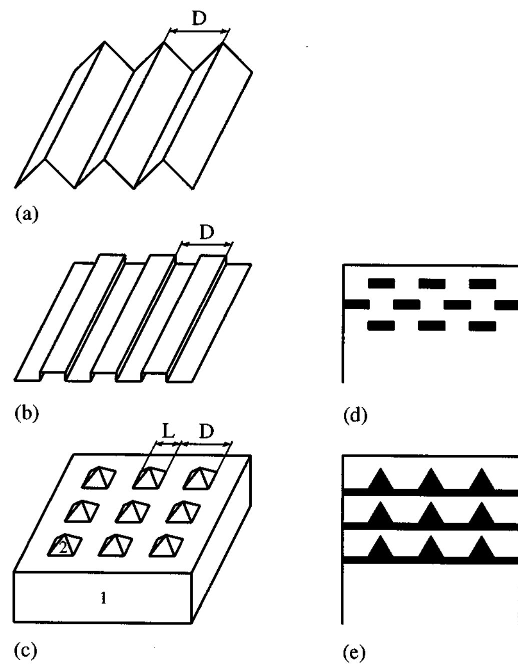

FIG. 1. Various classes of spontaneously ordered nanostructures: (a) periodically faceted surfaces; (b) surface structures of planar domains; (c) ordered array of three-dimensional coherently strained islands 2 lattice-mismatched to the substrate 1; (d) cross-sectional scheme of a multisheet array of two-dimensional islands; (e) cross-sectional scheme of a multisheet array of three-dimensional islands.

Multisheet arrays of islands, shown in Figs. 1(d) and 1(e), are nanostructures whose formation is governed by both equilibrium ordering and kinetic-controlled ordering. If the deposition of the first sheet of islands is followed by an interruption in growth, islands of the equilibrium structure are formed. For typical growth temperatures and growth rates, the structure of the buried islands of the first sheet does not change during the deposition of the second sheet. The second sheet of islands grows in the strain field created by the buried islands of the first sheet. And the structure of the second sheet of islands reaches partial equilibrium, that is, equilibrium under the constraint of the fixed structure of buried islands of the first sheet. The same is valid for subsequent sheets.

The role of long-range elastic interaction in the formation of periodic domain structures has been studied in detail for another class of elastic domains, namely, for compositional elastic domains in phase-separating alloys. The theory of compositional elastic domains in bulk samples of metals alloys was developed by Khachaturyan (1969) and is presented in his monograph (Khachaturyan, 1974; English translation 1983). Structures of compositional elastic domains in bulk samples of semiconductor alloys were studied by Ipatova (1990) and by Ipatova *et al.* (1991, 1993). The theory of compositional elastic domains in epitaxial films of semiconductor alloys was developed by Ipatova *et al.* (1993, 1994).

Another class of elastic domains in epitaxial films, namely, martensite-type domains, was studied by Roitburd (1976).

The five classes of spontaneously ordered nanostructures presented in Fig. 1 are the subject of the next five sections. In Sec. II the problem of the equilibrium crystal shape in relation to surface faceting is reviewed. A detailed discussion is presented of intrinsic surface stress, since it is the common driving force for the ordering of the first three types of nanostructures, Figs. 1(a)–1(c). The energetics of periodic faceting is considered, in which the elastic relaxation energy due to crystal edges always provides the optimum period of the faceted structure. An example of equilibrium faceting takes place on vicinal surfaces, i.e., on surfaces misoriented by a small angle from low index surfaces. On vicinal surfaces, periodic arrays of step bunches can occur, and such arrays are discussed as a particular class of periodically faceted surfaces. We also discuss the physical mechanism whereby cluster growth is favored in a GaAs/AlAs system with corrugated interfaces and thus direct fabrication of quantum wires and quantum-wire superlattices is made possible.

In Sec. III the ordering of surface structures of planar domains is considered. Although the geometry of these structures is very different from that of faceted surfaces, the basic energetics is the same, and the ordering of domains in both size and periodic lateral arrangement always occurs.

Section IV is devoted to ordering phenomena in arrays of three-dimensional coherently strained islands of a deposited material that are lattice-mismatched to the substrate. As concerns ordered arrays of 3D coherently strained islands (quantum dots), their origin is, at present, a highly debated issue. It was traditionally believed that an array of 3D islands is always unstable and that large islands will grow at the expense of evaporation or dissolving of small islands. This process is known as Ostwald ripening (Lifshits and Slyozov, 1958; Chakraverty, 1967). Formation of ordered arrays of 3D coherent islands implies the absence of Ostwald ripening. Among theoretical works that address the apparent absence of Ostwald ripening, there are two groups of papers. Thermodynamic theory states that, in a certain range of parameters, the equilibrium state of a heteroepitaxial system is a periodically ordered array of 3D coherently strained islands, and Ostwald ripening does not occur since it is not favored energetically (Shchukin, Ledentsov, *et al.*, 1995; Daruka and Barabási, 1997; Shchukin, Ledentsov, *et al.*, 1997). Kinetic theories state that the formation of coherent strained islands having a narrow size distribution is due to strain-induced barriers which hinder the evolution of the system towards Ostwald ripening (Chen *et al.*, 1995; Barabási, 1997; Jesson *et al.*, 1998). We focus on this debate in detail.

In the theoretical part of Sec. IV, we present the thermodynamic theory of arrays of 3D coherently strained islands. The complexity of these systems is due to two sources of the long-range strain field, the one being the lattice mismatch and the other being the discontinuity of the intrinsic surface stress tensor on the island edges. We evaluate the total energy of the system, which includes the elastic energy, the surface energy, and the edge energy. The elastic energy includes contributions from the two sources of the strain and the cross term, while the surface energy includes strain-induced renormalization terms. The total energy is calculated, and a phase diagram of the system is constructed which contains both a parameter region corresponding to the ordering in a *two-dimensional array of three-dimensional islands*, and a parameter region corresponding to Ostwald ripening of islands, which leads to the formation of large dislocated clusters.

In Sec. V, the formation of multisheet arrays of 3D islands in the semiconductor matrix is discussed. The formation mechanism involves both strain-driven equilibrium ordering and strain-driven growth kinetics.

In Sec. VI, the formation of multisheet arrays of 2D islands is considered and compared with the process for multisheet arrays of 3D islands.

In Sec. VII we summarize the review and discuss unsolved problems and future trends in the field.

II. PERIODICALLY FACETED SURFACES

A. Equilibrium crystal shape: Two distinct formulations of the problem

The phenomenon of equilibrium faceting plays the key role in determining the equilibrium crystal shape (ECS). We emphasize here two distinct problems related to the ECS which correspond to two different physical situations. The first problem is the ECS of a single crystal, which dates back at least to Wulff's paper (1901), and further developments of the ECS theory can be found in papers by Herring (1951a), Chernov (1961), and Mullins (1963). The exact thermodynamic formulation may be found, for example, in the review of Rottman and Wortis (1984), who discussed the shape of a single solid inclusion of a fixed volume ω which is in equilibrium with the liquid or with the vapor phase. The surface free energy of the inclusion is the integral over the surface of ω,

$$F_{\mathrm{surf}}(T,\omega)=\oint_{\partial\omega}\gamma(\hat{\mathbf{m}};T)\,dA. \tag{2.1}$$

Here $\gamma(\hat{\mathbf{m}};T)$ is the surface free energy per unit surface area, dependent on the orientation $\hat{\mathbf{m}}$ of the surface element dA relative to crystal axes. In the thermodynamics of the ECS a macroscopic inclusion of a fixed volume

$$V(\omega)=\int_{\omega}dV \tag{2.2}$$

takes at equilibrium that shape which minimizes the surface free energy (2.1) subject to the constraint (2.2).

ECS theory may be briefly summarized as follows (Rottman and Wortis, 1984). The orientational dependence of the surface free energy $\gamma(\hat{\mathbf{m}};T)$ is expected to

have cusps in symmetry directions leading to facets in the crystal shape at sufficiently low temperatures. These cusps represent discontinuities in the angular derivatives of the surface free energy, the discontinuities being associated with the free energy of the steps on a given facet. As the temperature is increased, step free energies decrease, cusps blunt, and corresponding facets shrink. A given facet will finally disappear at the roughening transition temperature T_R of the corresponding infinite planar surface, T_R being different for different symmetry directions. Above each T_R the corresponding region of the equilibrium crystal shape becomes smoothly rounded.

References to experimental data on equilibrium crystal shapes of micrometer-scale metal clusters is presented in the review paper of Rottman and Wortis (1984). Transmission electron microscopy studies of the equilibrium shape of voids in Si have revealed the orientational dependence of the surface free energy of Si (Eaglesham *et al.*, 1993).

Statistical mechanics is the tool for microscopic evaluation of the orientational dependence of the surface free energy $\gamma(\hat{\mathbf{m}};T)$ and for determining the ECS. An overview of theoretical results may be found in the review of Rottman and Wortis (1984).

The important issue of ECS theory is that there exist surface orientations that are not present in the crystal shape at a given temperature. At $T=0$ only several high-symmetry surface orientations are present in the ECS, and all others are passive in the sense that they do not contribute to the ECS. With an increase in temperature the domain of passive orientations shrinks as the crystal becomes more rounded.

The importance of this issue becomes plainer as one considers a second problem of ECS theory. This concerns a crystal that is in equilibrium with the liquid or with the vapor phase and has its volume fixed and all surfaces fixed but the top one. This formulation of the problem is relevant to any experimental situation in which only the top crystal surface is studied, e.g., to thermal annealing of the crystal or to growth interruptions introduced in crystal growth experiments.

The top crystal surface is not fixed and is allowed to rearrange into a hill-and-valley structure. The question that arises here is: when can the free energy of a plane surface be lowered by rearranging the atoms into hills and valleys? Since these hills and valleys are large compared to the lattice parameter, new tilt facets can be defined, and the free energy of the hill-and-valley structure can be written as a surface integral over the tilt facets:

$$F_{\mathrm{surf}}=\int \frac{\gamma(\hat{\mathbf{m}};T)}{(\hat{\mathbf{m}}\cdot\hat{\mathbf{n}})}\,dA. \tag{2.3}$$

Here $\hat{\mathbf{m}}$ is the coordinate-dependent unit vector locally normal to the surface at each point, and $\hat{\mathbf{n}}$ is the constant unit vector normal to the initially planar surface. The scalar product $(\hat{\mathbf{m}}\cdot\hat{\mathbf{n}})$ in the denominator of the integrand means that the surface element dA of a tilt facet is normalized per unit projected area of the nominally planar surface. Fixed side surfaces of the crystal imply that the average normal to the top surface coincides with the normal to the nominally planar surface, i.e.,

$$\frac{1}{A}\int \hat{\mathbf{m}}\,dA=\hat{\mathbf{n}}, \tag{2.4}$$

where A is the total area of the nominally planar surface.

The theorem proved exactly by Herring (1951a) reads: "If a given macroscopic surface of a crystal does not coincide in orientation with some portion of the boundary of the equilibrium shape, there will always exist a hill-and-valley structure which has a lower free energy than a flat surface, while if the given surface does occur in the equilibrium shape, no hill-and-valley structure can be more stable."

When the planar surface is unstable, the resulting hill-and-valley structure is determined by the minimum of the surface free energy [Eq. (2.3)] subject to the constraint (2.4). This minimization will yield the orientation of tilt facets as well as the fraction of the nominal planar surface onto which each facet is projected. Microscopic theory based on statistical mechanics can yield the orientational dependence of the surface free energy $\gamma(\hat{\mathbf{m}};T)$ and thus allow one to determine the ECS. Recent developments in this area have been made by Williams *et al.* (1993) for surfaces vicinal to Si(111) and by Mukherjee *et al.* (1994) for surfaces vicinal to Si(001).

The theory formulated by Eqs. (2.3) and (2.4) does not give, however, the linear scale of the equilibrium faceted structure, and therefore the formation of periodic structures was not discussed in the papers by Wulff (1901), Herring (1951a), Chernov (1961), Mullins (1963), and Rottman and Wortis (1984). The latter problem requires the additional concepts of *intrinsic surface stress* and of *capillarity effects on solid surfaces*, which are addressed in the next two subsections.

B. Intrinsic surface stress of a solid

Since atoms in the surface layer of any material are in a different environment than in the bulk, the surface layer energetically favors a lattice parameter different from the bulk value in the directions parallel to the surface. Being adjusted to the bulk lattice parameter, the surface layer is intrinsically stretched or compressed. Therefore the surface is characterized by intrinsic surface stress.

The intrinsic surface stress of a solid is analogous to the surface tension of a liquid. However, there is a fundamental difference between the thermodynamic properties of a liquid surface and of a solid surface, pointed out long ago by Gibbs (1928; see also Marchenko and Parshin, 1980; Needs, 1987). This is that any liquid is considered to be incompressible. When a liquid film is stretched, atoms or molecules move out from the bulk to form new surface, which is structurally identical to the existing surface. Thus an attempt to stretch a liquid film by 1% (say, by means of a thought experiment) results in a 1% increase in the number of surface atoms or mol-

ecules, whereas the spacing between surface atoms remains unchanged. Thus the processes of creation and deformation of a liquid surface are identical and are described by a single parameter γ, the energy required to create a unit area of the surface. However, when a crystal surface is stretched, the distance between atoms increases and the nature of the surface itself changes. This process is quite different from the creation of a new surface by the cutting of bonds. The energy to create unit area of the surface of a given orientation is characterized by the scalar quantity γ termed the surface energy, but the energy change due to deformation of the crystal surface is described by the intrinsic surface stress tensor $\tau_{\alpha\beta}$. The concept of the intrinsic surface stress tensor was proposed by Gibbs (1928) and discussed later by Shuttleworth (1950), Herring (1951b), and Marchenko and Parshin (1980). The linear term in strain in the change of the surface energy may be written as the following integral over the surface:

$$\int \tau_{\alpha\beta}(\hat{\mathbf{m}})\varepsilon_{\alpha\beta}\,dA, \tag{2.5}$$

where the intrinsic surface stress tensor $\tau_{\alpha\beta}$ has nonvanishing components only in the surface plane, $\alpha,\beta=1,2$ (Marchenko and Parshin, 1980). The principle values of the intrinsic surface stress tensor can be either positive (tensile) or negative (compressive). A tensile surface stress is associated with a surface that favors contraction, while a compressive stress is associated with a surface that favors expansion.

Values of the intrinsic surface stress for solids are known either from first-principles calculations or from comparison with indirect experimental data on parameters of surface domain structures (see also the next section). No direct experimental method for determining the intrinsic surface stress of a solid has been proposed so far. For most solid surfaces, the intrinsic surface stress is tensile (see, for example, Needs, 1987, and Fiorentini *et al.*, 1993), whereas the compressive surface stress is known for a Si(001) surface in the direction perpendicular to dimers (Garcia and Northrup, 1993; Dabrowski *et al.*, 1994). The order of magnitude of τ for both tensile and compressive surface stress is $100\,\text{meV}\,\text{Å}^{-2}$.

At this point it is worthwhile to note the following. Since a liquid surface is characterized by the single quantity γ, which is both the energy for creation of a unit surface area (i.e., the surface energy) and the quantity responsible to capillarity effects of the Laplace-pressure type, the term "surface tension" is widely used for the surface energy γ. Mainly for historical reasons, the use of this term has been extended to the surfaces and interfaces of solids. However, the use of "surface tension" for solids turns out to be totally ambiguous since it may produce a confusion between the surface energy γ and the intrinsic surface stress $\tau_{\alpha\beta}$. Therefore we make a distinction between the "surface energy" and the "intrinsic surface stress" and do not use the term "surface tension" for solids.

The change in the surface energy due to strain (2.5) indicates the interconnection that exists between surface effects and strain-related phenomena. Within the framework of the linear theory of elasticity where the bulk strain energy is a quadratic function of the strain, it is possible to expand the surface energy up to second-order terms in strain. The thermodynamics of solid surfaces and interfaces up to second-order terms in strain has been studied by Andreev and Kosevich (1981); further progress was made by Nozières and Wolf (1988; see also a review article by Kosevich, 1997). The dependence of the surface or interface free energy on strain may be written as the following expansion:

$$\gamma(\hat{\mathbf{m}};\varepsilon_{\alpha\beta})=\gamma_0(\hat{\mathbf{m}})+\tau_{\alpha\beta}(\hat{\mathbf{m}})\varepsilon_{\alpha\beta}+\frac{1}{2}S_{\alpha\beta\varphi\psi}(\hat{\mathbf{m}})\varepsilon_{\alpha\beta}\varepsilon_{\varphi\psi}+\frac{1}{2}h_{\alpha\beta i}(\hat{\mathbf{m}})\varepsilon_{\alpha\beta}\sigma_{ij}m_j. \tag{2.6}$$

Here $\hat{\mathbf{m}}$ is the normal to the surface or interface, Greek characters label two-dimensional indices in the surface plane whereas Roman indices are three-dimensional ones. The quadratic coefficients $S_{\alpha\beta\varphi\psi}$ and $h_{\alpha\beta i}$ have the meaning of *surface excess elastic moduli* and can be either positive or negative. σ_{ij} is the bulk elastic stress tensor, and the fourth term in Eq. (2.6) exists on solid-solid interfaces and vanishes on stress-free surfaces where the bulk stress tensor obeys the boundary conditions $\sigma_{ij}m_j=0$.

Following the conventional approach of elasticity theory (Landau and Lifshits, 1959) we use here and everywhere below all surface quantities defined per unit area of the undeformed surface. The dependence of the surface free energy on the strain (2.6) can be interpreted as the *strain-induced renormalization* of the surface free energy.

C. Capillarity phenomena on solid surfaces

Apart from the difference between a solid surface and a liquid surface emphasized in the previous subsection, there is a basic similarity between these two types of surfaces. Both liquid and solid surfaces are intrinsically stressed. Therefore solid surfaces exhibit capillarity (or surface stress-induced) phenomena similar to the familiar Laplace capillarity pressure near a curved liquid surface, and a strain field is generated at a curved surface of a solid. The existence of a surface stress-induced strain field was pointed out by Marchenko and Parshin (1980), who considered the elastic energy of a solid including both bulk and surface contributions:

$$E_{\text{elastic}}=\frac{1}{2}\int \lambda_{ijlm}\varepsilon_{ij}\varepsilon_{lm}\,dV+\int \tau_{\alpha\beta}(\hat{\mathbf{m}})\varepsilon_{\alpha\beta}\,dA. \tag{2.7}$$

Equation (2.7) yields the elastic energy as a function of strain for a given configuration of the surface. The presence of a term linear in the strain means that the unstrained state $[\varepsilon_{ij}(\mathbf{r})=0]$ does not correspond to mechanical equilibrium. The term linear in the strain

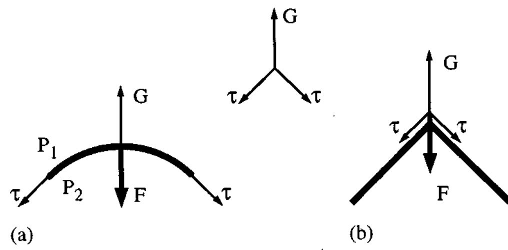

FIG. 2. Capillarity effects on liquid and on solid surfaces. (a) The balance of forces acting on an element of the curved surface layer of a liquid. Forces caused by the surface tension τ are balanced by the force **G** acting from the bulk of the liquid. According to Newton's third law, the *reactio* $\mathbf{F}=-\mathbf{G}$ is acting from the surface layer on the bulk of the liquid. This force results in the excess Laplace pressure $\Delta P=P_2-P_1$ below the curved surface of the liquid, P_1 and P_2 being the values of the pressure below and above the curved liquid surface. (b) The balance of forces acting on a crystal edge. Forces caused by the intrinsic surface stress τ are balanced by the force **G** acting from the bulk of the crystal. According to Newton's third law, the *reactio* $\mathbf{F}=-\mathbf{G}$ is acting from the surface layer on the bulk of the crystal, resulting in the strain field. The inset in the middle depicts the force balance, which is similar for a liquid and for a crystal. All forces in Fig. 2 are defined per unit length in the direction perpendicular to the figure.

implies effective forces applied to the crystal edges which give rise to elastic relaxation and to nonzero strain in the mechanical equilibrium.

To explain the origin of these forces, we note that the components of the tensor $\tau_{\alpha\beta}$ depend on the surface orientation $\hat{\mathbf{m}}$ (even the orientation of the axes where the tensor components do not vanish changes with $\hat{\mathbf{m}}$). Therefore a divergence of the surface stress tensor appears which gives the effective elastic force applied to the crystal,

$$F_i=\frac{\partial \tau_{i\beta}}{\partial r_\beta}. \tag{2.8}$$

The force F_i creates the elastic strain field in the crystal. It should be noted here that although elastic forces in Eq. (2.8), in Fig. 2, and below are denoted **F**, and the Helmholtz free energy is denoted F, there is no confusion at this point. The force is a vector quantity **F** denoted in bold throughout the text, or by using Cartesian subscripts F_i, whereas the free energy, being a scalar quantity, is denoted F.

The ultimate case of a curved solid surface is a sharp edge between neighboring facets. Figure 2 depicts the force balance on the curved surface of a liquid and at the crystal edge and thus demonstrates the similarity between capillarity effects in liquids and solids. The surface tension on a curved liquid surface results in an excess pressure below the surface, and, similarly, the intrinsic surface stress of crystal surfaces causes an effective force applied to the edge of the crystal. This force generates the strain field, which significantly affects the energetics of a faceted surface and promotes the formation of a periodic structure of facets.

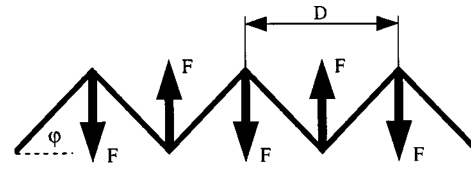

FIG. 3. Saw-tooth profile of a faceted surface. Effective forces of alternating sign are applied to neighboring edges.

D. Periodically faceted surfaces

If a planar crystal surface is unstable and breaks up into a system of tilt facets, the conservation of the average orientation of the normal to the surface [Eq. (2.4)] implies the coexistence of alternating facets [Fig. 1(a)]. At the intersection of neighboring facets there appear either sharp crystal edges or narrow rounded parts of the surface. Both these types of intersections may be described as linear defects at the surface. These linear defects give a short-range contribution to the surface free energy and a long-range contribution due to elastic strain energy.

It has been shown by Andreev (1980a) that if the order parameter related to the phase transition at the surface is linearly coupled to the strain field, i.e., if linear striction effects exist, they favor formation of a periodic structure whose period can be macroscopically large. For the faceting phase transition, the possibility of the formation of a faceted surface with a macroscopic period has been pointed out by Andreev (1980b).

The theory of a periodically faceted surface was developed by Marchenko (1981a), who found the period of the equilibrium structure. Following the paper by Marchenko (1981a) we consider a faceted surface with a one-dimensional periodic saw-tooth profile, depicted in Fig. 3. The free energy per unit projected area equals

$$F=F_{\mathrm{surf}}+E_{\mathrm{edges}}+\Delta E_{\mathrm{elastic}}. \tag{2.9}$$

Here F_{surf} is the free energy of the tilted facets, E_{edges} is the short-range energy of the edges, and $\Delta E_{\mathrm{elastic}}$ is the elastic energy due to the discontinuity of the surface stress tensor τ_{ij} at the crystal edges.

The free energy of tilted facets per unit projected area depends only on the orientation of the facets, $E_{\mathrm{surf}}=\gamma(\varphi)\sec(\varphi)$, and does not depend on the period of the structure D. The short-range energy of the edges per unit projected area equals

$$E_{\mathrm{edges}}=\frac{\eta(\varphi)}{D}\equiv\frac{\eta^{+}(\varphi)+\eta^{-}(\varphi)}{D}, \tag{2.10}$$

where $\eta^{+}(\varphi)$ is the short-range energy of the convex edge per unit length of the edge, and $\eta^{-}(\varphi)$ denotes the same energy of the concave edge.

While discussing the elastic strain energy, we note the following. First, E_{elastic} is given by the general formula (2.7) in which the energy is zero in the absence of strain and contains both linear and quadratic terms as a function of strain. Therefore the elastic strain energy in the equilibrium is negative, which corresponds to the relaxation of the surface stress at crystal edges. This negative

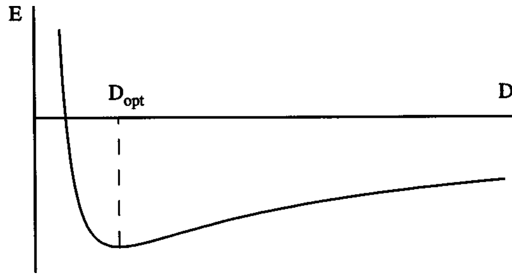

FIG. 4. The energy of a periodically faceted surface per unit surface area vs the period D. There always exists an optimum period of faceting $D_{\rm opt}$ due to the logarithmic dependence of the elastic relaxation energy on the period D.

elastic energy will henceforth be called the *elastic relaxation energy due to crystal edges*. Second, effective elastic forces acting at the edges are displayed in Fig. 3. *Force monopoles* are acting at each edge, and forces applied to neighboring edges are balanced, so that the total force applied to the system vanishes. Elastic strains generated by linear crystal edges propagate into the crystal over a distance of the order of D and decay at larger distances from the surface. Since the strain field is generated by linear defects at the surface, that is, by the linear crystal edges, the elastic relaxation energy depends logarithmically on the period D of the structure (Marchenko, 1981a):

$$\Delta E_{\rm elastic} = -\frac{\tilde{C}(\varphi)F^2}{YD}\ln\left(\frac{D}{a}\right) = -\frac{C(\varphi)\tau^2}{YD}\ln\left(\frac{D}{a}\right). \quad (2.11)$$

Here τ is the characteristic value of the intrinsic surface stress tensor, Y is the Young's modulus, a is the lattice parameter, and $C(\varphi)$ is the geometric factor which accounts for the particular symmetry of the tensor τ_{ij}, elastic anisotropy of the crystal, etc.

By substituting Eqs. (2.10) and (2.11) into Eq. (2.9), one obtains the following expression for the free energy of the faceted surface per unit projected area:

$$F = \frac{\gamma(\varphi)}{\cos\varphi} + \frac{\eta(\varphi)}{D} - \frac{C(\varphi)\tau^2}{YD}\ln\left(\frac{D}{a}\right). \quad (2.12)$$

The dependence of the free energy on the period of the faceted surface D is displayed in Fig. 4. Due to the logarithmic dependence of the elastic relaxation energy on the period D, there always exists an optimum period of faceting $D_{\rm opt}$ equal to

$$D_{\rm opt} = a\exp\left[\frac{\eta(\varphi)Y}{C(\varphi)\tau^2} + 1\right]. \quad (2.13)$$

All material parameters that enter the exponential in Eq. (2.13) have typical atomic values. Therefore the combination which appears as the argument of the exponential is of the order of 1. Since the exponential function is steep, and the argument can eventually be, say, equal to or larger than 3, the period D can exceed the lattice parameter a by at least an order of magnitude, i.e., can be macroscopically large. In this case the macroscopic approach is justified.

It should be noted that the free energy of facets, i.e., the first term in Eqs. (2.9) and (2.12), contains the entropy contribution which describes the dependence of the faceting itself and of the facet orientation on temperature. However, there exists another entropy contribution to F associated with possible deviations of the structure from a perfect periodic structure (the configuration entropy). For periodically faceted surfaces, the configuration entropy has not been considered in the literature so far. Therefore the present discussion refers, strictly speaking, to the case $T=0$. Below we shall omit everywhere the entropy contribution to F and discuss only the total energy of the system.

Periodic faceting with macroscopic periods has been observed on various surfaces of different materials, e.g., on surfaces vicinal to Si(111) (Hibino *et al.*, 1993; Williams *et al.*, 1993), on surfaces vicinal to GaAs(001) (Kasu and Kobayashi, 1993; Golubok *et al.*, 1994; Ledentsov, Gurianov *et al.*, 1994), on surfaces vicinal to Pt(100) (Watson *et al.*, 1993), on high-index surfaces of GaAs (Nötzel *et al.*, 1991) on Si(211) (Baski and Whitman, 1995), and on low-index surfaces of TaC(110) (Zuo *et al.*, 1993). The formation of facets has also been observed on Ir(110) (Koch *et al.*, 1991) although no periodicity has been revealed. All of the above-cited experimental observations of faceting refer to equilibrium conditions (e.g., thermal annealing).

E. Periodic arrays of macroscopic step bunches

An important particular example of surface faceting is the faceting of a vicinal surface. A homogeneous vicinal surface of a crystal consists of planar terraces with low Miller indices, the neighboring terraces being separated by equidistant monoatomic or monomolecular steps. The phenomenon of step bunching has been known for a long time as one of the possible kinetic instabilities of the crystal growth on vicinal surfaces (see, for example, Chernov, 1984). Recent experiments on surfaces vicinal to Si(111) (Williams *et al.*, 1993) and on surfaces vicinal to GaAs(100) (Kasu and Kobayashi, 1993; Golubok *et al.*, 1994; Ledentsov, Gurianov, *et al.*, 1994) have revealed step bunching which appears upon annealing of a cleaved surface or upon growth interruption. This indicates *equilibrium step bunching*. The height of step bunches was found to be homogeneous throughout the sample (Kasu and Kobayashi, 1993; Williams *et al.*, 1993; Golubok *et al.*, 1994; Ledentsov, Gurianov, *et al.*, 1994). The observation of equal-width terraces (or equidistant step bunches) was reported for vicinals to GaAs(100) (Kasu and Kobayashi 1993; Golubok *et al.*, 1994; Ledentsov, Gurianov, *et al.*, 1994).

The height of step bunches observed on vicinals to GaAs(100) (7–15 monolayers) allows us to consider them as macroscopic step bunches forming new facets (Fig. 5). Another example of faceting of a vicinal surface is its breaking into two vicinal surfaces with different concentration of steps, as observed for vicinals to Si(111) (Williams *et al.*, 1993).

Figure 5 depicts a periodic array of step bunches of a macroscopic height. The discontinuity of the intrinsic

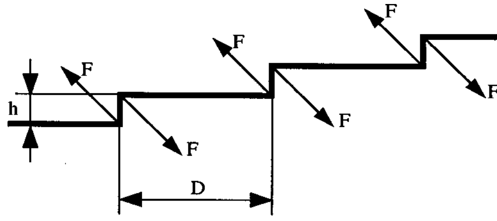

FIG. 5. A periodic array of macroscopic step bunches resulting from the faceting of a vicinal surface. Force monopoles are acting at the edges of the structure. The elastic interaction between the two edges of the same step bunch is the monopole-monopole interaction, whereas the interaction between different step bunches is the dipole-dipole one.

surface stress tensor τ_{ij} at the edges results in effective force monopoles acting at the edges. Thus the elastic interaction between the two edges of the same step bunch is the monopole-monopole interaction. Force monopoles acting at the two edges of the same bunch compensate each other, and the strain field due to a single step bunch is equal at large distances to the strain field of an elastic dipole. Therefore the elastic interaction between step bunches is the dipole-dipole interaction, which decreases with the separation L as L^{-2}, similar to the elastic interaction between steps of a microscopic height (Marchenko and Parshin, 1980). The total energy per unit surface area equals (where dipole-dipole interaction and higher terms are truncated)

$$E=\gamma_0+\gamma_1\frac{h}{D}+\frac{C_1\eta}{D}-\frac{C_2\tau^2}{YD}\ln\left(\frac{h}{a}\right). \tag{2.14}$$

Here γ_0 is the surface energy of a flat terrace, γ_1 is the surface energy of a step bunch, η is the energy of two edges, a convex one and a concave one, per unit length of the edges, similar to the coefficient in the second term in Eq. (2.12), and C_1 and C_2 are geometric factors.

Since the average orientation of the faceted surface in Fig. 5 coincides with the orientation of an initially homogeneous vicinal surface, there exists a relation between the height h of macroscopic step bunches and the period D of the structure, $h=D\varphi$, where φ is the misorientation angle of the initially homogeneous vicinal surface. By using this relation, it is possible to write Eq. (2.14) in a form similar to Eq. (2.12), $E=\gamma_0+\gamma_1\varphi+\varphi[C_1\eta h^{-1}-C_2\tau^2Y^{-1}h^{-1}\ln(h/a)]$. Due to the logarithmic dependence of the elastic relaxation energy on the height of the step bunch, there is always an optimum equilibrium height of step bunches.

F. Formation of quantum wires on faceted surfaces

Periodic surface faceting makes possible direct fabrication of ordered arrays of quantum wires. The growth of a deposited material 2 on the faceted surface of material 1 allows, in principle, the fabrication of quantum wires provided the growth proceeds in grooves of the faceted substrate. Here we focus on heteroepitaxial growth in the system GaAs/AlAs, where the two materials are nearly lattice matched.

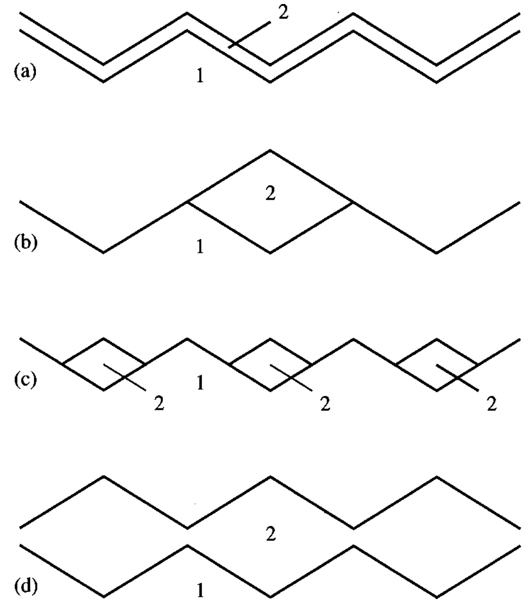

FIG. 6. Possible structures of a heteroepitaxial system in which material 2 is deposited on a periodically faceted surface of material 1: (a) homogeneous coverage; (b) separated "thick" clusters; (c) "thin" clusters; (d) high coverage, in which the periodic surface corrugation is restored, and the hills of the top surface appear over the valleys of the substrate, and vice versa. The heteroepitaxial system contains a continuous layer of material 2 with a periodically modulated thickness.

Two examples of heteroepitaxial growth on faceted surfaces in a GaAs/AlAs system are the growth on a faceted vicinal surface to the (001) surface (Kasu and Kobayashi, 1993) and the growth on a faceted surface (311) (Nötzel *et al.*, 1991; Alferov *et al.*, 1992).

The theory of quasi-equilibrium heteroepitaxial growth on periodically corrugated substrates has been developed by Shchukin, Borovkov, *et al.* (1995b). Here we focus on the practical case in which the surfaces of both material 1 and material 2 are unstable against faceting. This is the case for vicinals to both (001) surfaces (Kasu and Kobayashi, 1993) and (311) surfaces (Nötzel *et al.*, 1991) of GaAs and AlAs and offers several possibilities for the morphology of the heteroepitaxial system depicted in Fig. 6.

The total energy of the heteroepitaxial system equals (Shchukin, Borovkov *et al.*, 1995b)

$$E=E_{\text{surf}}+E_{\text{interface}}+E_{\text{edges}}+\Delta E_{\text{elastic}}. \tag{2.15}$$

Here, in addition to the three contributions to the energy of the faceted surface [see Eq. (2.9)], one more contribution enters, which is the interface energy. The total energies of several distinct types of heteroepitaxial structure, depicted in Fig. 6, have been compared by Shchukin, Borovkov, *et al.* (1995b), with the following conclusions.

The selection between two possible growth modes is determined by whether the deposited material wets or does not wet the substrate. If the deposited material wets the substrate, then homogeneous coverage of the periodically corrugated substrate occurs [Fig. 6(a)]. The

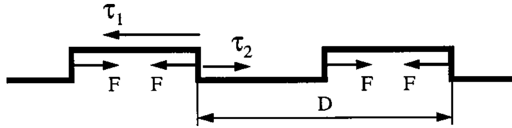

FIG. 7. Effective forces applied to domain boundaries in a system of planar surface domains.

example is the growth of AlAs on a periodically corrugated vicinal surface of GaAs(001), 3° off towards $[1\bar{1}0]$ (Kasu and Kobayashi, 1993).

If the deposited material does not wet the substrate, then isolated clusters of the deposited material appear on the periodically corrugated substrate [Fig. 6(b)]. This situation is likely to be realized for the growth of GaAs on a vicinal surface of AlAs(001) 3° off towards $[1\bar{1}0]$ (Kasu and Kobayashi, 1993) and for both GaAs/AlAs and AlAs/GaAs heteroepitaxial growth on a (311)A surface (Nötzel *et al.*, 1991; Alferov *et al.*, 1992).

In the case of inhomogeneous cluster coverage the periodic surface corrugation is restored after deposition of the first several monolayers. Then the hills of the top surface of a heteroepitaxial system appear over the valleys of the substrate, and vice versa, and a continuous layer of the deposited material with periodically modulated thickness is formed [Fig. 6(d)]. Thus the formation of clusters allows direct fabrication of quantum wires and quantum wire superlattices in heteroepitaxial semiconductor systems.

Since any periodically faceted surface is a structure of elastic domains, its geometrical parameters (e.g., the period) can be tuned in a controlled way by applying an external stress. Detailed consideration may be found in the paper by Shchukin, Borovkov, *et al.* (1995a).

To conclude the present section, we emphasize that spontaneous periodic faceting of semiconductor surfaces and cluster growth in grooves make possible direct fabrication of isolated quantum wires, of quantum wire superlattices, and of quantum well superlattices with modulated thickness of quantum wells.

III. SURFACE STRUCTURES OF PLANAR DOMAINS; HETEROEPITAXIAL SYSTEMS AT SUBMONOLAYER COVERAGE

Another class of spontaneously ordered nanostructures is associated with periodically ordered structures of planar surface domains [Fig. 1(b)]. Surface domain structures occur if different phases can coexist on the surface, e.g., phases of (2×1) and (1×2) surface reconstruction of Si(001), monolayer high islands in heteroepitaxial systems, etc. Then neighboring domains have different values of the intrinsic surface stress tensor τ_{ij}, and effective force monopoles are applied to the domain boundaries (Fig. 7),

$$F_\alpha=(\Delta\tau_{\alpha\beta})m_\beta\equiv(\tau^{(2)}_{\alpha\beta}-\tau^{(1)}_{\alpha\beta})m_\beta, \tag{3.1}$$

where m_β is the two-dimensional vector normal to the domain boundaries. The effective force from Eq. (3.1) gives rise to elastic relaxation. The elastic energy of such a system can be written in a form similar to Eq. (2.7), which contains a term linear in the strain. This indicates the existence of linear striction effects which favor formation of periodic structures with macroscopic periods (Andreev, 1980a). The theory of surface structures of planar domains governed by the discontinuity of τ_{ij} was developed by Marchenko (1981b). Although the geometry of these structures is very different from that of periodically faceted surfaces, the energetics is basically the same. The total energy of the domain structure per unit surface area equals

$$E=E_{\mathrm{surf}}+E_{\mathrm{boundaries}}+\Delta E_{\mathrm{elastic}}. \tag{3.2}$$

Here the surface energy E_{surf} does not depend on the period of the structure D, the energy of domain boundaries equals $E_{\mathrm{boundaries}}=C_1\eta D^{-1}$, where η is a short-range energy of domain boundaries, and the elastic relaxation energy equals $\Delta E_{\mathrm{elastic}}=-C_2(\Delta\tau)^2Y^{-1}D^{-1}\ln(D/a)$, where Y is the Young's modulus. Due to the logarithmic dependence of the elastic relaxation energy on the period of the structure D, the total energy (3.2) always has a minimum at a certain optimum period,

$$D_{\mathrm{opt}}=a\exp\left[\frac{C_1\eta Y}{C_2(\Delta\tau)^2}+1\right]. \tag{3.3}$$

The best-known system exhibiting surface stress domain structures is the Si(001) surface and corresponding vicinal surfaces. In this system domains of (2×1) and (1×2) surface reconstruction coexist on the surface and are separated by single-height atomic steps. Such a domain structure was first observed by Men *et al.* (1988), and the explanation was given by Alerhand *et al.* (1988). Comparison of the measured period of the domain structure with Eq. (3.3) allows one to extract the value of $(\Delta\tau)$ from experiment (provided the short-range energy of single-height atomic steps is known) and to compare $(\Delta\tau)$ with the results of first-principles calculations. A detailed discussion may be found, for example, in the paper of Dabrowski *et al.* (1994). Force monopoles applied to single-height atomic steps lead to a variety of structures on vicinal surfaces as a function of miscut angle. Both experimental and theoretical work on these structures is reviewed by Mukherjee *et al.* (1994).

It should be noted that force monopoles acting at opposite boundaries of a given domain are balanced, and the interaction between domains at large distances is the dipole-dipole interaction. Similar to elastic domain structures are domain structures known for systems with dipole-dipole electrostatic interactions (Langmuir monolayers at the water/air interface) or for systems with dipole-dipole magnetic interactions in ferromagnetic films or in planar-confined ferrofluid/water mixtures in magnetic fields. Corresponding references may be found in the paper by Ng and Vanderbilt (1995).

Although the scaling behavior of the energy is similar for all systems mentioned, the particular pattern of the domain structure depends strongly on the orientational dependence of the long-range interaction and of the en-

ergies of domain boundaries. For isotropic interactions, there is a transition from a 1D array of stripes to a 2D hexagonal array of disks (Vanderbilt, 1992; Ng and Vanderbilt, 1995), disks being more favorable if the coverage of the surface is close to 0 or to 1. Anisotropic interactions which always occur for elastic interactions, and anisotropic domain boundaries, which always occur for crystal surfaces, favor, generally speaking, striped domains over disk-shaped domains.

An important class of planar structures of surface domains includes periodic arrays of islands formed in heteroepitaxial systems at submonolayer coverage. A periodic structure of stripes has been observed by scanning tunneling microscopy in the system O/Cu(110) (Kern *et al.*, 1991). The first experimental studies of a submonolayer array of InAs islands on GaAs(001) were carried out for a structure covered by GaAs, i.e., for an array of InAs inclusions of a monolayer thickness in a GaAs matrix (Wang *et al.*, 1994, 1995). The anisotropy of photoluminescence intensity from these inclusions indicated that the inclusions were elongated in the $[\bar{1}10]$ direction. The existence of stripe-shaped monolayer high islands of InAs on an uncovered surface of GaAs(001) was confirmed by scanning tunneling microscopy (Bresller-Hill *et al.*, 1994); the islands were elongated in the $[\bar{1}10]$ direction.

The existence of a stable periodic structure of surface domains is a general phenomenon which occurs, at submonolayer coverage, in any heteroepitaxial system that grows according to the Stranski-Krastanow growth mode (see below, Sec. IV). This is distinct from homoepitaxial system where islands of the top (partially filled) monolayer undergo Ostwald ripening and tend to grow to an infinitely large size. No Ostwald ripening occurs for planar islands at submonolayer coverage in a heteroepitaxial system.

Zeppenfeld *et al.* (1994), established a relation between the size of a single surface domain (for low domain concentration) and the minimum separation between them at intermediate concentration. In the particular case of monolayer high islands, this result means that there exists an optimum island size for a dilute array of islands. The existence of the optimum size of islands confirms again that two-dimensional strained islands in a heteroepitaxial system do not undergo Ostwald ripening.

Surface structures of planar domains manifest themselves even if the coverage is equal to or larger than one monolayer (ML). Thus, an InAs/GaAs(001) system with the nominal 1-ML coverage has a corrugated surface that contains regions of 2 ML of InAs, regions of 1 ML of InAs, and regions of bare GaAs substrate (Guryanov *et al.*, 1996). The corrugation occurs in the [100] direction and is well pronounced for surface coverage 1–1.5 ML before the morphological transformation to three-dimensional islands of InAs occurs at the coverage ≈ 1.7 ML.

The above treatment demonstrates the existence of a stable periodic structure of islands and the absence of Ostwald ripening in a heteroepitaxial system at sub-

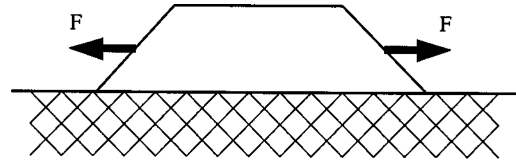

FIG. 8. Effective forces applied to side facets of a flat island.

monolayer coverage. This result can be extended to a system of planar islands with all three macroscopic dimensions, i.e., for islands where

$$a \ll h \ll L. \tag{3.4}$$

Here L is the lateral dimension of an island, and h is the island height.

If a uniform film of material 2 is coherently conjugated to a substrate of material 1, the elastic stress tensor in the film has nonvanishing in-plane components $\widetilde{\sigma_{\alpha\beta}}$ $(\alpha,\beta=1,2)$. In an island with a finite lateral size L, side facets lead to elastic relaxation. A nonuniform strain field can be described as the strain field created by effective forces with the density $P_\alpha = -\widetilde{\sigma_{\alpha\beta}} n_\beta$ applied to the side facets of the island, where n_β is the three-dimensional unit vector normal to the island surface (Fig. 8; see, for example, Maradudin *et al.*, 1991; Shchukin, Borovkov *et al.*, 1995a). If one considers the boundary of the island base, the total force per unit length of the boundary is then

$$F_\alpha = \widetilde{\sigma_{\alpha\beta}} h m_\beta, \tag{3.5}$$

where m_β is the two-dimensional unit vector normal to the boundary of the island base, as in Eq. (3.1). Equation (3.5) formally coincides with Eq. (3.1) if one sets

$$\Delta \tau_{\alpha\beta} = \widetilde{\sigma_{\alpha\beta}} h. \tag{3.6}$$

However, although the intrinsic surface stress $\tau_{\alpha\beta}$ can be qualitatively modeled as bulk stress in an epitaxial layer, Eq. (3.6) does not hold quantitatively for monolayer high islands. A substrate surface covered by a monolayer-thick epitaxial layer is, strictly speaking, a completely new surface distinct from both the substrate and the surface of the deposited material. This complex surface has its own surface energy and its own intrinsic surface stress tensor.

Nevertheless, apart from special cases in which the discontinuity of the intrinsic surface stress tensor $\Delta \tau_{\alpha\beta}$ differs significantly from Eq. (3.6) (see, for example, Grossmann *et al.*, 1996), in many lattice-mismatched heteroepitaxial systems Eq. (3.6) yields the correct sign and the correct order of magnitude of $\Delta \tau_{\alpha\beta}$ even for monolayer high islands. To clarify the physical reason for this, we make a rough estimate of the right-hand side of Eq. (3.6), by setting $\widetilde{\sigma_{\alpha\beta}} a \approx Y \varepsilon_0 a$, where Y is the Young's modulus, ε_0 is the lattice mismatch, and a is the lattice parameter. The substitution of $Y \approx 500$ meV Å^{-3}, $\varepsilon_0 \approx 0.07$, and $a = 3$ Å yields ≈ 100 meV Å^{-2} which is of the order of the characteristic value of τ for surfaces of pure crystals.

Due to the similarity between monolayer high islands and planar islands obeying the inequality (3.4), a stable structure of islands exists for both these classes. A dilute

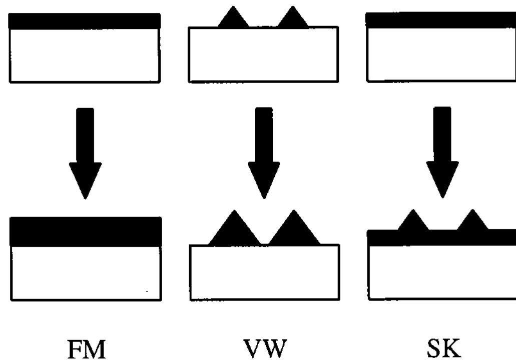

FIG. 9. Schematic diagrams of the three growth modes for heteroepitaxial systems: Frank-van der Merwe (FM), Volmer-Weber (VW), and Stranski-Krastanow (SK).

array of macroscopic strained islands was considered by Tersoff and Tromp (1993) for the case in which islands have a planar top surface and their height is *kinetically limited* to a value considerably smaller than the lateral size. An important issue is that there exists an optimum size in the system of planar strained islands and no Ostwald ripening occurs.

In the next section, another situation will be considered which occurs for essentially three-dimensional strained islands (e.g., pyramid-shaped islands), where two different regimes are possible, one being the regime where an optimum size of islands exists, and the other being the regime of ripening.

IV. ORDERED ARRAYS OF THREE-DIMENSIONAL COHERENTLY STRAINED ISLANDS

A. General morphology of lattice-mismatched systems

In the equilibrium theory of heteroepitaxial growth, three growth modes are traditionally distinguished (Bauer, 1958). They are Frank–van der Merwe (FM; Frank and van der Merwe, 1949), Volmer-Weber (VW; Volmer and Weber, 1926), and Stranski-Krastanow (SK; Stranski and Krastanow, 1937) growth modes. They may be described as layer-by-layer growth (2D), island growth (3D), and layer-by-layer plus islands (Fig. 9). The particular growth mode for a given system depends on the interface energies and on the lattice mismatch.

In lattice-matched systems, the growth mode is governed by the interface and surface energies only. If the sum of the epilayer surface energy γ_2 and of the interface energy γ_{12} is lower than the energy of the substrate surface, $\gamma_2+\gamma_{12}<\gamma_1$, i.e., if the deposited material wets the substrate, the Frank–van der Merwe mode occurs. A change in $\gamma_2+\gamma_{12}$ alone may drive a transition from the FM to the VW growth mode. For a strained epilayer with small interface energy, initial growth may occur layer-by-layer, but a thicker layer has a large strain energy and can lower its energy by forming isolated islands in which strain is relaxed. Thus the SK growth mode occurs.

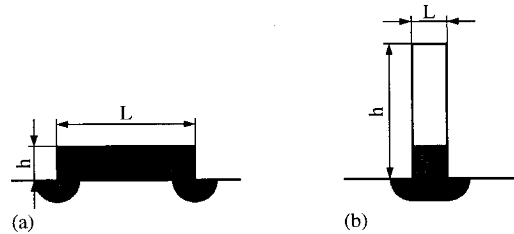

FIG. 10. Effect of island shape on the volume elastic relaxation of a coherently strained island. The dark area is that with a large elastic strain energy density: (a) island with height-to-width ratio $h/L \ll 1$ is weakly relaxed; (b) island with height-to-width ratio $h/L \gg 1$ is nearly completely relaxed.

It was traditionally believed that islands formed in the SK growth mode were dislocated. However, experiments on InAs/GaAs(001) (Goldstein *et al.*, 1985) and on Ge/Si(001) (Eaglesham and Cerullo, 1990; Mo *et al.*, 1990) have demonstrated the formation of *three-dimensional coherently strained*, i.e., dislocation-free, islands. This indicates the existence of a coherent mechanism of strain relaxation.

The relaxation of the elastic strain energy due to formation of coherently strained islands is related to the Asaro-Tiller-Grinfel'd instability of a strained layer against a long-wavelength corrugation of the surface (Asaro and Tiller, 1972; Grinfel'd, 1986; Srolovitz, 1989; Spencer *et al.*, 1991). To illustrate the physical mechanism of elastic relaxation, it is convenient to consider a strongly pronounced corrugation, e.g., an island, trough (Vanderbilt and Wickham, 1991), surface cusp (Jesson *et al.*, 1993), or crack (Yang and Srolovitz, 1993). The formation of troughs, cusps, and cracks can occur in a strained epitaxial film of a certain macroscopic thickness under annealing. At the same time, for the first stages of heteroepitaxial growth on a substrate, the formation of islands seems to be the only coherent mechanism of elastic relaxation.

Figure 10 shows two islands of a different shape. A flat island with a small height-to-width ratio is practically nonrelaxed, whereas a hypothetical island having the shape of a vertical bar with a large height-to-width ratio is relaxed almost completely. Thus the elastic relaxation depends strongly on the island shape. For a given shape, the elastic relaxation energy is proportional to the volume of the island (for details, see Appendix A). In order to distinguish this type of elastic relaxation from that due to capillarity effects (see Secs. II and III) we shall call it "volume elastic relaxation."

Volume elastic relaxation of coherently strained islands is a mechanism that competes with the formation of dislocations. The theory developed by Vanderbilt and Wickham (1991) compares the two mechanisms of elastic relaxation and yields a phase diagram of a lattice-mismatched system in which all possible morphologies are present, i.e., uniform films, dislocated islands, and coherent islands (Fig. 11). The formation of an island from a uniform film is accompanied, first, by relaxation of the elastic energy, $\Delta E_{\mathrm{elastic}}^{V}<0$, and, second, by a

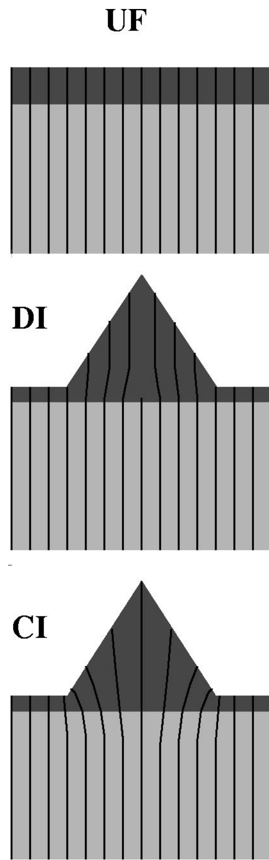

FIG. 11. Elastic strain relaxation during Stranski-Krastanow growth (schematic). Light grey areas denote the substrate, dark grey areas denote the lattice-mismatched epilayer. The lines symbolize lattice planes. It is assumed that surface and interface energies are such that the formation of a wetting layer is energetically preferred. Top (UF), uniformly strained film, $E_{UF}=\lambda\varepsilon_0^2 V$; middle (DI), dislocated relaxed islands, $E_{DI}=\gamma_2(\Delta A)+\gamma_{12}A_0$; bottom (CI), coherently strained islands, $E_{CI}=\gamma_2(\Delta A)+\lambda\varepsilon_0^2 V-|\Delta E_{\mathrm{elastic}}|$. From Pehlke *et al.* (1997) with the kind permission of the authors.

change of the surface area, $\Delta A>0$. The corresponding change in the surface energy is then caused by the formation of side facets of the islands and by the disappearance of certain areas of a planar surface. It is usually believed that the change in the surface energy is positive, $\Delta E_{\mathrm{surf}}>0$. It was shown by Vanderbilt and Wickham (1991) that the morphology of a mismatched system is determined by the relation between ΔE_{surf} and the energy of the dislocated interface $E_{\mathrm{interface}}^{\mathrm{disl}}$. The ratio of these two energies, denoted $\Lambda=E_{\mathrm{interface}}^{\mathrm{disl}}/\Delta E_{\mathrm{surf}}$, is the control parameter that governs the morphological phase diagram of Fig. 12.

If ΔE_{surf} is positive and large, or if the energy of the dislocated interface is relatively small, the corresponding value Λ on the phase diagram of Fig. 12 is smaller than Λ_0. Then formation of coherently strained islands is not favored. With an increase in the amount of deposited material, a transition occurs from a uniform film to dislocated islands, and coherently strained islands are not formed.

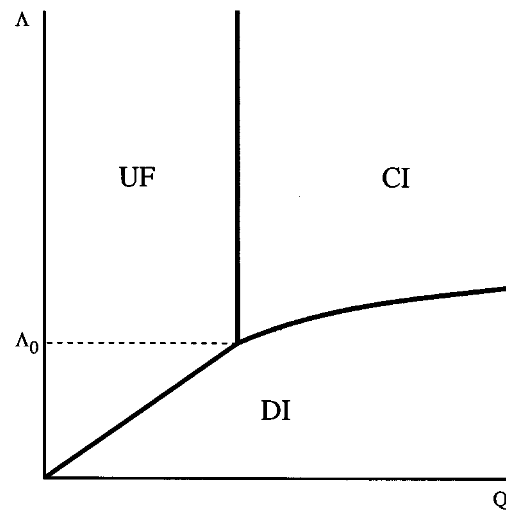

FIG. 12. Phase diagram showing the preferred morphology as a function of the amount of deposited material Q (horizontal axis) and of the quantity $\Lambda=\Delta E_{\mathrm{surf}}/E_{\mathrm{interface}}^{\mathrm{disl}}$, where ΔE_{surf} is the change in the surface energy due to island formation, and $E_{\mathrm{interface}}^{\mathrm{disl}}$ is the energy of a dislocated interface. The labels UF, CI, and DI refer to "uniform film," "coherent island," and "dislocated island," respectively. From Vanderbilt and Wickham (1991) with the kind permission of the authors.

If ΔE_{surf} is positive and small, or if the energy of the dislocated interface is relatively large, the corresponding value Λ on the phase diagram of Fig. 12 is larger than Λ_0. With an increase in the amount of deposited material, a transition from a uniform film to coherent islands occurs. Further deposition may cause the onset of dislocations in the islands. The theory of Vanderbilt and Wickham (1991) deals with islands having the shape of elongated prisms ("ridges"). The theory of Ratsch and Zangwill (1993) yields the same morphologies, i.e., uniform films, coherent islands, and dislocated islands in the case of pyramid-shaped islands.

As coherent islands are formed, the common understanding is that they will undergo Ostwald ripening in order to reduce the overall surface area and thus to reduce the total surface energy of the system. The process of ripening implies the growth of large islands at the expense of the evaporation of small islands (Lifshits and Slyozov, 1958; Chakraverty, 1987). Ripening yields a rather wide size distribution of islands, which evolves with time in a self-similar way, leading to an increase in the average volume of an island and to a corresponding decrease in island density. Although some slowing down has been predicted for a system of strained islands (Drucker, 1993), this mechanism does not yield substantial narrowing of the size distribution or the halt of island growth. After a given island reaches a certain critical volume for the onset of dislocations, plastic relaxation occurs, which accelerates the further growth rate of the island.

Surprisingly, experimental studies of coherent islands of InGaAs/GaAs(001) (Leonard *et al.*, 1993), and of InAs/GaAs(001) (Ledentsov *et al.*, 1994b; Leonard *et al.*, 1994; Madhukar *et al.*, 1994; Moison *et al.*, 1994)

have revealed a narrow size distribution of islands which does not follow from the Stranski-Krastanow growth mode itself. Such a narrow size distribution has been observed in a wide range of heteroepitaxial systems, including InAs/InP(001) (Ponchet *et al.*, 1995), AlInAs/GaAlAs(001) (Leon *et al.*, 1995), GeSi/Si(001) (Apetz *et al.*, 1995; Schittenhelm *et al.*, 1995; Jesson *et al.*, 1996), CdSe/ZnSe(001) (Xin *et al.*, 1996), InAs/InAlAs(001), and InAs/InGaAs(001) (Ustinov *et al.*, 1998), and InAs/Si(001) (Cirlin *et al.*, 1998).

The small size of these islands allows them to work as quantum dots and realize electron confinement in all three dimensions, while their narrow size distribution and the absence of misfit dislocations make them suitable for laser applications (Kirstaedter *et al.*, 1994; Bimberg, Kirstaedter, *et al.*, 1997b).

The narrow size distribution and the absence of Ostwald ripening are the subject of intense debates. Thermodynamic theory states that, under certain conditions, the equilibrium state of a lattice-mismatched heteroepitaxial system is an ordered array of three-dimensional coherently strained islands. No Ostwald ripening occurs in this case. Kinetic theories state that, once three-dimensional islands are formed, there will be a thermodynamic tendency towards ripening, but the growth of islands above a certain size can be kinetically slowed down (so-called kinetically self-limited growth).

Within this general debate, one can focus on two different questions. The first question is rather general: whether equilibrium arrays of 3D islands can indeed exist. The second question arises for any particular system: whether an observed array of 3D islands is in equilibrium or is kinetic controlled.

A number of papers report work in which 3D islands, after they are formed, are immediately capped by the substrate material (e.g., Leonard *et al.*, 1994; Leon *et al.*, 1995) or are immediately cooled down (e.g., Moison *et al.*, 1994). This approach allows one to obtain rather small dislocation-free islands which can work as quantum dots. However, it adds little to our understanding of the origin of arrays of 3D strained islands.

To determine experimentally whether an array of islands is an equilibrium one, it is necessary to stop deposition of the material and to interrupt growth before overgrowth of the islands, or before cooling down, or before any other change of the system. Then the heteroepitaxial system is a closed system with a fixed amount of deposited material and evolves towards equilibrium.

Ledentsov, Grundmann, *et al.* (1996) focused on the behavior of the system when epitaxial growth of InAs on GaAs(001) was interrupted. This work will be discussed in detail in Sec. IV.L.1. Briefly, those results indicate that, irrespective of the amount of deposited InAs, upon growth interruption, islands reach their optimum size ($\approx$140 Å), and their size and density does not change upon further growth interruption. Moreover, neighboring islands exhibit strongly correlated arrangements. This correlation is typical for a periodic square superlattice of islands (Bimberg *et al.*, 1995; Cirlin *et al.*, 1995; Grundmann *et al.*, 1995a, 1995b). These results indicate the existence of a new class of spontaneously ordered nanostructures, namely, ordered arrays of three-dimensional coherently strained islands.

Motivated by these observations, Shchukin, Ledentsov *et al.* (1995) developed a thermodynamic theory for the spontaneous formation of arrays of 3D coherently strained islands. In this theory, it is taken into account that there are two sources of strain in the system, the lattice mismatch, on the one hand, and the discontinuity of the surface stress tensor at the island edges, on the other hand. Secondly, the dependence of the surface energy on strain is taken into account. The analysis of Shchukin, Ledentsov *et al.* (1995) shows that, for a certain parameter region, the equilibrium in a system of 3D coherently strained islands corresponds to a periodically ordered array of identical islands, and Ostwald ripening does not occur.

There are two driving forces for the ordering of islands in size. The first is the elastic relaxation due to discontinuity of the intrinsic surface stress tensor at the island edges, similar to that described in Secs. II and III. The second is the strain-induced renormalization of surface energies. This renormalization may result in a decrease in the total surface energy (Shchukin, Ledentsov, *et al.*, 1996), despite an increase of the total surface area, owing to creation of a 3D island. In this case, there is no energy benefit in Ostwald ripening, and the latter does not occur.

In a subsequent paper, Shchukin, Ledentsov, *et al.* (1997) emphasized that the wetting layer formed in Stranski-Krastanow growth has a microscopic thickness and is surface distinct from the surface of the deposited material. Therefore the wetting layer has a different surface energy than the (001) surface of a bulk crystal of the deposited material (e.g., the surface energy of an InAs wetting layer on GaAs(001) differs from the surface energy of an (001) surface of bulk InAs). Thus the appearance of tilted facets via formation of a 3D island competes with the disappearance of a certain area of the wetting layer. In a heteroepitaxial system, the formation of a 3D island is accompanied, despite the increase of the surface area, by a decrease in the surface energy.

Following the approach of Shchukin, Ledentsov, *et al.* (1995), Daruka and Barabási (1997) constructed an equilibrium phase diagram of a lattice-mismatched heteroepitaxial system, which reproduces all possible morphologies observed in experiment, i.e., a flat film, an ordered array of islands over the wetting layer or over a bare substrate, ripened islands over the wetting layer or over a bare substrate, and a bimodal size distribution of islands including both ordered and ripened islands.

Other thermodynamic studies of lattice-mismatched systems focus on the equilibrium shape of a single isolated island. Kaminski and Suris (1996), Chen *et al.* (1997), and Duport *et al.* (1997) determined, under different assumptions about the facet energies, that the shape of a strained island changes with its volume, larger islands having steeper side facets. The same results for a particular system were obtained from *ab initio* calcula-

tions by Pehlke *et al.* (1996). Duport *et al.* (1997) suggested that the ultimate shape of an island as the volume increases corresponds to an overhanging island, nearly detached from the substrate, and the strain energy in such islands is completely relaxed. Spencer and Tersoff (1997) developed a model in which an asymptotic shape of a large coherent island is a ball sitting atop the wetting layer. Such a mode of *total relaxation* is an alternative to the onset of dislocations, which is unavoidable in large islands if the elastic relaxation is only partial (Vanderbilt and Wickham, 1991). Based on this effect of total elastic relaxation in overhanging coherent islands, Duport *et al.* (1997) and Spencer and Tersoff (1997) concluded that the equilibrium state of a lattice-mismatched system is in any case a single island formed via Ostwald ripening.

In Sec. IV.I we focus on the above statements of Duport *et al.* (1997) and of Spencer and Tersoff (1997). We show that, despite the possibility of the formation of totally relaxed overhanging islands, there exists, nevertheless, a parameter region where the equilibrium state of a lattice-mismatched heteroepitaxial system is an ordered array of 3D islands, and ripening does not occur.

The present section is organized as follows. In Sec. IV.B, the general equation is derived for the total energy of an array of 3D coherently strained islands. Provided the total amount of deposited material is fixed, i.e., the growth is interrupted, and evaporation is neglected, the system is a closed system and evolves towards the Helmholtz free-energy minimum. We omit the entropy term and seek the minimum of the total energy. Since the deposited material is, in general, distributed between 3D islands and the wetting layer, the total energy is a function of the amount of material in the islands, the shape, the volume, and the relative arrangement of the islands. First, we fix the amount of the material in the islands (and thus we fix the thickness of the wetting layer) and minimize the total energy under this constraint. In Sec. IV.C, we focus on a dilute array of islands, where the island-island elastic interaction is negligible, and obtain the equation for the energy of a single island. In Sec. IV.D we describe how the minimization of the energy of a single isolated island of a fixed volume can give the shape of the island. The main concern of the theoretical part of this section is to show that equilibrium arrays of 3D islands can exist and that Ostwald ripening does not occur for such arrays. In this connection, in Secs. IV.E–IV.G, we assume a constant island shape and seek an optimum island size, following papers by Shchukin, Ledentsov, *et al.* (1995, 1996, 1997). We demonstrate that, in a certain parameter region, the equilibrium corresponds to an ordered array of 3D coherently strained islands, and ripening is not energetically favored. In Sec. IV.H, we follow the paper by Daruka and Barabási (1997) and show how the thermodynamic theory reveals the phase diagram which reproduces all possible morphologies observed experimentally. In Sec. IV.I we refer to recent papers by Duport *et al.* (1997) and by Spencer and Tersoff (1997), who pointed out the possibility of formation of totally relaxed overhanging coherent islands, which should favor ripening in all systems. By taking into account the shape-versus-volume dependence of 3D islands, we demonstrate that there still exists a parameter region where ripening is not favored. In Sec. IV.J we give a brief description of kinetic theories of island formation, focusing on particular mechanisms that can eventually slow down Ostwald ripening and result in a narrow size distribution of islands. In Sec. IV.J we focus on how an experiment should be carried out in order to distinguish thermodynamic-controlled arrays of islands from kinetic-controlled ones.

In Sec. IV.K we discuss experimental techniques used for characterization of systems with 3D islands (quantum dots). We focus mainly on direct imaging techniques such as scanning tunneling microscopy, atomic force microscopy, and transmission electron microscopy. We compare these methods, discussing advantages and disadvantages, problems that can arise, and ways to overcome these problems. In Sec. IV.L we examine experimental data on the formation of 3D islands (quantum dots), mostly on InAs/GaAs and GaInAs/GaAs systems. Particular attention is paid to key experiments that allow one to distinguish thermodynamic-controlled arrays of islands from kinetic-controlled arrays. These experiments reveal two examples of reversible phase transitions. The first is, a reversible phase transition from 3D to 2D morphology in an InAs/GaAs system grown by molecular beam epitaxy (MBE); the transition is driven by lowering of As pressure (Ledentsov, Grundmann, *et al.*, 1996). The second example is a reversible phase transition from 3D to 2D morphology in an InGaAs/GaAs system grown by metalorganic vapor phase epitaxy (MOVPE) (Ozasa *et al.*, 1997). In the latter case, the transition is driven by switching off the AsH_3 flux and switching on the PH_3 flux. Such reversibility strongly indicates the thermodynamic nature of these arrays. Other materials systems, such as SiGe/Si and CdSe/ZnSe, are discussed. In the summary of this section, we formulate key experimental options that will allow us, for any particular materials systems, to distinguish thermodynamic-controlled arrays of islands from kinetic-controlled arrays.

B. Energetics of a heteroepitaxial system

We focus on the equilibrium structure of a heteroepitaxial lattice-mismatched system which may be achieved by interruption of growth. Let Q monolayers of material 2 be deposited on the (001) substrate of material 1. We treat both the substrate and the deposited material as elastically anisotropic cubic media with equal elastic moduli λ_{ijlm}, and the lattice mismatch between the two materials as being equal, $\varepsilon_0=\Delta a/a$, where a is the lattice parameter. The total energy of the uniform planar film per unit surface area may be written

$$E_{\mathrm{planar}}(Q)=\lambda\varepsilon_0^2 Qa+W(Q). \tag{4.1}$$

Here the first term is the strain energy of the uniform film, and the elastic modulus λ equals $(c_{11}+2c_{12})(c_{11}-c_{12})c_{11}^{-1}$, where c_{11} and c_{12} are elastic moduli in the

Voigt notation. If $Q\to 0$, the quantity $W(Q)$ is the surface energy of material 1, $W(0)=\gamma_1$. If the film thickness is macroscopic, $Q\gg 1$, the quantity $W(Q)$ is the sum of the surface and interface energies, $W(Q)=\gamma_2+\gamma_{12}^{\rm interface}$. For a film of arbitrary microscopic thickness, the contributions of surface, interface, and strain energy, respectively, cannot be separated, and only the total energy $E_{\rm planar}(Q)$ has a physical meaning. However, it is convenient to use Eq. (4.1) for arbitrary Q and to consider this equation as the definition of the quantity $W(Q)$ for arbitrary Q. The energy $W(Q)$ defined in this way takes into account effects of wetting or nonwetting as well as effects of possible surface reconstruction.

Since we are focusing on the equilibrium array of islands that appears in a closed system, the formation of islands obeys the conditions of matter conservation, i.e., the volume of initially deposited material 2 equals the sum of the volume of the wetting layer and the sum of the volumes of all islands. If we denote the thickness of the wetting layer as Q' monolayers, the remaining $(Q-Q')$ monolayers of the deposited material are assembled in the islands.

To obtain the structure of the equilibrium array of islands, we shall assume that all islands have the same shape and volume and form a two-dimensional periodic superlattice on the surface. If we denote the fraction of the surface covered by islands as q, the total energy of the array of islands per unit surface area may be written

$$E=\lambda\varepsilon_0^2Q'a+(1-q)W(Q')+\frac{1}{A_0}\left[\tilde{E}_{\rm island}+\frac{\tilde{E}_{\rm interaction}}{2}\right]. \tag{4.2}$$

Here the first two terms give the energy of the planar uniform film of thickness $Q'a$, the third term is the energy of a single island, and the fourth term is the interaction energy of a single island with all other islands, where A_0 denotes the unit cell area of the superlattice comprised of islands. By subtracting Eq. (4.1) from Eq. (4.2), one obtains the change in the energy due to formation of islands,

$$\Delta E=W(Q')-W(Q)+E_{\rm array}(Q',Q), \tag{4.3}$$

where the energy $E_{\rm array}(Q',Q)$ equals

$$E_{\rm array}(Q',Q)=(Q-Q')a\left[-\lambda\varepsilon_0^2+\frac{\tilde{E}_{\rm island}-W(Q')\tilde{A}_{\rm island}}{V}+\frac{\tilde{E}_{\rm interaction}}{2V}\right]. \tag{4.4}$$

Here V is the volume of a single island, and $\tilde{A}$ is the area of the island base. The change of energy ΔE in Eq. (4.3) is a function of the total amount of material assembled in all islands, $(Q-Q')$, of the shape of a single island, of the volume of a single island V, and of the lateral arrangement of islands, i.e., of the type of lateral superlattice comprised of islands.

Equation (4.3) indicates that the structure of the equilibrium array of islands and the thickness of the wetting layer should be determined in a self-consistent way by minimizing ΔE. We shall first fix the total amount of material assembled in all islands, $(Q-Q')$ (thus also fixing the thickness Q' of the wetting layer) and we shall seek the minimum of $E_{\rm array}$ with respect to the island shape, volume, and arrangement, following the paper by Shchukin, Ledentsov, *et al.* (1995). Afterwards, we shall substitute the minimum value of $E_{\rm array}$, which will be a function of Q', into Eq. (4.3) and will minimize ΔE with respect to Q'.

C. Dilute array of islands

The energy of a single island $\tilde{E}_{\rm island}$ which enters Eq. (4.4) may be written as a sum of three contributions,

$$\tilde{E}_{\rm island}=\tilde{E}_{\rm elastic}+\tilde{E}_{\rm surf}+\tilde{E}_{\rm edges}. \tag{4.5}$$

To write down the elastic energy of a heterophase system, we apply the concept of the stress-free strain $\varepsilon_{ij}^{(0)}(\mathbf{r})$ (Khachaturyan, 1974, 1983). Since different phases, having different values of the equilibrium lattice parameter, are coherently conjugated, the elastic field is characterized by the strain tensor $\varepsilon_{ij}(\mathbf{r})$ defined throughout the entire heterophase system. If locally the strain $\varepsilon_{ij}(\mathbf{r})$ coincides with the stress-free strain for a given material, $\varepsilon_{ij}^{(0)}(\mathbf{r})$, both the elastic stress and the elastic energy density vanish. A deviation of the strain from the stress-free strain leads to a nonzero stress and a nonzero value of the elastic energy density. For the latter we use the definition by Roitburd (1976), $f_{\rm elastic}=\frac{1}{2}\lambda_{ijlm}[\varepsilon_{ij}(\mathbf{r})-\varepsilon_{ij}^{(0)}(\mathbf{r})][\varepsilon_{lm}(\mathbf{r})-\varepsilon_{lm}^{(0)}(\mathbf{r})]$. The total elastic energy is then given by the integral

$$\tilde{E}_{\rm elastic}=\frac{1}{2}\int\lambda_{ijlm}[\varepsilon_{ij}(\mathbf{r})-\varepsilon_{ij}^{(0)}(\mathbf{r})]\times[\varepsilon_{lm}(\mathbf{r})-\varepsilon_{lm}^{(0)}(\mathbf{r})]dV. \tag{4.6}$$

For the heteroepitaxial system in question, it is natural to use the unstressed substrate as the reference frame, so that the stress-free strain vanishes in the substrate, $\varepsilon_{ij}^{(0)}(\mathbf{r})=\varepsilon_0\delta_{ij}\vartheta(\mathbf{r})$, where $\vartheta(\mathbf{r})=1$ in the deposited material, $\vartheta(\mathbf{r})=0$ in the substrate, $\delta_{ij}=1$ if $i=j$, and $\delta_{ij}=0$ otherwise. It should be noted that $\varepsilon_{ij}^{(0)}(\mathbf{r})=0$ does not mean the rigid substrate, since the strain field $\varepsilon_{ij}(\mathbf{r})$ penetrates, generally speaking, into the substrate.

The surface energy per unit area γ is renormalized in the strain field [Marchenko and Parshin, 1980; Andreev and Kosevich, 1981; see also Eq. (2.6)]:

$$\gamma(\varepsilon_{\alpha\beta})=\gamma_0+\tau_{\alpha\beta}(\varepsilon_{\alpha\beta}-\varepsilon_0\delta_{\alpha\beta})+\tfrac{1}{2}S_{\alpha\beta\mu\nu}(\varepsilon_{\alpha\beta}-\varepsilon_0\delta_{\alpha\beta})(\varepsilon_{\mu\nu}-\varepsilon_0\delta_{\mu\nu})+\cdots,$$

where $\tau_{\alpha\beta}$ is the intrinsic surface stress tensor, $S_{\alpha\beta\mu\nu}$ is the tensor of the "surface excess elastic moduli" (Wolf, 1993), and α, β, μ, ν are 2D indices in the local facet plane. The total renormalized surface energy of a heterophase system is

$$\tilde{E}_{\text{surf}} = \int \Bigg[\gamma_0(\hat{\mathbf{m}}) + \tau_{\alpha\beta}(\hat{\mathbf{m}})[\varepsilon_{\alpha\beta}(\mathbf{r}) - \varepsilon_0 \delta_{\alpha\beta}\Theta(\mathbf{r})] + \frac{1}{2} S_{\alpha\beta\mu\nu}(\hat{\mathbf{m}})[\varepsilon_{\alpha\beta}(\mathbf{r}) - \varepsilon_0 \delta_{\alpha\beta}\Theta(\mathbf{r})] \times [\varepsilon_{\mu\nu}(\mathbf{r}) - \varepsilon_0 \delta_{\mu\nu}\Theta(\mathbf{r})] \Bigg] (\hat{\mathbf{m}}\cdot\hat{\mathbf{n}})^{-1}\, dA. \tag{4.7}$$

Here $\hat{\mathbf{m}} = \hat{\mathbf{m}}(\mathbf{r})$ is the local normal to the facet, $\hat{\mathbf{n}} = (0,0,1)$ is the normal to the flat surface, and the integration in Eq. (4.7) is carried out over the reference flat surface. $\Theta(\mathbf{r}) = 1$ if the surface point belongs to the island facet, and $\Theta(\mathbf{r}) = 0$ on the surface of the wetting layer, since the wetting layer is considered to be a complex surface of the substrate material having the thickness Q' and the surface energy $W(Q')$.

The third term in Eq. (4.5) is the short-range energy of the edges.

For lattice-mismatched systems with edges, the total strain field is the sum of two contributions, one due to the lattice mismatch and another due to the discontinuity of the intrinsic surface stress tensor τ_{ij} at the edges. Since excess elastic moduli $S_{\alpha\beta\mu\nu}(\hat{\mathbf{m}})$ exist on the surface only, their contribution to the energy is smaller by a factor of $\sim a/L$ than the elastic energy, where L is the characteristic size of the island, and may be treated by perturbation theory.

In the zero approximation in $S_{\alpha\beta\mu\nu}(\hat{\mathbf{m}})$, the elastic energy, including both bulk and surface contributions, is given in terms of the sources of the strain field (Shchukin *et al.*, 1995a),

$$\tilde{E}_{\text{elastic}} = \lambda \varepsilon_0^2 V - \frac{1}{2}(c_{11} + 2c_{12})\varepsilon_0 \oint dA \times \int dA' m_i(\mathbf{r}) G_{i\alpha}(\mathbf{r},\mathbf{r}') \widetilde{\sigma_{\alpha\beta}}\, m_\beta(\mathbf{r}') - \int dl \int dA' F_i(\mathbf{r}) G_{i\alpha}(\mathbf{r},\mathbf{r}') \widetilde{\sigma_{\alpha\beta}}\, n_\beta(\mathbf{r}') - \frac{1}{2}\int dl \int dl' F_i(\mathbf{r}) G_{ij}(\mathbf{r},\mathbf{r}') F_j(\mathbf{r}'). \tag{4.8}$$

Here the first term is the elastic energy of the volume V in a planar, uniformly strained film. The second term is the energy of the volume elastic relaxation, the contribution to this energy coming from tilted facets of the island where $m_\beta \neq 0$. The third term is the energy of the interaction of two strain fields, the one due to lattice mismatch and the other due to the intrinsic surface stress discontinuity at the edges. The fourth term is the energy of elastic relaxation due to surface stress discontinuity at the edges. Here $G_{ij}(\mathbf{r},\mathbf{r}')$ is the static Green's tensor of elasticity theory defined for a semi-infinite crystal with a stress-free surface of a given profile, $\widetilde{\sigma_{\alpha\beta}} = -(c_{11}+2c_{12})(c_{11}-c_{12})c_{11}^{-1}\varepsilon_0\delta_{\alpha\beta}$ is the stress tensor in a planar heteroepitaxial film, the forces $F_i(\mathbf{r})$ are due to discontinuity of the surface stress tensor at the edges, the integration $\oint dA$ is defined over both the side facets of the island and the interface between the island and the wetting layer, the integration $\int dA'$ contains nonvanishing contributions from the side facets of the island only, and the integrations $\int dl$ and $\int dl'$ are carried out over the edges of the island.

The scaling properties of the Green's tensor in the elasticity theory for a three-dimensional elastic field allow one to obtain the scaling behavior of each of the contributions to the elastic energy in Eq. (4.8). For an infinite homogeneous medium the Green's tensor behaves as $G_{ij}(\mathbf{r},\mathbf{r}') \sim |\mathbf{r}-\mathbf{r}'|^{-1}$ (Landau and Lifshits, 1959), and for an arbitrary geometry of the system one finds that $G_{ij}(\mathbf{r},\mathbf{r}')$ scales as L^{-1}. By substituting this into Eq. (4.8), one obtains the following scaling behavior of different contributions into the elastic energy of the island $\tilde{E}_{\text{elastic}}$ (Shchukin *et al.*, 1995a; Shchukin, Ledentsov *et al.*, 1995): $E_{\varepsilon_0-\varepsilon_0} \sim L^3$, $E_{\varepsilon_0-\tau} \sim L^2$, $E_{\tau-\tau} \sim -L \ln L$. The excess elastic moduli of the surface give the correction to the energy of the volume elastic relaxation, which is proportional to L^2, and corrections to all other terms are of the order of L or smaller. Thus, summing up the scaling analysis of the energy of a single island, one can write it in the following schematic form (Shchukin, Ledentsov, *et al.*, 1995):

$$\tilde{E}(V) = \left[-f_1 \lambda \varepsilon_0^2 V + (\Delta\Gamma) V^{2/3} - \frac{f_2 \tau^2}{\lambda} V^{1/3} \ln\left(\frac{V^{1/3}}{2\pi a}\right) + f_3 \eta V^{1/3} \right]. \tag{4.9}$$

The first term in Eq. (4.9) is the energy of the volume elastic relaxation $\widetilde{\Delta E}^{V}_{\text{elastic}}$. It is always negative. The second term is the change in the renormalized surface energy of the system due to island formation. For concreteness, we shall write $(\Delta\Gamma)$ for an island having the shape of a pyramid with a square $L \times L$ base and a tilt angle of side facets φ_0. Then $\widetilde{\Delta E}^{\text{renorm}}_{\text{surf}} = (\Delta\Gamma)(\frac{1}{6}\tan\varphi_0)^{2/3} L^2$, and

$$(\Delta\Gamma) = (6\cot\varphi_0)^{2/3}[\gamma_2(\varphi_0)\sec\varphi_0 + \gamma_{12}^{\text{interface}} - W(Q') - g_1(\varphi_0)\tau\varepsilon_0 - g_2(\varphi_0) S \varepsilon_0^2]. \tag{4.10}$$

Here the change in the surface energy includes contributions from several sources: the appearance of tilted facets of the island; the appearance of the interface between the deposited material and the substrate underneath the island; the disappearance of the planar surface area; and renormalization terms, both linear and quadratic in ε_0.

The key point is that the quantity $(\Delta\Gamma)$ can be *of either sign*. The third term in Eq. (4.9) is the contribution of the edges of the island to the elastic relaxation energy, $\widetilde{\Delta E}^{\text{edges}}_{\text{elastic}} \sim -V^{1/3}\ln V^{1/3}$. It is always negative. The fourth term in Eq. (4.9) is the short-range energy of the edges, where η is a characteristic energy per unit length of the edge. Coefficients f_1, f_2, f_3 are geometric factors depending on the island shape. We note that the parametrization of the energy (4.10) differs from that in papers by Shchukin, Ledentsov *et al.* (1995, 1997). Unlike those papers, where we focused only on pyramid-shaped is-

lands, here, in Sec. IV.I, we shall consider islands of different shapes. That is why we have written the island energy (4.9) not in terms of the island's lateral size, but in terms of its volume.

D. Ordering of islands in shape

For a dilute array of islands, where the average distance between islands is large compared to the island size L, the equilibration of the island shape by atomic migration on the island facets is faster than material exchange between islands. Then for any given volume of an island, there exists an equilibrium shape. For sufficiently large islands, the first two terms in the island energy (4.9), $\widetilde{\Delta E}^V_{\text{elastic}}$ and $\widetilde{\Delta E}^{\text{renorm}}_{\text{surf}}$ are the two dominant ones.

Several theoretical studies have been carried out in which an equilibrium shape of a single three-dimensional coherently strained island has been calculated. Tersoff and Tromp (1993) obtained an equilibrium shape of an island under the assumption that the height of the island was kinetically limited to a certain value h. The global geometry of such an island is 2D rather than 3D. That is the reason why this discussion is put into Sec. III.

The equilibrium shape of a single three-dimensional coherently strained island has been calculated by Pehlke *et al.* (1996) and by Kaminski and Suris (1996) by minimizing the island's total energy. The total energy was approximated by the sum of the elastic energy and of the surface energy, i.e., by the first two terms of Eq. (4.9).

Kaminski and Suris (1996) showed that rather general assumptions about surface energies of island facets yield a phase diagram containing not only regimes of 2D and 3D growth, but also a regime in which a 2D-3D transition occurs. Pehlke *et al.* (1996) focused on InAs islands on a GaAs(001) substrate. They obtained surface energies of (100), (110), (111), and $(\overline{111})$ surfaces of InAs from *ab initio* calculations, and applied the Wulff's construction to these energies. This gave an equilibrium shape of InAs in As-rich conditions (Pehlke *et al.*, 1997) which agrees with the observed shape of large, and thus presumably fully relaxed, InAs islands grown by metal-organic vapor phase epitaxy (MOVPE) on a GaAs(001) substrate (Steimetz *et al.*, 1997).

To derive the equilibrium shape of a coherently strained InAs island, Pehlke *et al.* (1996) considered a variety of possible configurations, which were restricted to surface orientations present on the equilibrium crystal shape of InAs. The elastic energy for each configuration was calculated in the frame of a continuum theory of elasticity via the finite-element method. Their results are displayed in Fig. 13. The optimum island shape for a given volume of the island $V_0 = 2.88\times 10^5$ Å^3 is determined by that point where the line of constant total energy $E_{\text{total}}/V_0 = E_{\text{elastic}}/V_0 + E_{\text{surf}}/V_0$ touches the manifold of island energies from below. Even when the volume is different it is possible to reveal the optimum

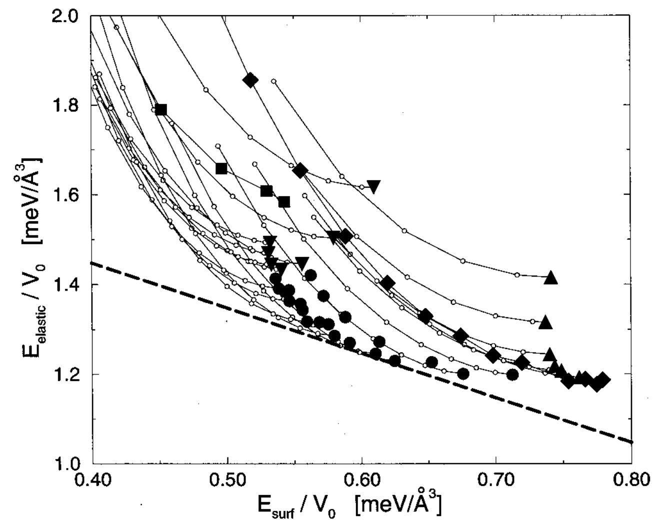

FIG. 13. Elastic energy per volume E_{elastic}/V vs surface energy per volume E_{surf}/V_0 for InAs islands having the volume $V = 2.88\times 10^5$ Å^3. ■, square-based pyramids with {101} faces and (001)-truncated {101} pyramids; ♦, square-based pyramid with {111} and $\{\overline{111}\}$ faces and (001)-truncated pyramids; ▲, "huts" with {111} and $\{\overline{111}\}$ faces; ▼, square based {101} pyramids with $\{\overline{111}\}$-truncated edges; ●, islands with {101}, {111}, and $\{\overline{111}\}$ faces. Filled symbols denote numerical results, while open circles correspond to a simple analytical approximation for (001)-truncated "mesa-shaped" islands. It is assumed that the elastic energy does not change when the (almost fully relaxed) top of an island is cut off. Solid lines connect islands that are created in this way, varying the height of the (001) surface plane. The dashed line is the curve of constant total energy $E_{\text{elastic}} + E_{\text{surf}}$ that selects the equilibrium shape. From Pehlke *et al.* (1996), with the kind permission of the authors.

shape from the same graph. By using the scaling relations $E_{\text{elastic}} \sim V$ and $E_{\text{surf}} \sim V^{2/3}$, one obtains

$$\frac{E_{\text{total}}(V)}{V} = \frac{E_{\text{elastic}}(V_0)}{V_0} + \left(\frac{V_0}{V}\right)^{1/3} \frac{E_{\text{surf}}(V_0)}{V_0}. \quad (4.11)$$

Equation (4.11) reads that only the slope of the total energy line changes with a change in volume, and the whole evolution of the island shape can be extracted from Fig. 13. For an island with volume $V_0 = 2.88\times 10^5$ Å^3, the optimum shape deduced from Fig. 13 is a hill bounded by {101}, {111}, and $\{\overline{111}\}$ facets and by a (001) surface on the top. The shape is similar to that of InP islands on GaInP observed by Georgsson *et al.* (1995). However, since the surface energies of InP could be different from those of InAs, a direct comparison of the calculated shape of InAs islands with the observed shape for InP islands is not possible. Various shapes have been observed for InAs islands grown on a GaAs substrate. Moison *et al.* (1994) reported rather flat islands having {104} facets. Leonard *et al.* (1994) described their islands as planoconvex lenses with a radius-to-height aspect ratio of about 2. Ruvimov *et al.* (1995) reported the pyramid shape with {101} side facets. All the observed shapes differ from the equilibrium shape predicted theoretically.

There are several possible reasons for this disagreement, discussed, for example, by Pehlke *et al.* (1997). First, the diversity of experimental results indicates that the islands in most cases are not equilibrium shapes, but kinetically controlled ones. We shall argue below that the pyramids observed by Ruvimov *et al.* (1995) are most likely the equilibrium islands. But this does not lift the existing disagreement with the theory (Fig. 13).

Secondly, *ab initio* calculations of surface energies by Pehlke *et al.* (1996) refer to infinitely large surfaces, whereas one cannot exclude the possibility that finite nanometer-scale facets do not allow formation of reconstructions with large surface unit cells, and actual surface energies of island facets may be different from those for infinite flat surfaces. Moreover, the contribution of the edges to the island energy and finite-temperature corrections to the surface energies, which might affect the equilibrium shape of the islands, are not taken into account in Fig. 13.

Below, in Sec. IV.K, we shall argue that different measured shapes of InAs islands are due, first, to different growth conditions, and, second, to different measurement techniques. In our review, we shall focus below on the particular system of InAs islands described by Ruvimov *et al.* (1995). We shall point out that carefully performed high-resolution electron microscopy (HREM) measurements combined with HREM simulations (Ruvimov and Scheerschmidt, 1995) reveal a pyramid bounded by {101} facets to be the true shape of InAs islands grown at temperature 450–480 °C. We shall also review a set of experiments especially aimed at distinguishing equilibrium islands from kinetically controlled ones, which indicate that the InAs pyramids having {101} facets seem to be equilibrium islands.

E. Ordering of islands in size versus Ostwald ripening

In this subsection we consider the driving forces governing the narrow size distribution of islands, as well as the conditions under which Ostwald ripening does not occur. To focus on essential physics, we use an approximation of a constant island shape, which is a pyramid having a square $L\times L$ base and the tilt angle φ_0 of the side facets.

Equilibrium in an array of islands can be reached by the exchange of material between islands via surface migration. For a dilute array, the elastic interaction between islands via the strained substrate may be neglected. Then the energy of the array is the sum of contributions of single islands [Eq. (4.9)].

The condition for equilibrium is the total energy minimum under the constraint of a fixed amount of material in all islands. It is possible to use an equivalent procedure and to minimize the energy *per one atom in the island* $E(L)$. Dividing $\tilde{E}(L)$ from Eq. (4.9) by the volume of a single island $\frac{1}{6}\tan\varphi_0 L^3$ and multiplying by the atomic volume Ω, one obtains (Shchukin, Ledentsov, *et al.*, 1995)

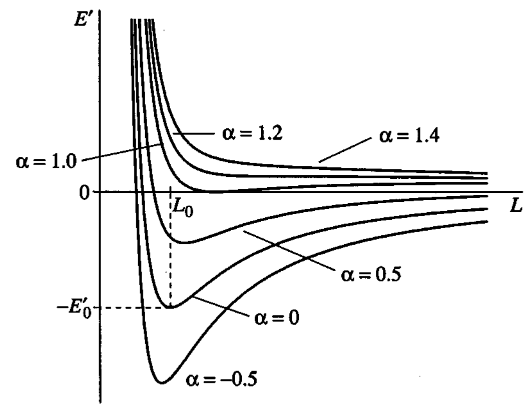

FIG. 14. The energy of a dilute array of 3D coherently strained islands per one atom vs size of the island. The parameter α is the ratio of the change in the surface energy due to the formation of islands, $\Delta E_{\rm surf}^{\rm renorm}$, and of the contribution of the edges to the elastic relaxation energy, $|\Delta E_{\rm elastic}^{\rm edges}|$.

$$E(L)=\Omega\Bigg[-f_1(\varphi_0)\lambda\varepsilon_0^2+(6\cot\varphi_0)^{1/3}\frac{(\Delta\Gamma)}{L}-(6\cot\varphi_0)^{2/3}\frac{f_2(\varphi_0)\tau^2}{\lambda L^2}\ln\left(\frac{L}{2\pi a}\right)+(6\cot\varphi_0)^{2/3}\frac{f_3(\varphi_0)\eta}{L^2}\Bigg]. \quad (4.12)$$

It is worth noting that the volume elastic relaxation energy $\Delta E_{\rm elastic}^{V}$ [the first term in Eq. (4.12)] does not depend on the island size L. To seek the minima of $E(L)$ from Eq. (4.12) we introduce the characteristic length

$$L_0=2\pi a\exp\left[\frac{f_3(\varphi_0)\eta\lambda}{f_2(\varphi_0)\tau^2}+\frac{1}{2}\right] \quad (4.13)$$

and the characteristic energy per one atom,

$$E_0=\frac{1}{2}\,\frac{\Omega f_2(\varphi_0)(6\cot\varphi_0)^{2/3}\tau^2}{\lambda L_0^2}. \quad (4.14)$$

Then we may write the sum of all L-dependent terms in $E(L)$ as (Shchukin, Ledentsov *et al.*, 1996)

$$E'(L)=E_0\left[-2\left(\frac{L_0}{L}\right)^2\ln\left(\frac{e^{1/2}L}{L_0}\right)+\frac{2\alpha}{e^{1/2}}\left(\frac{L_0}{L}\right)\right]. \quad (4.15)$$

The function $E'(L)$ is governed by the control parameter

$$\alpha=\frac{e^{1/2}\lambda L_0}{f_2(\varphi_0)(6\cot\varphi_0)^{1/3}\tau^2}(\Delta\Gamma), \quad (4.16)$$

which is the ratio of the change in surface energy due to island formation and the contribution of the edges to the elastic relaxation energy, $|\Delta E_{\rm elastic}^{\rm edges}|$. The energy of the dilute array of islands per one atom versus the size of the island L is displayed in Fig. 14 for different values of α. If $\alpha\leqslant 1$, there exists an optimum island size $L_{\rm opt}$, corresponding to the absolute minimum of the energy, $\min E'(L)\equiv E(L_{\rm opt})<0$. On the other hand, the ripening

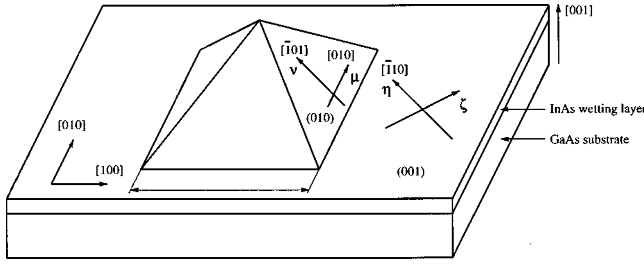

FIG. 15. Geometry of an InAs pyramid over an InAs wetting layer deposited on a GaAs(001) surface.

of islands would correspond to $L\rightarrow\infty$ where the energy $E'(L)\rightarrow 0$. This means that an array of identical islands of the optimum size L_{opt} is a stable array, and islands do not undergo ripening. If $1<\alpha<2e^{-1/2}\approx 1.2$, there exists only a local minimum of the energy, corresponding to a metastable array where $E'(L')>0$. If $\alpha\geqslant 1.2$, the local minimum in the energy $E'(L)$ disappears. For both these cases where $\alpha>1$, there exists a thermodynamic tendency towards ripening. The energy minimum then corresponds to a single huge cluster where all deposited material is collected.

If $(\Delta\Gamma)<0$ (and $\alpha<0$), the formation of a 3D island leads not only to a decrease in the strain energy due to relaxation, but also to a *decrease in the renormalized surface energy*.

For an InAs pyramid with {101}-type side facets over the InAs wetting layer deposited on a GaAs(001) surface, the evaluation of $(\Delta\Gamma)$ yields (Shchukin, Ledentsov, *et al.*, 1997)

$$(\Delta\Gamma)=6^{2/3}\{1.41\gamma_{\mathrm{InAs}}^{(101)}+\gamma_{\mathrm{interface}}-\gamma_{WL}^{(001)} \tag{4.17a}$$

$$-[0.72\tau_{\mu\mu}^{(101)}+0.40\tau_{\nu\nu}^{(101)}$$

$$+0.15(\tau_{\zeta\zeta}^{(001)}+\tau_{\eta\eta}^{(001)})]\varepsilon_0 \tag{4.17b}$$

$$+[0.22S_{\mu\mu\mu\mu}^{(101)}+0.08S_{\nu\nu\nu\nu}^{(101)}$$

$$+0.25S_{\mu\mu\nu\nu}^{(101)}+0.10S_{\mu\nu\mu\nu}^{(101)} \tag{4.17c}$$

$$+0.01(S_{\zeta\zeta\zeta\zeta}^{(001)}+S_{\eta\eta\eta\eta}^{(001)})+0.03S_{\zeta\zeta\eta\eta}^{(001)}$$

$$+0.01S_{\zeta\eta\zeta\eta}^{(001)}]\varepsilon_0^2\}, \tag{4.17d}$$

where the axes μ,ν,ζ,η are defined in Fig. 15. The change in the surface energy due to the formation of a pyramid contains contributions due to the appearance of tilted {101} facets of InAs [the first term in Eq. (4.17a)], the appearance of the InAs/GaAs interface underneath the pyramid [the second term in Eq. (4.17a)], the disappearance of the L^2 area of the wetting layer [the third term in Eq. (4.17a)], linear renormalization terms (4.17b), and quadratic renormalization terms [Eqs. (4.17c), (4.17d)].

It should be noted that the decrease in the surface energy in an InAs/GaAs(001) system, $(\Delta\Gamma)<0$, may occur despite the fact that the (001) surface of bulk InAs is stable against faceting. The reason is that the appearance of tilted {101} facets of InAs competes with the disappearance of a certain area of the wetting layer. The wetting layer of InAs having a microscopic thickness 1–2 monolayers, should be regarded as a surface whose surface energy is not equal to the surface energy of InAs(001).

The quantity $(\Delta\Gamma)$ could be evaluated if *all* quantities entering Eq. (4.17) were known from *ab initio* calculations. By using the values obtained so far for $\gamma_{\mathrm{InAs}}^{(101)}=41\,\mathrm{meV/\AA}^2$ from Pehlke *et al.* (1996), for the interface energy, for the intrinsic surface stress $\tau_{\alpha\beta}$, and for the excess surface elastic moduli $S_{\alpha\beta\varphi\psi}$ from Moll *et al.* (1998), we can show that the criterion $(\Delta\Gamma)<0$ is equivalent to $\gamma_{\mathrm{WL}}^{(001)}>55\,\mathrm{meV/\AA}^2$. Whether this condition holds could be determined by *ab initio* calculations.

However, one should be very careful about applying *ab initio* surface energies to the evaluation of crucial quantities in macroscopic theory. First, preferred surface reconstructions and corresponding values of surface energies were obtained in the above-cited papers only for temperatures $T=0$, while typical growth temperatures are 450 °C and higher. It is known that surface reconstruction can change and does change with temperature, and so does the surface energy. Second, calculated surface energies refer to infinitely large surfaces, while reconstruction on nanometer-scale facets could be different from that on a plane. Third, to apply the macroscopic theory to finite temperatures, one has to take into account an entropy contribution to the free energy, which has been neglected so far. Thus substantial theoretical effort from both *ab initio* and macroscopic approaches is required in order to ascertain the nature of ordering in a given system.

F. Lateral arrangement of islands

For a dense system of islands, elastic interaction between islands via the substrate is essential. The system of interacting islands is then a system of elastic domains where the energy minimum corresponds to a periodic domain structure (Marchenko, 1981b; Khachaturyan, 1983; Vanderbilt, 1992; Ipatova *et al.*, 1993, 1994). To obtain the elastic energy of interacting islands, we calculate the second term on the right-hand side of Eq. (4.8), which is the major contribution to the interaction energy. We focus on a small tilt angle of the island facets where the elastic relaxation energy given by the second term of Eq. (4.8) reduces to (Shchukin, Ledentsov, *et al.*, 1995)

$$\widehat{\Delta E}_{\mathrm{elastic}}=-C_0\int dA\int dA'\,n_\alpha(\mathbf{r}_\parallel)$$

$$\times G_{\alpha\beta}(\mathbf{r}_\parallel-\mathbf{r}'_\parallel;z,z')\Big|_{\substack{z=0\\ z'=0}} n_\beta(\mathbf{r}'_\parallel). \tag{4.18}$$

Here $C_0=(1/2)(c_{11}+2c_{12})^2(c_{11}-c_{12})^2c_{11}^{-2}\varepsilon_0^2$, the integration is carried out over the planar substrate, and the integrand is nonzero only on the projections of the tilted facets of the islands where $\mathbf{n}_\alpha\neq 0$, $\alpha=1,2$. $G_{\alpha\beta}(\mathbf{r}_\parallel-\mathbf{r}'_\parallel;z,z')$ is the static Green's tensor of the semi-infinite elastic medium bounded by a planar, stress-free surface $z=0$.

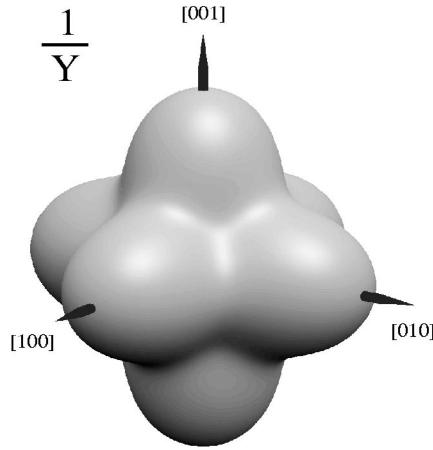

FIG. 16. Inverse Young's modulus of an elastically anisotropic cubic crystal. Typical behavior for Si, Ge, III-V, and II-VI semiconductors is shown. $1/Y$ reveals pronounced maxima, and Y has minima at elastically soft directions ⟨100⟩.

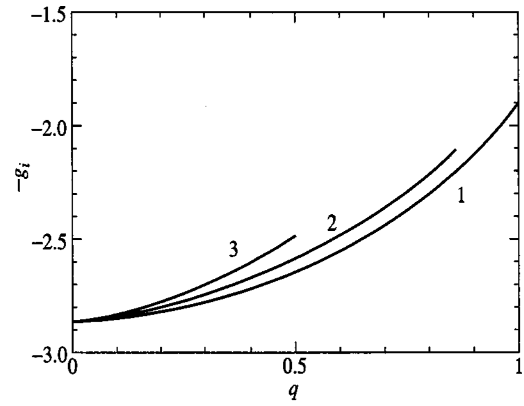

FIG. 17. The energy per unit area $\Delta E^V_{\text{elastic}}+E_{\text{interaction}}=(Q-Q')a\bar{\lambda}\varepsilon_0^2\varphi_0\times(-g_i(q))$ for different arrays of coherently strained islands vs areal coverage q: curve 1, 2D square lattice of pyramids with primitive lattice vectors (1,0,0) and (0,1,0); curve 2, 2D hexagonal lattice of pyramids with primitive lattice vectors $(-\frac{1}{2},-\sqrt{3}/2,0)$ and (1,0,0); curve 3, "checkerboard" square lattice of pyramids with primitive lattice vectors $(\sqrt{2}/2,-\sqrt{2}/2,0)$ and $(\sqrt{2}/2,\sqrt{2}/2,0)$. Curves 2 and 3 terminate at maximum possible coverages for given arrays.

To get a hint of what will be the preferred arrangement of interacting islands, we evaluate the energy (4.18) for a pair of separated islands. We take into account that Si, Ge, III-V, and II-VI semiconductors are cubic crystals with a strong elastic anisotropy. The anisotropy is illustrated in Fig. 16, where the inverse Young's modulus of a cubic crystal is plotted as a function of crystallographic direction. The general equation for $1/Y$ is given, for example, by Landau and Lifshits (1959; see the problem in Sec. 10), and particular calculations for GaAs have been carried out by Grundmann *et al.* (1995c). To evaluate Eq. (4.18), we use the Fourier transform for the static Green's tensor $\widehat{G_{\alpha\beta}}(\mathbf{k}_\parallel;z,z')$ obtained by Portz and Maradudin (1977) for elastically anisotropic cubic crystals bounded by a planar, stress-free (001) surface. We interpolate the angular dependence of the exact Green's tensor by the lowest-order angular polynomial having cubic symmetry, $B_1+B_2(8k_x^2k_y^2/k_\parallel^4-1)$, the accuracy of interpolation being less than 2%. Then we carry out a reciprocal Fourier transformation and obtain the Green's tensor in **r**-space. By integrating in Eq. (4.18) by parts, subtracting the volume elastic relaxation energy of isolated islands, retaining only the lowest-order, i.e., dipole-dipole interaction between islands, we obtain

$$\tilde{E}_{\text{interaction}}=\frac{C_0}{2\pi}V^2\frac{B_1+15B_2(1-8m_x^2m_y^2)}{R^3}, \tag{4.19}$$

where V is the island volume, R is the distance between the two islands, and $\mathbf{m}=(m_x,m_y)$ is the unit vector in the surface plane, parallel to the direction between the islands. For an elastically isotropic medium, $B_2=0$ and the interaction between far separated islands is the isotropic dipole-dipole repulsion. In systems with a strong elastic anisotropy, like most III-V and II-VI semiconductors, the dipole-dipole interaction changes its sign as a function of **m**. This results in an attraction between islands whose directions **m** are close to the elastically soft directions [100] or [010]. Therefore a very dilute array of islands will be arranged in weakly coupled chains parallel to the [100] or [010] direction where dipole-dipole attraction is balanced by higher-order (e.g., dipole-octopole) repulsion. Such an arrangement manifests itself also for a moderate areal coverage.

To discover the optimum arrangement of islands, one has to evaluate the energy from Eq. (4.18) for a number of periodic superlattices of islands on the surface. By expressing the normal vector via the surface profile gradient, $n_\alpha(\mathbf{r}_\parallel)\approx-\nabla_\alpha\zeta(\mathbf{r}_\parallel)$, one obtains the elastic energy of the array of interacting islands per one atom as a sum over the vectors of the reciprocal lattice corresponding to a given periodic array of islands,

$$\widehat{\Delta E}_{\text{elastic}}=-C_0A_0\frac{\Omega}{V}\sum_{\mathbf{K}_\parallel}|\tilde{\zeta}(\mathbf{K}_\parallel)|^2 \times K_\alpha K_\beta\widehat{G_{\alpha\beta}}(\mathbf{K}_\parallel;z,z')\Big|_{\substack{z=0\\z'=0}}. \tag{4.20}$$

Here $\tilde{\zeta}(\mathbf{K}_\parallel)$ is the Fourier transform of the surface profile $\zeta(\mathbf{r}_\parallel)$ describing the shape of the islands, A_0 is the unit cell area of the superlattice comprised of islands, V is the volume of the island, and Ω is the atomic volume.

In the paper by Shchukin, Ledentsov, *et al.* (1995), interaction energies were compared for three arrays of islands, namely, for square, hexagonal, and checkerboard arrays. A comparison of the energies for the three arrays is given in Fig. 17, which reveals that the square array is the most favorable of the three.

Later these calculations were extended and all possible superlattices were considered (Shchukin and Bimberg, 1998) having primitive translation vectors $(\mathbf{e}_1,\mathbf{e}_2)$ where $\mathbf{e}_1$ is parallel to the elastically soft direction [100], and $\mathbf{e}_2$ has an arbitrary absolute value and orientation.

The energy (4.20) yields the sum of the energy of the

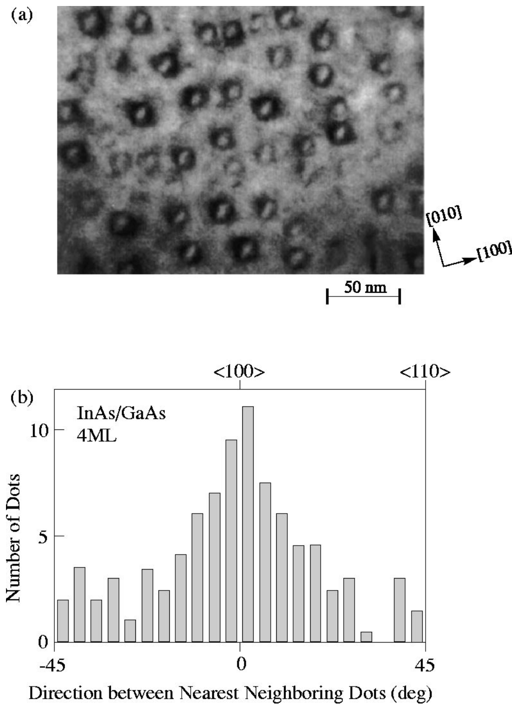

FIG. 18. Ordering of quantum dots: (a) plan-view transmission electron microscopy (TEM) micrograph of a single sheet of InAs dots grown in molecular beam epitaxy by four-monolayer deposition of InAs. Dots are preferentially aligned in rows parallel to ⟨100⟩. (b) Histogram of the direction between the nearest neighboring dots.

volume elastic relaxation of the islands and of the interaction energy between islands. Comparison of energies for different arrays has revealed the following. If the fraction q of the surface covered by islands (areal coverage) is less than 0.06, islands form a chainlike arrangement along the [100] (or [010]) direction with a weak coupling between chains. For $0.06 \leqslant q \leqslant 0.17$, the favorable arrangement is a base-centered rectangular superlattice, whose unit cell is a parallelogram with the angle between primitive lattice vectors changing from 78° for $q=0.06$ to 73° for $q=0.17$. Such an arrangement with the corresponding angle $\approx 75°$ has been observed by Ledentsov, Bimberg, *et al.* (1997). For $0.17 \leqslant q \leqslant 0.33$, the preferred arrangement is rectangular, the aspect ratio of the rectangular unit cell decreasing from 1.7 for $q=0.17$ to 1 for $q=0.33$, where the rectangle transforms into a square. For $0.33 \leqslant q \leqslant 1.0\%$, a square superlattice is the most favorable one. A perfect hexagonal superlattice with the angle 60° is never favored. Energy calculations for optimum arrays performed by Shchukin and Bimberg (1998) revealed that the difference in energies between the square array and the optimum array, if different from the square one, is considerably smaller than the difference between the checkerboard array and the square array. Therefore one may approximate the energy of the square array as the minimum energy of an array of interacting islands for any areal coverage.

Figure 18(a) shows the transmission electron micrograph of a single-sheet array of InAs quantum dots grown by molecular beam epitaxy (Bimberg *et al.*, 1995). Preferential alignment of dots in rows parallel to elastically soft ⟨100⟩ directions is visible. Figure 18(b) displays the histogram of the direction between a given dot and a nearest neighboring dot. This histogram reveals a pronounced maximum for ⟨100⟩ directions, in agreement with the above theoretical results. It should be noted that, since the interaction energy itself and, moreover, the difference in energies between different arrangement of islands, are rather small, the system of islands exhibits strong correlations only in the nearest-neighbor arrangement.

Two factors favor the square lattice. The first is the cubic anisotropy of elastic moduli of the medium, and the second is the square shape of the base of a single island.

The approximation of small tilt angles used in the present subsection does not have a significant impact on results. First, this approximation works well for the volume elastic relaxation of isolated islands, even if the tilt angle of the facets is 45°. The approximation of small tilt angles yields a volume elastic relaxation energy equal to (-64%) of the strain energy of a flat film, whereas exact calculations by the finite-element method give the elastic relaxation energy of a pyramid equal to (-60%) of the strain energy of a flat film (Shchukin, Ledentsov, *et al.*, 1996).

There is also a close similarity between the approximation of small tilt angles and the exact numerical solution for arrays of interacting islands. The elastic energy for arrays of interacting islands, obtained by the finite-element method for the tilt angle $\varphi_0 = 45°$, reveals that the cubic anisotropy of elastic moduli in this case favors a 2D square lattice of islands with primitive lattice vectors parallel to the elastically "soft" directions [100] and [010].

G. Phase diagram of 2D array of islands

The main part of the elastic interaction energy in a system of strained islands is from dipole-dipole elastic interactions. The energy per atom is proportional to $\lambda \varepsilon_0^2 \Omega (L/D)^3$ where D is the period of the lateral superlattice comprising the islands. For a square superlattice, the filling factor of the surface equals $q = L^2/D^2$, and the interaction energy per atom is equal to

$$E_{\text{interaction}} = \lambda \varepsilon_0^2 \Omega f_4(\varphi_0) q^{3/2}, \tag{4.21}$$

where $f_4(\varphi_0)$ is a geometrical factor. Due to the conditions of matter conservation, the size of the islands L and the period of the lateral superlattice D are not independent quantities. To obtain the relation between L and D, we note that $(Q-Q')$ monolayers of the deposited materials are assembled in the islands, i.e., the volume $D^2(Q-Q')a$ of the deposited material equals the volume of the island,

$$D^2(Q-Q')a = V. \tag{4.22}$$

For pyramid-shaped islands with a square $L \times L$ base and a tilt angle of the side facets φ_0, we express the

volume V in terms of L, $V=\frac{1}{6}\tan\varphi_0 L^3$. Hence the interaction energy per one atom takes the form

$$E_{\text{interaction}}=\frac{\lambda\varepsilon_0^2\Omega f_4(\varphi_0)(6\cot\varphi_0)^{3/2}[(Q-Q')a]^{3/2}}{L^{3/2}}. \tag{4.23}$$

To consider in detail L-dependent terms in the energy per one atom $E'(L)=E_{\text{dilute}}(L)+E_{\text{interaction}}(L)$, we introduce the characteristic length L_0 from Eq. (4.13) and the characteristic energy E_0 from Eq. (4.14). Then the sum of all L-dependent terms in $E(L)$ may be written as a function of the dimensionless length L/L_0:

$$E'(L)=E_0\left[-2\left(\frac{L_0}{L}\right)^2\ln\left(\frac{e^{1/2}L}{L_0}\right)+\frac{4\beta}{e^{3/4}}\left(\frac{L_0}{L}\right)^{3/2}+\frac{2\alpha}{e^{1/2}}\left(\frac{L_0}{L}\right)\right]. \tag{4.24}$$

This function is governed by two control parameters, where α is defined in Eq. (4.16) and

$$\beta=[(Q-Q')a]^{3/2}\times\frac{e^{3/4}f_4(\varphi_0)(6\cot\varphi_0)^{5/6}(\lambda\varepsilon_0)^2L_0^{1/2}}{2f_3(\varphi_0)\tau^2}. \tag{4.25}$$

The parameter β is the ratio $E_{\text{interaction}}/|\Delta E_{\text{elastic}}^{\text{edges}}|$. It increases with the amount of material $(Q-Q')$ assembled in all islands as $(Q-Q')^{3/2}$.

By seeking the minima of the energy $E'(L)$ from Eq. (4.24) for different α and β, we obtain the phase diagram of Fig. 19. For region 1 of the phase diagram, there exists an optimum island size L_{opt}, corresponding to the absolute minimum of the energy, $\min E'(L)\equiv E'(L_{\text{opt}})<0$. On the other hand, the ripening of islands would correspond to $L\to\infty$, where the energy $E'(L)\to 0$. This means that a 2D periodic square lattice of islands of the optimum size L_{opt} is a stable array, and islands do not undergo ripening. For region 2 of the phase diagram, there exists only a local minimum of the energy, corresponding to a metastable array where $E'(L')>0$. For region 3, the local minimum in the energy $E'(L)$ disappears. In both regions 2 and 3, there is a thermodynamic tendency towards ripening. If the system initially corresponds to region 1, and the amount of the deposited material Q increases, then the point in the phase diagram moves to regions 2 and 3, and islands undergo ripening.

If $\alpha\leqslant 0$, there exists an absolute minimum of the energy $E'(L)$ for an arbitrary value of β, and $\min E'\equiv E'(L_{\text{opt}})<0$. Besides the absolute minimum of $E'(L)$, there may also exist a local minimum at $L=L'$, where the energy of a corresponding metastable state is $E'(L')<0$ in region 4 and $E'(L')>0$ in region 5; and no metastable state exists in region 6. The same phase diagram, given in the paper by Shchukin, Ledentsov, *et al.* (1995), unfortunately, contains an error. Figure 19 of the present paper gives the correct phase diagram.

To estimate characteristic values of α and β, we substitute $\tau\approx 100$ meV/Å^2, $\lambda\approx 500$ meV/Å^3, $L_0\approx 100$ Å, and

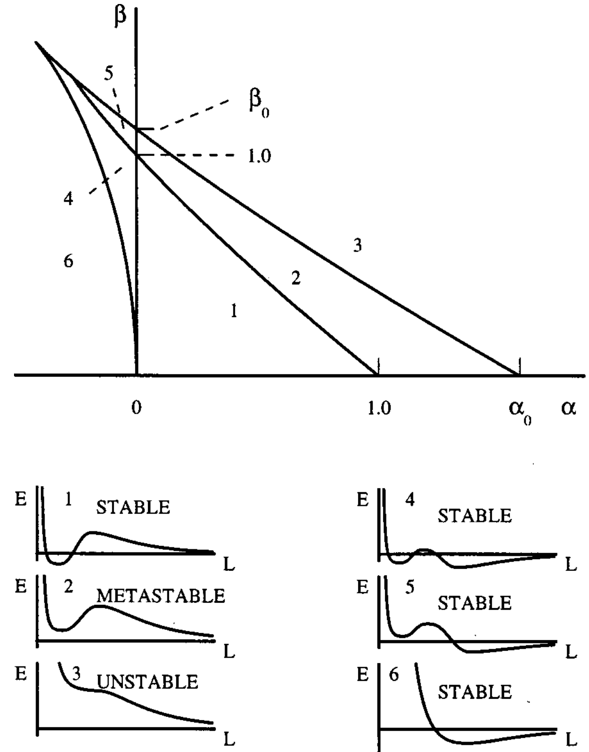

FIG. 19. Phase diagram of the stability of a square lattice of coherently strained islands in the plane of control parameters $\alpha-\beta$. Here α and β are defined in Eqs. (4.16) and (4.25). In the lower part of the figure, the energy of the interacting array of islands vs their size is plotted, with plots corresponding to different regions of the phase diagram. In regions 1, 4, 5, and 6, there exist stable arrays of islands which do not undergo ripening. In regions 2 and 3, all arrays of islands undergo ripening. $\alpha_0=2e^{-1/2}\approx 1.213$; $\beta_0=(4/3)e^{-1/4}\approx 1.038$.

$a=3$ Å into Eq. (4.25). This gives $\beta\approx 1$ for $|\varepsilon_0|\approx 1\%$ and $(Q-Q')=0.5$ monolayers. Therefore, if $\alpha>0$, the array of islands may correspond to region 1 of the phase diagram only for small values of $(Q-Q')$. It was argued in Sec. IV.E that the parameter α for an InAs/GaAs(001) system is very likely to be negative. If $\alpha<0$, then the increase of $|\varepsilon_0|$, e.g., by the increase of x for the heteroepitaxial system $In_xGa_{1-x}As$/GaAs(001), results in the decrease of L_{opt}. This agrees with the experimental data of Ledentsov, Grundmann, *et al.* (1994).

The key difference between arrays of three-dimensional coherently strained islands and periodically faceted surfaces or periodic structures of surface domains is the existence of both an ordering regime and a ripening regime, where a possible transition between these two regimes is governed by the surface energy of island facets.

For III-V semiconductor systems, it is possible to tune surface energies experimentally by varying the pressure of group-V element(s) in the vapor. It is known (see, for example, Qian *et al.*, 1988; Moll *et al.*, 1996) that the stoichiometry of the (001) surface of GaAs and, correspondingly, the surface energy depend strongly on the arsenic pressure in the vapor. This tendency should be rather general for all III-V systems, including the InAs

wetting layer on GaAs(001). Therefore one might expect that variation in arsenic pressure could drive the system from the regime of size-ordered islands to the regime of Ostwald ripening. Such a phase transition, driven by As pressure, has been observed experimentally by Ledentsov, Grundmann *et al.* (1996). This transition will be discussed below, in Sec. IV.L.3.

H. Equilibrium thickness of the wetting layer

The above analysis of Secs. IV.E–IV.G, following the paper of Shchukin, Ledentsov, *et al.* (1995) reveals the equilibrium structure of an array of 3D coherently strained islands under the constraint of a fixed amount of material assembled in the islands. The treatment is based only on the scaling behavior of various contributions to the total energy, and leads to a criterion for whether Ostwald ripening occurs or optimum-sized coherent islands form.

A more profound understanding of the equilibrium morphology of the system can be achieved if one takes into account the existence of the wetting layer. A common experiment on growth interruption implies a fixed amount of deposited material, which is distributed between the wetting layer and 3D islands. Therefore neither the thickness of the wetting layer nor the total volume of all islands are fixed separately. To determine each of these quantities, one has to assume a certain microscopic model for the dependence of the energy of the wetting layer W on its thickness Q'. Such a model was introduced by Daruka and Barabási (1997). The energy per atom of a thick epitaxial film coherent to the substrate is given by $\lambda\varepsilon_0^2\Omega-\Phi_{22}$, where $-\Phi_{22}$ is the energy of chemical bonds in the bulk of the deposited material 2, defined per atom. At the wetting layer-substrate interface, chemical bonds between the substrate atoms and the film atoms have the energy $-\Phi_{12}$ such that $\Delta=\Phi_{22}-\Phi_{12}<0$ (wetting condition). Due to the finite range of intermolecular interactions, the binding energies of the atoms in the second and successive monolayers of the film are also modified: as we move away from the substrate, the binding energy density increases from $-\Phi_{12}$ in the first monolayer to its asymptotic value $-\Phi_{22}$. These intermolecular forces are responsible for a critical layer thickness larger than one monolayer (Tersoff, 1991; Roland and Gilmer, 1993). A model of the wetting layer energy proposed by Daruka and Barabási (1997) takes this effect into account. The explicit form of the energy is

$$W(Q')=\int_0^{Q'}d\tilde{q}\left\{-\Phi_{22}+\Delta\left[\vartheta(1-\tilde{q})+\vartheta(\tilde{q}-1)\exp\left(-\frac{\tilde{q}-1}{\tilde{a}}\right)\right]\right\}. \qquad (4.26)$$

Here $\vartheta(x)=1$ if $x\geqslant 0$, $\vartheta(x)=0$ if $x<0$, and $\tilde{a}$ is the characteristic attenuation length of interatomic interaction.

By substituting $W(Q')$ from Eq. (4.26) into Eq. (4.3), it is possible, in principle, to find the optimum thickness of the wetting layer as a function of the total amount of deposited material Q. It follows from Eq. (4.3) that the formation of coherently strained islands leads to a decrease in the total energy, the decrease being a linear function of $(Q-Q')$. At the same time, the elastic repulsion between islands defined per unit surface area is proportional to $(Q-Q')^{5/2}$ [the last term in Eq. (4.3)] which exhibits a steep increase with Q at sufficiently large Q and hinders the formation of a dense array of islands. To take this effect into account, Daruka and Barabási (1997) considered the possible coexistence of small islands of optimum size L_{opt} and of "ripened" islands considerably larger than L_{opt}. The total energy *per unit cell* of the substrate is

$$E=E_{\mathrm{WL}}(Q_1)+Q_2E_{\mathrm{island}}(Q_2)+(Q-Q_1-Q_2)E_{\mathrm{rip}}. \qquad (4.27)$$

Here the energy of the wetting layer equals $E_{\mathrm{WL}}(Q_1)=\lambda\varepsilon_0^2Q_1+W(Q_1)$, where $W(Q_1)$ is given by Eq. (4.26). Equation (4.27) implies that Q monolayers of material 2 are deposited, Q_1 monolayers form the wetting layer, Q_2 monolayers are assembled in 3D coherently strained islands of a given pyramidlike shape and volume, and the rest of the material 2, namely, $(Q-Q_1-Q_2)$ monolayers, is assembled in ripened islands. The energy of 3D pyramids per atom equals $E_{\mathrm{island}}=[1-f_1(\varphi_0)]\lambda\varepsilon_0^2\Omega-\Phi_{22}+E'(L)$, where the $f_1(\varphi_0)$ is the geometrical factor describing the volume elastic relaxation [see Eq. (4.9)], and $E'(L)$ is defined in Eq. (4.24). Hence the energy of "ripened" islands can be obtained if one takes the limit $L\to\infty$, $E_{rip}=[1-f_1(\varphi_0)]\lambda\varepsilon_0^2\Omega-\Phi_{22}$.

Equation (4.27) defines the total energy of the wetting layer and 3D pyramidal islands, where the latter may exhibit *bimodal behavior*, i.e., both small islands of size L_{opt} and large islands considerably larger than L_{opt} may be present in the system. By minimizing the energy from Eq. (4.27) with respect to Q_1 and Q_2, Daruka and Barabási (1997) obtained the equilibrium phase diagram of a lattice-mismatched heteroepitaxial system as a function of the lattice mismatch ε_0 and of the total amount of the deposited material Q. The domains of the phase diagram in Fig. 20 correspond to the following physical situations:

FM phase: The deposited material contributes to the pseudomorphic growth of the wetting layer, and 3D islands are absent, reminiscent of the Frank-van der Merwe (FM; Frank and Van der Merwe, 1949) growth mode. The total energy has its minima at $Q_2=0$ and $Q_1=Q$, indicating that the thickness of the wetting layer coincides with the nominal thickness of the deposited material Q.

R_1 phase: Above a certain value of $Q_{c1}(\varepsilon_0)$, the total energy has new minima at $Q_2=0$ and $0<Q_1<Q$. This implies that after formation of a wetting layer, the excess material contributes to the formation of ripened islands. These ripened islands, being infinitely large, have zero areal density.

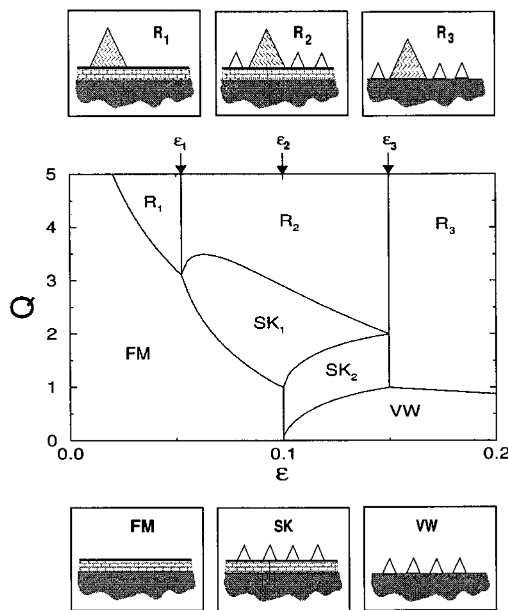

FIG. 20. Equilibrium phase diagram of a lattice-mismatched heteroepitaxial system as a function of the total amount of deposited material Q and the lattice mismatch ε_0. The small panels on the top and bottom illustrate the morphology of the surface in the six growth modes described in the text. The small empty triangles indicate the presence of stable islands, while the large shaded ones refer to ripened islands. From Daruka and Barabási (1997) with the kind permission of the authors.

SK_1 phase: The total energy develops new minima at nonzero Q_1 and Q_2 such that $Q_1+Q_2=Q$, i.e., the deposited material (Q monolayers) is distributed between Q_1 monolayers of the wetting layer, and finite islands accumulating Q_2 monolayers of the deposited material, similar to the Stranski-Krastanow growth mode. It should be noted that with an increase in the total amount of deposited material Q, the thickness of the wetting layer Q_1 continues to grow sublinearly. This is the consequence of island-island repulsive interactions: in the dilute system limit, the wetting layer thickness is constant.

R_2 phase: In this phase, the total energy has minima at $0<Q_1<Q$ and $0<Q_2<Q$, indicating that the deposited material is distributed between a wetting layer, finite islands, and ripened islands. The finite islands formed in the SK_1 phase will be preserved, being stable against ripening. Thus finite and ripened islands coexist in the R_2 phase.

VW phase: For large mismatch and for small coverages, the total energy has its minima at $Q_2=Q$ and $Q_1=0$, indicating that all deposited material is accumulated in finite islands. Due to large mismatch, the wetting layer is absent and the islands are formed directly on the substrate, similar to the Volmer-Weber (VW; Volmer and Weber, 1926) growth mode.

SK_2 phase: By increasing Q, we reach the SK_2 phase. The behavior of the system is different from the SK_1 growth mode. For a given ε_0, islands are already formed in the VW phase. In the SK_2 phase, the island density and island size remain unchanged, and a wetting layer starts forming until its thickness reaches 1 monolayer, at which point we enter the SK_1 phase.

R_3 phase: The total energy has its minima at $Q_1=0$ and $0<Q_2<Q$, indicating the formation of ripened islands. Finite islands formed in the VW mode are preserved, and coexist with ripened islands. However, in contrast to the R_2 phase, the wetting layer is absent.

Thus the papers of Shchukin, Ledentsov, *et al.* (1995) and Daruka and Barabási (1997) solve the theoretical problem of the equilibrium state of a lattice-mismatched heteroepitaxial system.

I. Two exact theorems on shape-versus-volume dependence for 3D islands

The thermodynamic theories developed by Shchukin, Ledentsov, *et al.* (1995c, 1996, 1997) and by Daruka and Barabási (1997) and presented in Secs. IV.E–IV.H above are based on the approximation of a fixed shape of a single island. These theories reveal that, in a certain parameter range, the equilibrium state of a lattice-mismatched system is an ordered array of 3D coherently strained islands, and Ostwald ripening does not occur. On the other hand, Duport *et al.* (1997), and Spencer and Tersoff (1997) have pointed out that the equilibrium shape of a sufficiently large coherent island is an overhanging ball nearly detached from the substrate or from the wetting layer. Since such islands are totally relaxed, these authors concluded that equilibrium always corresponds to a single overhanging island formed as a result of ripening.

In the present subsection we show that, despite the possible existence of totally relaxed overhanging islands (or totally relaxed dislocated islands), there is, nevertheless, a parameter region where equilibrium corresponds to an ordered array of 3D coherently strained islands, and ripening is not favored energetically. The transition from a dense array of 3D coherent, partially relaxed islands over a wetting layer to a single overhanging, totally relaxed island is accompanied, first, by a reduction in the strain energy and, secondly, by a change in the surface energy. When the surface energy of the wetting layer is higher than the surface energies of the island facets, the disappearance of islands implies an increase in the total surface energy. If the amount of deposited material is not too large, the above-mentioned increase in surface energy can outweigh the reduction in the strain energy, and the formation of a single island via ripening will not be favored energetically.

In order to show this, we take into account the dependence of an island's shape on its volume and discuss how this can affect the conclusions of Secs. IV.E–IV.H. The dependence of the equilibrium shape of a 3D coherently strained island on its volume has been obtained, under certain model assumptions about facet energies, by Kaminski and Suris (1996), by Chen *et al.* (1997), by Duport *et al.* (1997), and by Spencer and Tersoff (1997) and, from *ab initio* calculations of surface energies, by

Pehlke *et al.* (1996). Unlike the equilibrium shape of unstrained crystals, for which exact theorems have been formulated and proved by Wulff (1901) and Herring (1951a), there is still a lack of theorems concerning the shapes of strained islands. Here we shall formulate and prove two exact theorems. Since the main concern of this subsection is the existence of an optimum volume of the island versus ripening, we shall consider the energy per one atom of the material in the islands.

If, in the energy of a single island, we retain only the elastic strain energy and the surface energy, i.e., the first and the second terms in Eq. (4.9), and express the energy in terms of the island volume and island shape, we obtain the energy per atom as

$$E=\Omega\left[\lambda\varepsilon_0^2 R+\frac{(\Delta\Gamma)}{V^{1/3}}\right]. \qquad (4.28)$$

Unlike Eq. (4.9), which gives the change in the energy due to formation of a 3D island from a uniformly strained flat film, Eq. (4.28) gives the energy of an island itself. Here the shape-dependent coefficient R ($0\leqslant R\leqslant 1$), determined by the volume elastic relaxation, is related to f_1 from Eq. (4.9) as $R=1-f_1$. The shape-dependent coefficient $(\Delta\Gamma)$ includes effects due to the appearance of side facets and, eventually, of the top facet, disappearance of a certain area of the wetting layer underneath the island, and strain-induced renormalization of the surface energies. Since the optimum shape of the island depends on the island's volume, the coefficients $R=R_{\mathrm{opt}}$ and $(\Delta\Gamma)=(\Delta\Gamma)_{\mathrm{opt}}$ depend on volume, too.

Theorem 1. For the optimum shape of a 3D coherently strained island, the coefficient $R=R_{opt}$ in Eq. (4.28) is a non-increasing function of the island volume V, and the coefficient $(\Delta\Gamma)=(\Delta\Gamma)_{opt}$ is a non-decreasing function of the island volume.

This theorem is, in fact, intuitively clear. Its validity has been demonstrated on several particular examples, e.g., by Kaminski and Suris (1996), by Pehlke *et al.* (1996), and by Duport *et al.* (1997). However, to the best of our knowledge, no strict proof of the general statement has been given in literature so far. We give this proof here.

Proof. Let an island of volume V_1 have an equilibrium shape 1, where the corresponding coefficients are $R=R_1$ and $(\Delta\Gamma)=(\Delta\Gamma)_1$. For an island of volume V_2, let the corresponding coefficients be R_2 and $(\Delta\Gamma)_2$. For an island of the volume V_1, the minimum energy is achieved by the shape 1. Islands of any other shape, in particular, of shape 2, have larger energy. Hence

$$\lambda\varepsilon_0^2 R_2+\frac{(\Delta\Gamma)_2}{V_1^{1/3}}\geqslant\lambda\varepsilon_0^2 R_1+\frac{(\Delta\Gamma)_1}{V_1^{1/3}}. \qquad (4.29)$$

A similar consideration of islands of volume V_2 yields

$$\lambda\varepsilon_0^2 R_1+\frac{(\Delta\Gamma)_1}{V_2^{1/3}}\geqslant\lambda\varepsilon_0^2 R_2+\frac{(\Delta\Gamma)_2}{V_2^{1/3}}. \qquad (4.30)$$

Now let us, in Eqs. (4.29) and (4.30), put the combination (R_1-R_2) on one side of the inequality, and the

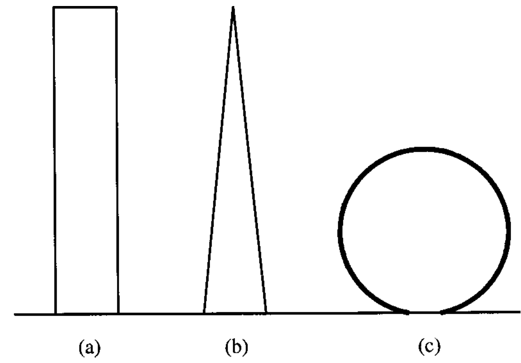

FIG. 21. Sample shapes of coherent islands having asymptotically small elastic energy, i.e., $R\to 0$: (a) vertical prism; (b) vertical pyramid; (c) overhanging island.

combination $[(\Delta\Gamma)_2-(\Delta\Gamma)_1]$ on the other side of the inequality. This procedure yields a double inequality,

$$\frac{(\Delta\Gamma)_2-(\Delta\Gamma)_1}{V_2^{1/3}}\leqslant\lambda\varepsilon_0^2(R_1-R_2)\leqslant\frac{(\Delta\Gamma)_2-(\Delta\Gamma)_1}{V_1^{1/3}}. \qquad (4.31)$$

For concreteness, let $(R_1-R_2)\geqslant 0$. Then, from the right inequality of (4.31), it follows that $(\Delta\Gamma)_2-(\Delta\Gamma)_1\geqslant 0$. Comparison of the left and right parts of the double inequality (4.31) yields $V_2\geqslant V_1$. A similar consideration shows that, for $(R_1-R_2)<0$, one obtains $(\Delta\Gamma)_2-(\Delta\Gamma)_1<0$ and $V_2<V_1$. The theorem is proven.

One should keep in mind that the proof of the above theorem is based on the assumption that, for a given volume of the material, the island chooses its optimum shape from *all possible shapes*. This assumption is no longer valid if the discrete nature of the material becomes important. For example, the height of the islands cannot be less than one monolayer. The latter is important for sufficiently small island volume V, where islands are two dimensional.

As the volume increases, the equilibrium shape becomes three dimensional, and the above theorem applies. In particular, the coefficient R decreases. As the island volume tends to infinity, the coefficient R tends asymptotically to zero. Such behavior is realized, for example, by the island shapes given in Fig. 21. For all islands in Fig. 21, the elastic energy is concentrated in a small volume in the island and in the substrate in the vicinity of the interface. In Eq. (4.10) where the quantity $(\Delta\Gamma)$ is defined, the first term, i.e., the positive surface energy of the island surface, dominates due to a large side surface of the island. Therefore $(\Delta\Gamma)$ is always positive for sufficiently large islands.

To discuss the possible dependence of the energy per atom on the island's volume, we shall differentiate (4.28) over V. We have to take into account that there are two contributions to the change of E with the island volume. The first contribution comes from the fact that the larger the volume, the smaller the fraction of atoms that are surface atoms. This corresponds to the factor $V^{-1/3}$ in the second term in Eq. (4.28). The second contribution comes from the change in the island shape versus volume. This corresponds to the dependence of R and $(\Delta\Gamma)$

in Eq. (4.28) on volume. In the derivative dE/dV these two contributions enter as

$$\frac{dE}{dV}=\frac{\partial E}{\partial V}\bigg|_{\mathcal{G}=\mathcal{G}_{\text{opt}}}+\frac{d\mathcal{G}}{dV}\frac{\partial E}{\partial \mathcal{G}}\bigg|_{V=\text{const}}. \tag{4.32}$$

Here $\mathcal{G}$ denotes the set of variables that define the island's shape. For example, for truncated square-based pyramids these are the facet tilt angle and the level of truncation. The definition of the optimum shape reads that $\partial E/\partial \mathcal{G}=0$. Hence

$$\frac{dE}{dV}=\frac{\partial E}{\partial V}\bigg|_{\mathcal{G}=\text{const}}=-\frac{1}{3}\,\Omega\,\frac{(\Delta\Gamma)_{\text{opt}}}{V^{4/3}}. \tag{4.33}$$

It follows from Eq. (4.33) that if, for a given volume V of the island, $(\Delta\Gamma)_{\text{opt}}>0$, then the energy per atom is a locally decreasing function of the volume. Alternatively, if, for a given volume V, $(\Delta\Gamma)_{\text{opt}}<0$, then the energy per atom is a locally increasing function of the volume. Since $(\Delta\Gamma)_{\text{opt}}$ is an increasing function of the island volume (see Theorem 1), it is either positive for all volumes or it changes sign once. From the behavior of $(\Delta\Gamma)_{\text{opt}}$ one can reveal the possible dependence of the energy per atom on volume. Figures 22(a), (b), and (c) demonstrates three possible behaviors of the energy per atom versus island volume for a dilute array of islands.

For small volumes, islands are either two dimensional or form a dense array of 3D interacting islands, and the above approximation of a dilute array of 3D islands does not apply. Therefore the behavior of the energy at small volumes is not shown.

If $(\Delta\Gamma)_{\text{opt}}>0$ for all volumes [Fig. 22(a)], then the energy per atom decreases monotonically with the island volume. The minimum energy corresponds to $V\rightarrow\infty$, i.e., to Ostwald ripening. If, for some volume $(\Delta\Gamma)_{\text{opt}}<0$, then there are two possibilities. Figure 22(b) is related to the situation in which the absolute minimum still corresponds to $V\rightarrow\infty$, i.e., to Ostwald ripening. However, there exists a local minimum for small volumes. This local minimum corresponds either to 2D islands or to a dense array of 3D islands. In Fig. 22(c), the absolute minimum is attained either by 2D islands or by a dense array of 3D islands.

An analysis of the behavior of the energy per atom versus island volume gives us a proof of the following theorem:

Theorem 2. If, for some island volume, $(\Delta\Gamma)_{\text{opt}}<0$, then there exists a stable or a metastable array of islands of a finite optimum volume.

For a dense array of islands, it is necessary to take into account the island-island elastic interaction. As was shown in Sec. IV.F, this interaction can be attractive only at a very small surface coverage ($<1\%$) and is otherwise repulsive. The interaction energy per atom in the islands depends on the island volume as $E_{\text{interaction}}\sim C(\mathcal{G})(Q-Q')^{3/2}V^{-1/2}$ where the coefficient $C(\mathcal{G})$ depends on the island shape. Therefore, for a given volume of the island, the optimum shape depends on the total amount of material in all islands $(Q-Q')$. Such a dependence manifests itself in experiment (Floro *et al.*, 1998). Thus, for GeSi/Si(001) islands, the shape transition from a pyramid bounded by {105} facets to a dome bounded by steeper {113} facets occurs in dense arrays for a smaller volume of islands than in dilute arrays.

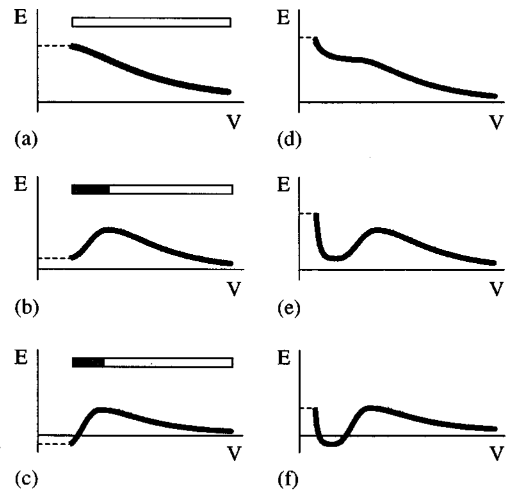

FIG. 22. The energy per atom for an array of 3D islands vs the volume of the islands, $E(V)$. If the amount of material in all islands is less than one monolayer, islands of small volumes are two-dimensional. If the amount of material in all islands exceeds one monolayer, islands of a certain volume cover 100% of the surface, and islands of smaller volumes cannot exist. In all graphs, a dashed line plotted in the region of small volumes implies that the real dependence $E(V)$ is not considered for such volumes. (a)–(c). An approximation of a dilute array of noninteracting 3D islands. White bars in the insets correspond to island volumes $(\Delta\Gamma)_{\text{opt}}>0$. Dark bars correspond to $(\Delta\Gamma)_{\text{opt}}<0$: (a) $(\Delta\Gamma)_{\text{opt}}>0$ for all volumes. The stable state corresponds to a single huge island formed via Ostwald ripening; (b) $(\Delta\Gamma)_{\text{opt}}<0$ for some volumes. The stable state corresponds to a single huge island formed via Ostwald ripening. A metastable state exists, corresponding to an array of finite islands of an optimum volume; (c) $(\Delta\Gamma)_{\text{opt}}<0$ for some volumes. The stable state corresponds to an array of finite islands. Ostwald ripening is not favored energetically and will not occur. (d)–(f) an approximation of an array of interacting 3D islands; (d) The stable state corresponds to a single huge island formed via Ostwald ripening; (e) the stable state corresponds to a single huge island formed via Ostwald ripening. A metastable state exists, corresponding to an array of finite 3D islands of optimum volume; (f) the stable state corresponds to an array of finite 3D islands of optimum volume. Ostwald ripening is not favored energetically and will not occur.

Two factors govern the effect of island-island interaction on the variation of the energy per atom with island volume $E(V)$. First, this energy is a repulsive one. Second, it decreases with island volume. A quantitative analysis, based on a particular model of island will be published elsewhere (Shchukin and Bimberg, 1999). However, qualitatively, the effect of island-island interaction can be understood, if one adds to the curves of Figs. 22(a)–22(c) a positive decreasing function. Then, if $(\Delta\Gamma)_{\text{opt}}>0$ for all island volumes, the tendency towards Ostwald ripening remains unchanged [Fig. 22(d)]. If $(\Delta\Gamma)_{\text{opt}}<0$ for some volume, then the local minimum in

Fig. 22(b) is shifted to larger volumes [Fig. 22(e)]. The same is valid for the absolute minimum of energy in Fig. 22(c), which is shifted to larger volumes [Fig. 22(f)]. This shift means that the stable [Fig. 22(f)] or a metastable [Fig. 22(e)] state of the system corresponds not to an array of 2D islands, but to an array of 3D islands. For a sufficiently large amount of material assembled in all islands, the local minimum in Fig. 22(e) or the absolute minimum in Fig. 22(f) will disappear, and the islands will undergo ripening.

We note that elastic relaxation due to island edges, which has not been considered in this subsection, also contributes to the creation of a local or an absolute minimum on the curve $E(V)$ and hinders the tendency towards ripening.

Summing up the discussion of this section, we emphasize the main effect of the shape-versus-volume dependence for 3D coherently strained islands. The parameter region where the absolute minimum of the total energy corresponds to an ordered array of 3D islands is narrower than that obtained in Sec. IV.G. Otherwise, an ordered array of 3D islands would no longer be a stable state, but rather a metastable one. It is worth noting that this metastable state has nothing to do with the self-limiting kinetics of island growth. This metastable state is determined by energetic arguments only, i.e., by a local minimum in the dependence of the energy per atom versus island volume. On a rather long time scale, no difference between the situations of Figs. 22(e) and 22(f) can be observed in experiment. Such metastable arrays behave like stable ones, including the reversibility of the 2D-to-3D morphology transition, the control of the island volume by vapor pressure of the group V element, etc. In this sense, both the above-described metastable array and a stable array are *thermodynamically controlled*. Below, in Sec. IV.L we shall focus on key experiments that allow us to distinguish thermodynamically controlled arrays from kinetically controlled ones.

J. Kinetic theories of ordering

The kinetic approach is a basic one in the theoretical description of crystal growth. The importance of strain effects in the kinetics of growth has been recognized for a number of growth-related phenomena. Thus the step-flow growth of a material lattice-mismatched to the substrate results in the step's bunching (Tersoff *et al.*, 1995). The step-flow growth of an alloy can be unstable either against vertical modulation of composition due to stress induced by step bunching (Tersoff, 1996), or against lateral modulation of composition due to stress induced by "frozen" fluctuation of composition (Ipatova *et al.*, 1998).

In this connection, it is necessary to distinguish two types of kinetics. The most common situation (that described above) corresponds to the kinetics in an open crystal growth system where a deposition is present and where the deposition of atoms proceeds simultaneously with the evolution of a surface nanostructure. A steady-state structure, if one exists, does not correspond to equilibrium, but is determined by the particular growth kinetics.

Another type of kinetics is that in a closed system. This is realized upon growth interruption or annealing, where the total amount of deposited material is preserved provided the evaporation is negligibly small. The kinetic evolution pathway of the nanostructure leads towards thermodynamic equilibrium.

One should keep in mind the importance of kinetic effects even in closed systems. First, thermodynamic equilibrium relies on elementary kinetic processes in a detailed balance. Secondly, it is possible to emphasize kinetic effects in the formation of 3D coherently strained islands by rapid freezing of a certain configuration, e. g., by cooling down or burying the structure underneath a cap layer before it can reach thermodynamic equilibrium.

All debates on whether the narrow size distribution of 3D islands or the absence of Ostwald ripening have a thermodynamic or a kinetic origin are relevant only if a closed system is considered and the system is subject to annealing or growth interruption, i.e., is allowed to equilibrate.

Several kinetic models of 3D island formation and of ordering have been proposed (Chen *et al.*, 1995; Madhukar *et al.*, 1995; Chen and Washburn, 1996; Barabási, 1997; Dobbs *et al.*, 1997; Jesson *et al.*, 1998). Such models take into account microscopic processes on the crystal surface like deposition, diffusion, attachment to islands, and detachment from islands.

Dobbs *et al.* (1997) formulated a mean-field theory for the density of adatoms in 2D and 3D islands, attempting to explain data from Seifert *et al.* (1996). Three-dimensional islands, as soon as they nucleate, act as traps for adatoms and atoms detaching from flat 2D islands. The increase in the density of 3D islands with increasing deposition of material is steep and saturates quickly. After this, additional material leads to no further increase in island density, but to an increase in the size of 3D islands. This model might be adequate for the initial stages of 3D island formation but does not predict any favored island size or narrow size distribution.

Madhukar *et al.* (1995) and Chen and Washburn (1996) pointed out the influence of strain fields created by islands on the motion of adatoms. Inhomogeneous strain fields in the vicinity of 3D islands act as repulsive forces, leading to the drift of adatoms away from existing islands and thus increasing the nucleation rate of new islands. In addition, smaller islands grow more rapidly than larger ones. Thus the above effects tend to equalize the sizes of the islands. Barabási (1997) has established a one-dimensional model using a Monte Carlo method including strain relaxation of the lattice at each step. This model takes into account the above impact of island-induced strain fields on the motion of adatoms, and eventually leads to a narrow size distribution for sufficiently large mismatch ($>5\%$). Increasing deposition leads mainly to a higher density of islands of the same size.

Chen *et al.* (1995) and Jesson *et al.* (1998) emphasized the importance of nucleation of every new atomic layer in the growth of faceted islands. If an island has a shape with smooth facets which do not contain any steps or kinks, a new layer starts to nucleate at the edge between the island facet and the substrate, i.e., in a highly strained area. Strain provides a barrier for such nucleation, and the height of the barrier is larger for larger islands. This leads to self-limited growth and may result in a narrow size distribution.

All of the above-mentioned kinetic theories imply that, in a system of 3D coherently strained islands, there is always a thermodynamic tendency towards Ostwald ripening but that it does not occur on an experimentally available time scale due to various kinds of strain-induced barriers. Such models seem to be relevant to particular experiments. However, as we shall emphasize below in Sec. IV.L, there are experimental data on InAs/GaAs and GaInAs/GaAs islands which cannot be explained via kinetic concepts. First, these are the data on the reversible 3D-to-2D phase transition driven by changes in As pressure for MBE-grown InAs/GaAs islands or by replacing of AsH_3 by PH_3 for MOVPE-grown InGaAs/GaAs islands. Second, these are the data on the irreversible transition from an ordered array of 3D islands to ripening driven by the increase of As pressure. At the same time, these observations agree well with the thermodynamic theory of island formation.

K. Experimental techniques

Experimental studies of spontaneous morphological transformation effects on crystal surfaces using scanning tunneling microscopy (STM), atomic force microscopy (AFM), and transmission electron microscopy (TEM) have attracted a great deal of interest in modern solid-state physics.[1]

The primary methods for structural characterization can be divided into *direct imaging* methods such as scanning tunneling microscopy, atomic force microscopy (Güntherodt and Wiesendanger, 1994), and transmission electron microscopy (Reimer, 1984; Cerva and Oppolzer, 1990; Ourmazd *et al.*, 1990; Bimberg *et al.*, 1992; Neumann *et al.*, 1996); and *diffraction* methods such as reflective high-energy electron diffraction (RHEED; Joyce *et al.*, 1984; Larsen and Dobson, 1988) its ellipsometric equivalent, reflectance anisotropy spectroscopy (RAS; Aspnes, 1985; Richter and Zahn, 1996), and x-ray diffraction (Bartels and Nijman, 1978; Tapfer and Ploog, 1986; Segmüller *et al.*, 1989; Krost *et al.*, 1996).

[1]These studies include those of Goldstein *et al.*, 1985; Glas *et al.*, 1987; Mo *et al.*, 1989, 1990; Guha *et al.*, 1990; Snyder *et al.*, 1991; Leonard *et al.*, 1993; Bressler-Hill *et al.*, 1994; 1995; Moison *et al.*, 1994; Nötzel *et al.*, 1994; Cirlin *et al.*, 1995; Guryanov *et al.*, 1995; Ruvimov *et al.*, 1995; Häusler *et al.*, 1996; Jeppesen *et al.*, 1996; Kurtenbach *et al.*, 1995; Kobayashi *et al.*, 1996; Ledentsov, Grundmann, *et al.*, 1996; Ngo *et al.*, 1996; Nötzel, 1996).

We emphasize that none of these techniques is superior to the others. In this section we discuss advantages and disadvantages of each of the techniques.

1. Direct imaging methods

Scanning tunneling microscopy has the advantage of revealing directly the morphology of a surface on an atomic level and permitting manipulation of surface atoms, e.g., creating lines and figures on the surface. With respect to the formation of 3D islands (quantum dots, or QDs) STM has proven to be very successful (see, for example, Mo *et al.*, 1990). In this method, the tunneling current and voltage between the surface and the ultrasharp metal microscope tip are measured as a function of the tip position. Atomic force microscopy has, in principle, atomic resolution. Typically, a lateral resolution of a few nm and a much finer z resolution of 0.1 nm is achieved. The actual resolution depends on the specific size and shape of the tip. Tip effects can modify slightly the apparent height and to a large extent the lateral size of the islands. STM and AFM deliver a convolution of the island geometry with the tip-surface interaction function. Therefore STM and AFM are suitable for determining only heights and positions (densities) of islands, but not the shape of islands. Moreover, plan-view scanning tunneling techniques usually cannot distinguish between coherent and dislocated islands, unless dislocations extend to the surface.

One should keep in mind that STM and AFM plan-view measurements of uncovered islands are not usually performed at growth temperature. The sample is first cooled down and then subject to STM or AFM studies. The surface morphology actually investigated can thus be completely different from that directly after growth. For example, the lateral size, facet angle, and density of 3D islands in an InAs/GaAs(001) system have all been shown to depend on particular growth conditions like growth temperature (Ledentsov, Grundmann, *et al.*, 1996). At the same time, the disappearance of InAs 3D islands has been reported due to switching off of the arsenic flux and deposition of only 0.15 monolayer of pure indium (for details, see Sec. IV.L.3). These examples demonstrate that the surface kinetics is sufficiently fast to result in severe modifications of dot size and density due to changes in growth conditions. In view of these results, the question arises for any particular system, whether the surface morphology does or does not change upon cooling down. To answer this question, it is important to establish under which conditions the surface morphology is the same after cooling as it is during growth. A straightforward experimental option is to investigate how the surface morphology measured in STM or AFM depends on the rate of cooling. It would be worthwhile to perform such a study for any materials system. However, to the best of our knowledge, no such studies have been reported in the literature so far.

Problems connected with the cooling of a sample are not encountered if STM cross-section experiments are performed on covered samples (Wu *et al.*, 1997).

Most of the problems mentioned can be solved by using transmission electron microscopy and, particularly, high-resolution electron microscopy (HREM), which provides information about covered islands. In most cases islands are covered by the substrate material, forming inclusions of material 2 (quantum dots) in the matrix of material 1. The shape and the size of quantum dots can be obtained with the high accuracy, and this technique provides reliable information about their coherent or incoherent nature (Ruvimov *et al.*, 1995). The particular importance of TEM is related to the fact that most applications of quantum dots require covered dots, and the covered dots are the ones whose shape and size should be optimized for device applications.

There exist however, certain problems related to TEM and HREM. These techniques are time consuming, and real shape of the quantum dots is affected by strain fields. However, the problem of strain contrast in TEM is at present solved to a major extent.

Ruvimov and Scheerschmidt (1995) have carried out molecular dynamic modeling to check visualization of coherently strained nanometer-scale InAs islands (QDs) embedded in a GaAs matrix. A pyramidal shape of InAs quantum dot has been used in simulations. It has been demonstrated that the visualization by using conventional TEM is rather complicated owing to the high strain level around the island. Being of pyramidal shape, an InAs island always looks truncated independent of the usual defocus variation. On the other hand, HREM contrast of the island is shown to be rather sensitive to both foil thickness and defoci. Optimum HREM imaging conditions (particular focus and foil thickness, which is about twice the base length of the dot) are found to be most favorable for revealing the shape of such objects owing to the difference in structure factors between In and Ga atoms.

The results of simulations coincide with the observed TEM and HREM images. Top-view TEM indicates that the islands have a square base, principal axes are close to the two orthogonal $\langle 100\rangle$ directions, and the average base length is about (12 ± 1) nm. In the cross-section micrographs the QDs always look like truncated pyramids, due to specific strain contrast. In the cross-section HREM image, the pure pyramidal shape of the QD is fully proved. The height of the pyramid is about 6 nm, the side facets close to $\{101\}$ (see also Ruvimov *et al.*, 1995).

The above discussion and comparison of different techniques allows us to understand the origin of a seeming discrepancy between the results of different groups. On the one hand, HREM cross-section measurements carried out independently by Xie *et al.* (1994) and by Ruvimov *et al.* (1995) indicated similar pyramidal shapes of InAs quantum dots. In both papers, the growth temperature was the same (480 °C).

On the other hand, InAs islands on GaAs(001) grown by MBE at a temperature of 530 °C by Leonard *et al.* (1994) and measured by AFM revealed the shape of a planoconvex lens with a height-to-radius ratio 1:2. Moison *et al.* (1994) performed MBE growth of InAs islands at a temperature of 500 °C. Their AFM measurements revealed both islands bounded by $\{104\}$ facets and islands bounded by $\{101\}$ facets. The difference between these two groups of results may be owing first, to different growth temperatures, and, second, to different measurement techniques, if one takes into account that AFM can overestimate the lateral size of islands due to the finite size of the tip.

Certainly, one should keep in mind that the overgrowth process can, in some cases, affect the shape, the size, and the chemical composition of QDs, and measured QDs can be, in principle, different in shape from free-standing islands on the surface. Modifications of QDs, induced by overgrowth, are particularly pronounced at elevated temperatures (530–580 °C). These modifications include the elongation of initially isotropic islands in the [110] direction, a craterlike suppression in the middle of the islands, and the intermixing of Ga and In (Garcia *et al.*, 1997).

To carefully control such modifications induced by overgrowth, it is especially important to perform structural characterization for both uncovered and covered islands. Thus Lian *et al.* (1998) controlled the morphology of an InAs/GaAs(001) system by *in situ* STM and AFM measurements before overgrowth and then examined capped structures *ex situ* by TEM and scanning TEM. A comparison of *in situ* and *ex situ* results showed that overgrowth at 530–580 °C resulted in partial or complete evaporation of InAs islands and in the reduction of island density. Incoherent and large coherent islands were shown to evaporate first. This effect can eventually narrow the size distribution of QDs and eliminate incoherent islands, at the expense of the reduction of QD density.

If the overgrowth of InAs islands by GaAs is performed at a moderate temperature (e.g., 480 °C), but the islands are only partially capped, the uncovered parts of the islands start to evaporate and to form a second wetting layer on a GaAs surface (Ledentsov, Shchukin, *et al.*, 1996). This will be discussed further in Sec. V.

However, if the overgrowth of InAs islands is performed at a moderate temperature (480 °C), and the islands are capped completely, no significant island evaporation occurs (Xie *et al.*, 1994). For overgrowth of InAs islands, five periods of $(Al_{0.25}Ga_{0.75}As)_3/(GaAs)_{15}$ have been grown, with layers of AlGaAs used in between as marker layers. Marker layer images on the cross-sectional TEM micrograph indicate the evolution of the GaAs overlayer profile. This evolution involves, first, the preferential growth of GaAs over the wetting layer, where the lattice parameter is close to that of GaAs, and, second, the suppression of GaAs growth on island facets and over the island where, due to partial strain relaxation, the lattice parameter has an intermediate value between GaAs and InAs. The suppression of overgrowth facilitates potential evaporation of InAs islands at higher temperatures (see Lian *et al.*, 1998), but has no essential effect on island shape and size at moderate temperatures.

Summing up this discussion, we emphasize that problems of strain contrast in conventional TEM can be overcome if HREM measurements combined with HREM simulations are used. The problem of possible transformation of island morphology during overgrowth can be overcome if islands are completely capped at a moderate temperature (e.g., 480 °C for InAs islands on GaAs). Obviously, the temperature of the overgrowth can be higher for materials systems with greater thermal stability, e.g., for SiGe/Si.

In comparing the advantages and disadvantages of different characterization techniques, many studies indicate the complementary nature of TEM, on the one hand, and STM and AFM, on the other hand. Thus Kamins *et al.* (1997) emphasizes that AFM provides statistically significant data and accurate height information, but does not provide an unambiguous value for island diameter because of the finite size and shape of the AFM tip. Cross-sectional TEM provides more detailed information about the island diameter and shape, but samples fewer islands. Complementary TEM and AFM data on the same sample allow the apparent enlargement of the island diameter by AFM to be quantified, so that AFM can provide statistical confirmation of the trends observed by TEM.

In general, most of conclusions which follow from STM and AFM results agree with the data available from TEM studies (see, for example, Ledentsov, Grundmann, *et al.*, 1996). By combining the results of all these techniques, one can build a picture of the main effects in lattice-mismatched epitaxy.

2. Diffraction methods

Reflection high-energy electron diffraction (RHEED) is a highly surface-sensitive ultrahigh-vacuum technique used to monitor growth in MBE systems. Upon transformation of an initially two-dimensional ordered surface with monolayer high islands into a corrugated structure, the RHEED pattern changes from streaky to spotty (see, for example, Nabetani *et al.*, 1994; Guryanov *et al.*, 1996). RHEED is thus a very valuable tool for *in situ* monitoring of the formation of 3D islands.

Reflectance anisotropy spectroscopy (RAS) allows one to monitor the asymmetry of the dielectric properties of the surface. Surface reconstruction (Kamiya *et al.*, 1992) and oscillations due to monolayer growth (Reinhardt *et al.*, 1993) can be identified. Formation of larger objects can be found by means of scattered (stray) light intensity (Olson and Kibbler, 1986).

X-ray diffraction techniques are useful for structural investigation after growth. Results for single-sheet arrays of quantum dots (Krost *et al.*, 1996) and multisheet arrays (Darhuber, Holy *et al.*, 1997; Darhuber, Schittenhelm *et al.*, 1997) have been reported for InAs/GaAs and Ge/Si systems. The diffraction signal due to dots is rather weak, since the dots are much larger (~ 10 nm) than the probing wavelength (~ 0.1 nm). X-ray diffraction has been shown to be a powerful tool for measuring the alloy composition of InGaAs in the wetting layer (Krost *et al.*, 1996). The observed interference pattern is caused by the phase shift between the diffracted waves from the upper GaAs cap layer and the lower GaAs substrate, the phase shift depending on the strain-thickness product, which allows one to determine the In composition in an InGaAs wetting layer.

3. Optical methods

For quantum dots based on direct band-gap semiconductors, e.g., InAs QDs in a GaAs matrix, photoluminescence spectroscopy is an additional powerful tool for characterization of QDs. First, the position of the photoluminescence line contains information about the size of the QDs and about the depth of the confinement potential. The increase in QD size and in the depth of the confinement potential results in a redshift of the photoluminescence line. The broadening of the spectrum is related to the width of the QD size distribution. Second, the loss of coherence and the onset of misfit dislocations create a high concentration of centers of nonradiative recombination and reduce significantly the integral intensity of the photoluminescence spectrum.

In the following, we discuss MBE and MOVPE growth of 3D islands in the InAs/GaAs and InGaAs/GaAs materials systems, experimental characterization of the obtained structures, and their relation to theoretical models.

L. Experimental studies of 3D islands in lattice-mismatched heteroepitaxial systems

The first experimental evidence of the formation of 3D coherently strained islands was obtained by TEM and was reported by Goldstein *et al.* (1985) for an InAs/GaAs system. Eaglesham and Cerullo (1990) and Mo *et al.* (1990) observed coherent islands of $Ge_{1-x}Si_x$/Si(001) and Ge/Si(001) by STM. The shape of the Ge/Si(001) islands was revealed with atomic accuracy by the STM measurements of Mo *et al.* (1990).

The explosion of interest in the formation of 3D coherently strained islands is related to the discovery of the narrow size distribution of InGaAs islands on GaAs(001) (Leonard *et al.*, 1993), and of InAs islands on GaAs(001) (Ledentsov, Grundmann, *et al.*, 1994; Leonard *et al.*, 1994; Moison *et al.*, 1994) and to the apparent absence of Ostwald ripening. Later, similar properties of 3D islands, namely, a narrow size distribution and the absence of ripening have been observed for a large variety of heteroepitaxial systems, e.g., for InAs/InP(001) (Ponchet *et al.*, 1995), for AlInAs/GaAlAs(001) (Leon *et al.*, 1995), for GeSi/Si(001) (Apetz *et al.*, 1995; Chen *et al.*, 1995; Schittenhelm *et al.*, 1995; Jesson *et al.*, 1996), for CdSe/ZnSe(001) (Xin *et al.*, 1996), for InAs/InAlAs(001) and InAs/InGaAs(001) (Ustinov *et al.*, 1998), and for InAs/Si(001) (Cirlin *et al.*, 1998).

As has been discussed above, the nature, thermodynamic or kinetic, of arrays of 3D islands (quantum dots) is a highly debated issue. In this section we formulate

criteria that allow us to test, for any particular system, whether an observed array is an equilibrium one or a kinetic-controlled one. To resolve this question, it is important to verify experimentally whether the following equilibrium properties are present in a given system.

(1) Upon growth interruption or upon annealing, the system evolves towards equilibrium. When the equilibrium is reached, no further changes occur.
(2) The equilibrium state of the system depends only on thermodynamic parameters, and not on prehistory. For the heteroepitaxial systems in question, these are the amount of deposited material and the temperature. For III-V and II-VI compound semiconductors, a third thermodynamic parameter, the vapor pressure of anions, can affect the morphology of the system. Growth interruption is provided by switching off the supply of cations while a given vapor pressure of the anions (e.g., arsenic) is maintained.
(3) For a system in equilibrium, it is possible, by varying the thermodynamic parameters of the system, to cause reversible changes in the morphology.

These will be the main features in our discussion of experimental data on quantum dot arrays. Despite the large amount of experimental work on the formation of QDs in various semiconductor systems, there are only a few papers that focus on whether dots are equilibrium or kinetic controlled. In our discussion, we shall pay special attention to these experimental data.

1. Effect of growth interruption on the morphology of InAs/GaAs systems

Studies of the behavior of an InAs/GaAs heteroepitaxial system upon growth interruption have been carried out by Ledentsov, Grundmann, *et al.* (1996). The system was grown by molecular beam epitaxy, then growth interruption was introduced, and the system was overgrown by GaAs afterwards. The capped structure was studied by transmission electron microscopy (TEM) and by photoluminescence spectroscopy. A series of experiments was carried out, at the same growth temperature 480 °C, with different amounts of deposited material and with different times of growth interruption.

These studies revealed the following. When the average critical thickness of InAs deposition was reached [1.6–1.7 monolayers (ML)], a morphological transition to three-dimensional InAs islands occurred. Since the process of dot formation was very fast at this stage, freezing it for STM and AFM studies would have been impractical. Therefore TEM investigation of immediately covered dots was the only reliable method for dot characterization.

TEM and photoluminescence studies of dots formed after 2 ML deposition of InAs demonstrated that the dots were small, did not show well-resolved crystalline shape, and exhibited a wide spread in sizes.

If 4 ML of InAs were deposited, a dense array of well-developed dots was formed. In plan-view the base of the dots had a square shape, the sides being parallel to the [100] and [010] directions. The average lateral side of the dots was ~140 Å.

The introducing of growth interruption resulted in dramatic changes in the heterophase morphology with respect to as-grown samples. If 3 ML of InAs were deposited, and a 10-s the growth interruption is introduced, the dots reached the same lateral size ~140 Å. If 2.5 ML of InAs were deposited, and a growth interruption of 40 s was introduced, the dots reached the same lateral size ~140 Å. If only 2 ML of InAs were deposited, the use of a very long (100-s) growth interruption forced initially small dots to reach the same lateral size. When the dots reached this lateral size, further growth interruption did not produce any changes in the shape, the size, or the density of dots.

The above cited data support the conclusion that the size of InAs dots ~140 Å is *the equilibrium size* which can be attained by growth interruption. However, one should keep in mind that the allowed time for growth interruption has a natural upper limit. For growth temperatures ~480 °C, an interruption much longer than 100 s can lead to evaporation of In, to alloying of quantum dots or of the wetting layer with the substrate, or to migration of intrinsic defects from the substrate to the surface. Any of these processes makes both the energetics and the kinetics in the system much more complex.

The conventional consideration of the energetics of a QD array, or of the kinetics of dot formation, is based on the assumption that there is no evaporation of deposited material or intermixing with the substrate and that the properties of the substrate, e.g., its lattice parameter, do not change. If any of these assumptions is no longer valid, growth interruption does not give an answer on the nature of the dot array.

2. Reversible 3D-to-2D transitions in heteroepitaxial systems

For III-V compound semiconductors, the vapor pressure of group V elements is the control parameter that can affect the morphology of the heteroepitaxial system. The dependence of the morphology of an InAs/GaAs heteroepitaxial system on the arsenic pressure has been studied in detail by Ledentsov, Grundmann *et al.* (1996). Growth of InAs by molecular beam epitaxy at temperature $T=480\,^\circ\mathrm{C}$ and standard MBE arsenic pressure ($P_{As}^0 \approx 2.0\times 10^{-6}$ Torr) results in an array of dots of high density ($5\times 10^{10}\,\mathrm{cm}^{-2}$). The dot array is stable, and islands do not undergo Ostwald ripening upon growth interruption.

The growth at arsenic pressure $1/6P_{As}^0$ does not lead to formation of 3D islands, and only two-dimensional InAs islands (~1000 Å) appear (Fig. 23). These growth conditions are close to ‘‘virtual surfactant epitaxy’’ (Tournié *et al.*, 1994), and the corresponding reflection high-energy electron diffraction (RHEED) pattern is streaky, indicating a planar surface morphology. The photoluminescence peak shifts towards higher energies than in the case of 3D dots. The broadening of the photoluminescence peak corresponds to a highly nonuniform corrugated 2D layer of InAs.

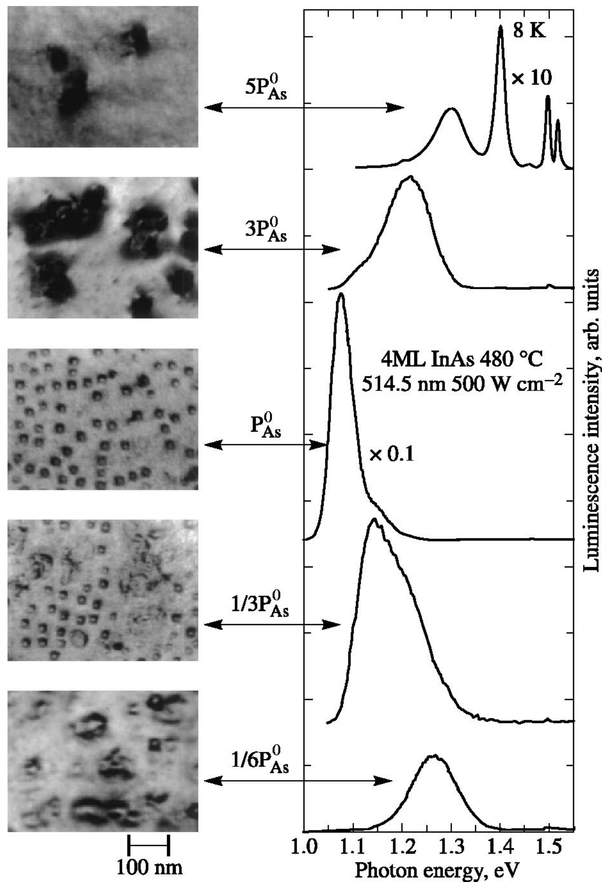

FIG. 23. Effect of As pressure on InAs/GaAs quantum dot arrays. Plan-view TEM and photoluminescence spectra for five values of arsenic pressure are given, $P^0_{As}=2\times10^{-6}$ Torr. The dense array of 3D coherent dots existing for $P=P^0$ undergoes a reversible transition to a planar morphology with lowering of pressure to $P=\frac{1}{6}P^0_{As}$. An increase of pressure results in Ostwald ripening, formation of dislocated clusters at $P=3P^0_{As}$, and complete disappearance of coherent dots at $P=5P^0_{As}$.

The same state of the system can be obtained in quite a different way. If 3D islands are formed at the standard arsenic pressure P^0_{As}, the As flux is interrupted, and 0.15 ML of In is deposited, then 3D islands disappear, and the RHEED pattern converts from spotty to streaky within a few seconds. The similarity of the final morphology in the two above-mentioned cases indicates the *reversibility of the phase transition* between the corrugated 2D layer of InAs and an array of 3D coherently strained islands of InAs.

A similar reversible 3D-to-2D transition was observed independently by Ozasa *et al.* (1997) for GaInAs quantum dots grown by chemical beam epitaxy. The experiments were carried out on GaAs(001) substrates using triethylgallium (TEGa), trimethylindium (TMIn), and AsH_3 as sources. Quantum dots were grown at a temperature of 480 °C, and the indium fraction in GaInAs was 0.50. The onset of 3D island formation was detected *in situ* by the change in the RHEED pattern, from streaky to spotty. The density, height, and diameter of the QDs were 7×10^{10} cm^{-2}, approximately 13 nm, and 24 ± 3 nm, respectively. These values were obtained by atomic force microscopy (AFM) observations and by high-resolution scanning electron microscopy observations.

After stopping the supply of TEGa and TMIn, Ozasa *et al.* switched off the AsH_3 flux, and switched on the PH_3 flux. The spotty RHEED pattern was gradually changed into a streaky pattern. The change indicates that the 3D dot structure became a flatter layer of InGaAsP through the replacement of arsenic in the dots by phosphorus. This transition can be attributed to a smaller lattice mismatch in the InGaAsP/GaAs system than in the InGaAs/GaAs system. The RHEED pattern obtained 12 s after switching from AsH_3 to PH_3 still revealed spots, but a shift of the spots was observed. The shift was explained by the partial replacement of As by P in the dots, so that the composition of the dots was $In_{0.52}Ga_{0.48}As_{0.68}P_{0.32}$. The shifted spots became thinner after 12 s and finally fused into streaks. The shift of spots/streaks stopped at around 30 s, but the diffusion of the spots into streaks continued with a slower speed thereafter. The observed RHEED change revealed that the dot structure became a flatter surface upon exposure to phosphorus via two steps: first, some arsenic in the dots was replaced by phosphorus with preservation of dot shapes. Then the dot started to flatten with further arsenic/phosphorus replacement. The RHEED pattern obtained at 85 s after switching from AsH_3 to PH_3 was similar to that of the InGaAs layer observed before the onset of dot formation. The resultant two-dimensional layer had an estimated composition of $In_{0.52}Ga_{0.48}As_{0.23}P_{0.77}$.

When the AsH_3 beam was reapplied instead of PH_3, a reverse transition from the InGaAsP flat surface to InGaAs dot structure occurred. The RHEED pattern at 120 s was identical to that obtained for the initial 3D dot formation with the InGaAs deposition. Photoluminescence studies of the capped reproduced dots, on the one hand, and of capped as-grown dots, on the other hand, indicated a minor difference in peak positions which can be attributed to some residual phosphorus in the dots.

The reversible 3D-to-2D transition is driven by a reduction in the lattice mismatch upon replacement of arsenic by phosphorus, in agreement with the equilibrium phase diagram of Fig. 20. These data indicate that the morphology of the heteroepitaxial system is determined by the vapor pressure of arsenic and phosphorus. The reversibility of such a transition clearly indicates the equilibrium nature of the quantum dot arrays in question.

3. Transition from an ordered array of InAs quantum dots to Ostwald ripening

An increase in arsenic pressure affects the morphology of an InAs/GaAs system in a different way. The effect of arsenic pressure on MBE-grown InAs quantum dots has been studied in detail by Ledentsov, Grundmann, *et al.* (1996). As mentioned above, in Sec. IV L 2, the growth of InAs at temperature $T=480$ °C and stan-

dard MBE arsenic pressure ($P_{As}^0 \approx 2.0\times 10^{-6}$ Torr) results in an array of dots of high density (5×10^{10} cm^{-2}). No qualitative changes in the morphology occur if arsenic pressure is changed by $\approx 50\%$ around P_{As}^0. An increase in As pressure by a factor of 3 ($3P_{As}^0$) results in a dramatic change in the morphology. The size of dots reduces, and a high density of large (~500–1000 Å) dislocated InAs clusters appears, as shown in Fig. 23 (see also Madhukar *et al.*, 1994). Further increase in arsenic pressure ($5P_{As}^0$) suppresses the formation of small dots nearly completely, and only dislocated InAs clusters can be resolved on the InAs wetting layer. Photoluminescence emission is dominated by the wetting layer peak at low temperatures, and no emission from the dots can be resolved at 300 K. The integral intensity of the photoluminescence strongly degrades in agreement with the formation of large dislocated clusters.

We emphasize here that the kinetics of surface migration is very fast in the above experiments. At the arsenic pressure P_{As}^0, 3D coherent islands of InAs have a base length of 140 Å and a typical separation of 250–350 Å. At high As pressure, dislocated clusters of InAs are separated by 0.2–1 μm. This means that the migration kinetics is sufficient to rearrange InAs and to deliver material over a distance of about 0.2–1 μm. Such fast kinetics confirms that the array of 3D coherent InAs islands of approximately the same size is formed not due to "frozen" kinetics, but due to the fact that this array corresponds to thermodynamic equilibrium.

The change in the morphology of InAs/GaAs systems with an increase in arsenic pressure can be explained by considering the surface energies. The stoichiometry of (001) surfaces of III-V semiconductors that are in equilibrium with the vapor is known to depend on the pressure of the group-V element in the vapor. Thus a change in As pressure leads to a change in the surface energy of the GaAs(001) surface and even to a change in the surface reconstruction (Qian *et al.*, 1988; Moll *et al.*, 1996). The wetting layer of InAs on a GaAs(001) surface may be considered as a complex surface of a semiconductor, which is expected to exhibit similar behavior with arsenic pressure. An increase in the arsenic pressure results in a decrease in the surface energy of GaAs(001) (Qian *et al.*, 1988; Moll *et al.*, 1996) and of InAs(001) (Pehlke *et al.*, 1997). It is natural to assume that the same tendency will be present in the *InAs wetting layer on GaAs(001)*. A decrease in the surface energy of the (001) surface results in an increase in the control parameter α in Eq. (4.16) and favors the transition from the ordering regime to the ripening regime. This is likely to be the case when the arsenic pressure increases from P_{As}^0 to $3P_{As}^0$.

The effect of arsenic pressure on the formation of InAs quantum dots is even more pronounced for QDs grown by metalorganic vapor phase epitaxy (MOVPE). A comparison of QD growth by MOVPE and by molecular beam epitaxy is valuable, among other reasons, because it allows one to extract and to distinguish the effects of both energetics and kinetics on the formation of quantum dots.

A "standard" MOVPE procedure for growing arsenids of group-III elements requires the AsH_3 flux to be switched on during the whole epitaxy process, i.e., during the growth and the growth interruptions. This "standard" procedure is mandatory to guarantee group-V stabilization of the crystal surface at elevated temperatures and to prevent formation of group-III droplets. However, the absence of AsH_3 for just a few seconds is not critical. Heinrichsdorff *et al.* (1998) found quite the opposite: for the growth of InAs/GaAs quantum dots the *presence* of AsH_3 degrades the structure quality.

A set of experiments was carried out in which after the deposition of 1.65 ML of InAs, growth was interrupted during $t_{\mathrm{GRI}}=14$ s. For the same $t_{\mathrm{GRI}}=14$ s, the flux of AsH_3 was switched off during the first time interval $t_{\mathrm{GRI}}^{\mathrm{off}}$ and switched on during the rest $t_{\mathrm{GRI}}-t_{\mathrm{GRI}}^{\mathrm{off}}$. If AsH_3 was switched off for 12 s, a high-quality array of QDs was formed. If the AsH_3 was switched off for only 3 seconds, the photoluminescence peak decreased by a factor of ≈ 2. The presence of AsH_3 ($P=0.7$ mbar) during the entire period of growth interruption reduced the QD luminescence intensity by more than two orders of magnitude. Dislocated clusters with low areal density were formed which gave rise to macroscopic surface roughness. In short, AsH_3 pressure during growth interruption is the key parameter for the growth of defect-free InAs QDs in MOVPE for two reasons:

(i) The QD nucleation seems to be hindered by AsH_3. Fewer and larger objects are formed in the presence of AsH_3.

(ii) Even after nucleation, an exposure to AsH_3 leads to a redistribution of material and to the formation of larger dots and dislocated clusters.

The simplest possible explanation for the preferred cluster formation under the pressure of AsH_3 is based on the fact that typical MOVPE growth conditions can be regarded as As-rich compared to the MBE case. For As-rich conditions in molecular beam epitaxy, the QD density reduces, and dislocated clusters are formed (see above).

A major difference between MOVPE and MBE growth is associated with the reactants used for the epitaxy. Particularly, an atomic hydrogen stemming from AsH_3 decomposition in MOVPE is expected to affect both the energetics and kinetics of QD formation, since hydrogen radicals are known to interact with the surface by breaking of bonds due to high reactivity and to get incorporated into the bulk crystal (Li and Jagadish, 1996). Nevertheless, it is clear that switching off the AsH_3 flux during growth interruption makes the QD nucleation and development more "MBE-like," since it reduces both the As and the H pressure.

The effect of AsH_3 pressure during the growth of QDs is similar to the effect of AsH_3 pressure during growth interruption. High AsH_3 pressure results in a redshift of the photoluminescence spectrum and in an overall decrease in the integral photoluminescence intensity. This corresponds to an increase in the QD size, broadening of the QD size distribution, and the onset of misfit dis-

locations, thus indicating that an increase in the AsH_3 pressure promotes Ostwald ripening.

Thus the effect of arsenic pressure on the formation of InAs quantum dots on a GaAs(001) substrate is similar for both MBE and MOVPE growth. Low arsenic pressure results in the formation of a dense array of QDs, whereas high arsenic pressure leads to Ostwald ripening and formation of dislocated clusters. These results indicate that the morphology of an InAs/GaAs system depends rather on energetics than on kinetics, the latter being quite different for MBE and MOVPE growth.

4. Other materials systems

Among other materials systems, Ge and SiGe islands on Si(001) are particularly interesting given the prominence of Si technology for electronic device applications. Formation of Ge and SiGe islands upon deposition on Si(001) was the subject of a number of works (e.g., Eaglesham and Cerullo, 1990; Mo *et al.*, 1990; Chen *et al.*, 1995; Schittenhelm *et al.*, 1995; Kamins *et al.*, 1997). However, only in a few works was an attempt made to distinguish equilibrium arrays of islands from kinetic-controlled ones.

Chen *et al.* (1995) deposited $Si_{0.5}Ge_{0.5}$ on a Si(001) substrate at the low temperature of 400 °C. Post-deposition annealing at 590 °C for six minutes resulted in an array of islands bounded by {105}-facet planes and showing a narrow size distribution.

When the sample was annealed at a much higher temperature ($\geqslant$650 °C) for 10 minutes, a much broader distribution of island size was observed. This indicates that islands were undergoing Ostwald ripening. Based on these observations, Chen *et al.* (1995) concluded that formation of an array of islands with a narrow size distribution at 590 °C is a kinetic effect, rather than one due to the thermodynamics of the 3D island system. A kinetic model of self-limited growth was proposed by Chen *et al.* (1995) in which the evolution of the island towards Ostwald ripening was stopped due to strain-induced barriers associated with the nucleation of every new facet layer. Since it is easier to overcome such barriers at a higher temperature, the average island size increases with temperature, and Ostwald ripening will occur only at sufficiently high temperatures.

In principle, these observations agree with the model of self-limiting growth kinetics. However, this does not give an unambiguous proof of the kinetic nature of the array of 3D islands. The equilibrium state of a heteroepitaxial system depends on temperature, via the entropy contribution to the free energy. This entropy contribution should account for a finite concentration of adatoms, as well as for fluctuations in island shape, size, and relative arrangement. The entropy for an array of 3D islands has not been considered in the literature so far, but plainly it is not possible to distinguish equilibrium arrays of islands from kinetic-controlled ones if islands are formed at one temperature and further annealing is performed at another temperature. To obtain an unambiguous answer, one must ensure that the islands are formed and further annealing (or growth interruption) is carried out under identical conditions, particularly, at the same temperature.

Such a careful study has been carried out by Kamins *et al.* (1997) for Ge islands on Si grown by chemical vapor deposition. Six monolayers of Ge deposited at approximately 580 °C produced a narrow size distribution of Ge islands. The layers were annealed for times up to 20 min without cooling or exposing the wafers to air between deposition and annealing. The distribution of islands became less uniform as the annealing continued, indicating some transfer of Ge from small to large islands (Ostwald ripening). This also indicates that the array of Ge islands, with its narrow size distribution, is a kinetic-controlled array rather than an equilibrium one.

Recent results of Kamins *et al.* (1998) have revealed a reversible transition between two shapes of Ge islands on Si(001), a square-base pyramid bounded by {105} facets, and an octagonal-base "dome." Ge islands are pyramids when they are small and transform to domes when they exceed a certain critical volume. Annealing at 650 °C results in some alloying of Ge islands with the Si substrate, the lattice mismatch reduces, and the island shape can change from a dome back to a pyramid, even though the island size increases substantially. However, this result does not mean real reversibility, since the overall morphology of the heteroepitaxial system, including island size, density, and chemical composition, is not restored.

The stability of CdSe 3D islands on ZnSe(001) substrates was examined by Xin *et al.* (1996). The dots were grown by molecular beam epitaxy at a temperature of 350 °C, then taken out of the growth chamber, cooled to room temperature, and exposed to the atmosphere. Atomic force microscopy measurements of the same sample area were repeated at 48-h intervals. This revealed that the uncapped CdSe dots changed in two ways: their total density decreased and their size distribution broadened, the effect being visible in six days. These observations were interpreted as Ostwald ripening at room temperature. However, one should keep in mind that the formation of these dots, on the one hand, and their further evolution towards Ostwald ripening, on the other hand, occurred in different vapor environments. Thus this experiment does not give a decisive answer as to whether there is a tendency towards ripening when dots are being formed.

Other systems, in which the formation of 3D coherently strained islands (quantum dots) has been observed, include GaSb islands on GaAs(001) (Hatami *et al.*, 1995); GaN islands on $Al_{1-x}Ga_xN$ (Tanaka *et al.*, 1996), and InAs islands on Si(001) (Cirlin *et al.*, 1998). However, no special experiments aimed at distinguishing equilibrium and kinetic control have been performed so far for these systems.

5. Discussion

Many of the experimental observations of three-dimensional InAs/GaAs(001) or InGaAs/GaAs(001) is-

lands have produced results that support the equilibrium nature of ordering. These results include the following: (i) the evolution of dot size up to the equilibrium value upon growth interruption for MBE-grown InAs quantum dots; (ii) a reversible phase transition in an InAs/GaAs system from 3D to 2D morphology, driven by a reduction in As pressure; (iii) a reversible phase transition from 3D to 2D morphology in a GaInAs(P)/GaAs system driven by switching off/on of AsH_3 and switching on/off of PH_3; (iv) an irreversible phase transition from coherently strained islands to dislocated clusters, i.e., the ''switching on'' of Ostwald ripening driven by the increase in As pressure; (v) formation of coherent InAs quantum dots by metalorganic vapor phase epitaxy (MOVPE), which is possible only in MBE-like conditions, at very low AsH_3 pressure; (vi) the general tendency towards Ostwald ripening with an increase in arsenic pressure in both MBE and MOVPE; (vii) the preferred alignment of nearest neighboring dots along elastically soft directions ⟨100⟩.

To sum up the discussion of this section, we formulate experimental options that would allow us to distinguish equilibrium arrays of quantum dots from kinetic-controlled ones.

(1) The behavior of a system upon growth interruption or annealing is a key indicator of the equilibrium or kinetic nature of a QD array. To give adequate information about the nature of a QD array, growth interruption or annealing must be carried out under the same conditions as when the dots are formed, i.e., at the same temperature, at the same group-V element vapor pressure (for III-V systems), without exposure to the atmosphere. If the array of QDs does not change upon growth interruption or annealing, this indicates the equilibrium nature of the array. However, there is a natural limit on the duration of growth interruption or annealing: it should not be so long as to permit evaporation of the deposited material or alloying of the deposit and the substrate.

(2) For III-V materials systems, upon growth interruption, one can control the morphology of the QD array by varying the vapor pressure of group-V elements (e.g., arsenic). A change in the vapor pressure may result in a change in the density, shape, or size of the QDs, and even in a 3D-to-2D morphological transition. If a QD array is an equilibrium one, such changes should be reversible as long as dislocated clusters do not appear.

(3) For equilibrium arrays of QDs, the change in the morphology with temperature should be reversible as well. To check whether such changes are reversible, the following experiment could be carried out. Let four growth runs be performed for the same heteroepitaxial system. (i) The system of QDs is grown at temperature T_1, annealed at temperature T_1, then capped and measured by transmission electron microscopy (TEM). (ii) The system of QDs is grown at temperature $T_2 > T_1$, annealed at temperature T_2, then capped and measured by TEM. (iii) The system of QDs is grown at temperature T_1, annealed at temperature T_1, heated up to temperature T_2, annealed at temperature T_2, capped and measured by TEM. (iv) The system of QDs is grown at temperature T_2, annealed at temperature T_2, cooled to temperature T_1, annealed at temperature T_1, capped and measured by TEM.

The difference in morphology between systems (i) and (ii) will indicate some temperature dependence. The crucial difference between equilibrium and kinetic-controlled arrays of QDs is as follows. The morphology of the equilibrium array depends only on the current temperature and does not depend on the prehistory of the system. The morphology of a kinetic-controlled array is determined by the highest temperature in its prehistory. In this connection, the morphology should be the same in cases (ii) and (iii) for both equilibrium and kinetic-controlled arrays. However, the measurements of system (iv) will resolve the question of the nature of the QD array. For equilibrium arrays, system (iv) should have the same shape, size, and density of QDs as system (i). For kinetic-controlled arrays, the shape, size, and density of QDs in system (iv) should be the same as in systems (ii) and (iii).

It should be noted that in the present review we have focused on the calculation of the total energy. Therefore the equilibrium morphology of the system revealed above refers, strictly speaking, only to temperature $T = 0$. At finite temperatures, one should take into account the entropy contribution to the free energy. As is known for stepped vicinal surfaces (see, for example, the paper by Joós *et al.*, 1991) the entropy term prevents the ''collision'' of steps and results in effective repulsion between steps. One would expect that, for an array of islands, the entropy term would also lead to an effective repulsion between islands. The role of the entropy term for the equilibrium morphology of an array of 3D islands is not yet known. Our discussion on the possible dependence of the QD array on temperature is based only on the general thermodynamic concept that the equilibrium state of a system should depend on thermodynamic parameters only, and not on prehistory.

To conclude the present section, we have described the debate setting thermodynamic theories against kinetic theories of the formation of arrays of 3D coherently strained islands (quantum dots). We have presented the thermodynamic theory in detail and demonstrated that, in a certain region of materials parameters, the equilibrium state of a heteroepitaxial system is an ordered array of equal-shape and equal-size islands, where Ostwald ripening is not favored energetically. Experimental data on InAs/GaAs quantum dots show that the formation of arrays of QDs in this system is governed rather by thermodynamics than by kinetics. We have proposed key experiments which would allow us for any given materials system, to distinguish between an equilibrium and a kinetic-controlled array of QDs.

V. MULTISHEET ARRAYS OF THREE-DIMENSIONAL ISLANDS

Multisheet arrays of islands are distinct from other types of nanostructures for the two following reasons:

First, formation of multisheet arrays of 3D or 2D islands is a process governed by both equilibrium ordering and kinetic-controlled ordering. If the deposition of the first sheet of islands of material 2 on the substrate material 1 is followed by growth interruption, or if the growth rate is sufficiently low, islands of equilibrium structure are formed. If then the islands are capped by material 1, and a second cycle of material 2 is deposited, a new growth mode occurs. For typical growth temperatures and growth rates, the structure of the buried islands of the first sheet does not change during the deposition of the second sheet. The second sheet of islands grows in the strain field created by the buried islands of the first sheet. And the structure of the second sheet of islands reaches equilibrium under the constraint of the fixed structure of buried islands of the first sheet.

Secondly, varying of the separation between successive sheets makes possible additional tuning (as compared to single-sheet arrays) of the geometrical and electronic characteristics of nanostructures.

A remarkable feature of multisheet arrays of 3D islands is that the buried islands in successive sheets are spatially correlated. The surface islands grow above buried islands. This type of vertical correlation has been observed in InAs/GaAs(001), InGaAs/GaAs(001), and Ge/Si(001) heteroepitaxial systems by Goldstein *et al.* (1985), Kuan and Iyer (1991), Yao *et al.* (1991), Xie *et al.* (1994, 1995), Ledentsov, Böhrer, *et al.* (1996), Ledentsov, Grundmann, *et al.* (1996), Ledentsov, Shchukin, *et al.* (1996), Tersoff *et al.* (1996), and Heinrichsdorff *et al.* (1997).

To explain this type of vertical correlation, one has to calculate the strain field created by buried islands. This can be done by using the continuum elasticity theory. If one approximates buried islands by elastic point defects and considers the elastically isotropic medium, the results of Maradudin and Wallis (1980) apply to the problem. This yields the hydrostatic part of the surface strain created by an island buried at a depth z_0 and lateral position $x_0=y_0=0$ as

$$\varepsilon_{ii}(x,y,0)=-\frac{C}{(x^2+y^2+z_0^2)^{3/2}}\left[1-\frac{3z_0^2}{x^2+y^2+z_0^2}\right]. \tag{5.1}$$

The "strength" of the point defect C is proportional to the island volume and to the lattice mismatch between the island material and the matrix. If the island material has a larger lattice parameter than the matrix (which is the case for InAs/GaAs and Ge/Si systems), then the coefficient C in Eq. (5.1) is positive.

The modulated strain field on the surface leads to modulation of the chemical potential of surface adatoms (Srolovitz, 1989), which in turn results in a migration of adatoms on the surface governed by diffusion and drift (Mullins, 1957; sometimes the term "directional migration" is used for the drift of adatoms). This drift is a driving force of kinetic self-organization in this complex growth mode. The same kinetic mechanism is responsible for the instability of epitaxial growth in a homogeneous alloy (Malyshkin and Shchukin, 1993; Guyer and Voorhees, 1995, 1996; Ipatova *et al.*, 1997, 1998) and may result in structure with modulated composition.

Since for InAs islands in a GaAs matrix, the coefficient C in Eq. (5.1) is positive, the position above the buried island, i.e., at $x=y=0$, corresponds to the maximum of the tensile strain ε_{ii}. The migration of In atoms on the surface of GaAs, in the strain field due to a buried island of InAs, was considered by Xie *et al.* (1994, 1995). It was argued that In atoms with a larger radius than Ga atoms are attracted to surface regions with the maximum tensile strain ε_{ii}, i.e., to positions directly above buried islands.

Tersoff *et al.* (1996) pointed out that nucleation of islands of the second sheet occurs preferentially above buried islands, thus explaining vertical stacking in a Ge/Si(001) system. Experimental data and theoretical modeling by Tersoff *et al.* (1996) show that the lateral ordering in subsequent sheets of islands is better pronounced than in the first sheet.

Multisheet arrays of 3D coherently strained islands (quantum dots) form *a new class of spontaneously formed nanostructures* where the ordering occurs both in the lateral plane and in the vertical direction.

However, as concerns the application of QDs, vertically stacked islands do not provide any significant improvement over a single-sheet array. The reason is that vertically stacked islands are essentially separated, i.e., the 3D islands of the first sheet are completely covered by a cap layer, and the deposition of the second sheet of islands starts only afterwards. In this case both electron and hole wave functions are localized inside each quantum dot. Therefore the regularity of the above arrangement does not affect the basic electronic properties of the structures. In order to realize advantages from vertically correlated arrays of quantum dots, *electronically coupled quantum dots* were fabricated (Heinrichsdorff *et al.*, 1996; Ledentsov, Shchukin, *et al.*, 1996; Solomon *et al.*, 1996).

Ledentsov, Shchukin, *et al.* (1996) performed a multicycle InAs-GaAs growth experiment in which the deposition of 5.5 Å of InAs was alternated with deposition of 15 Å of GaAs. The deposition of the first sheet of InAs resulted in the formation of InAs pyramids over the wetting layer of InAs. Since the characteristic height of InAs pyramids is ≈60 Å, the cap layer of GaAs covered the pyramids only partially, and then the next layer of InAs was deposited.

In Fig. 24, cross section (a) and plan-view (b) transmission electron microscopy (TEM) images are presented of a structure containing InAs vertically coupled quantum dots formed by three-cycle InAs-GaAs deposition. Figure 24(b) reveals the average lateral size of the islands at the top as 170±10 Å. The islands have a square base with their main axes along the [100]- and [010] directions. The histogram of nearest-neighbor dot orientation [Figs. 24(c) and 24(d)] shows the preferred

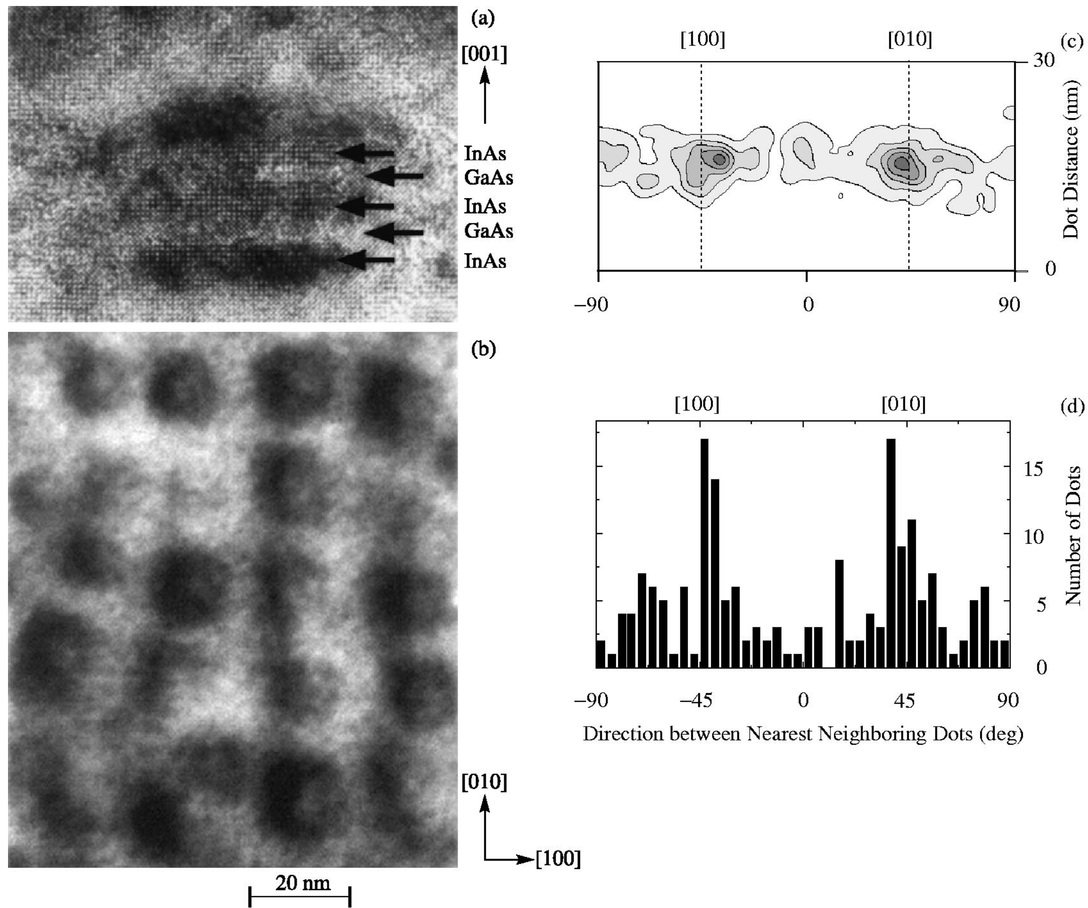

FIG. 24. Vertically coupled InAs quantum dots (QDs) in a GaAs matrix: (a) high-resolution electron microscopy [010] cross-section image formed by nine beams. Defocusing is 60 nm; note the different spot densities in the InAs and GaAs regions; (b) bright field plan-view transmission electron microscopy micrograph under [001] zone axis illumination; (c) 2D histogram of nearest two neighbors' center-to-center distance and direction for vertically coupled QDs from Fig. 24(b); (d) projection of Fig. 24(c) onto an angular axis. Maxima in the [100] and [010] directions prove the correlation in the nearest-neighbor arrangement of the islands, which corresponds to a lateral square superlattice composed of vertically coupled QDs.

orientation in the [100] and [010] directions typical for a 2D square lattice with primitive lattice vectors along the same directions. Each vertically coupled quantum dot is composed of three vertically aligned parts separated by 2–4-ML-thick GaAs regions [see Fig. 24(a)]. The top parts have a larger lateral size ($\approx$170 Å) than the lower part ($\approx$110 Å).

The important properties of the resulting structure are as follows:

(i) larger lateral size of the InAs islands in the top sheet than in the bottom sheet,
(ii) splitting of the InAs pyramids and the appearance of thin layers of GaAs separating the parts of these pyramids,
(iii) lateral correlation in the nearest-neighbor dot orientation, which is typical for a 2D square lattice and is more pronounced than in a single-sheet structure.

The increase in lateral size of the InAs islands can be explained by the transfer, during growth, of In from buried parts of the structure, where InAs is strained, to the top part where InAs is partially relaxed. The enhancement of the lateral correlation is similar to that observed for Ge/Si(001) vertically stacked islands by Tersoff *et al.* (1996). However, since the InAs islands of each sheet are covered only partially by GaAs, the detailed growth kinetics is different from that modeled by Tersoff *et al.* (1996). A semiqualitative kinetic model for the system in question was proposed by Ledentsov, Shchukin, *et al.* (1996).

Since successive parts of vertically coupled InAs quantum dots are separated only by very thin barriers, they are electronically coupled. By varying the thickness of the deposited GaAs or InAs in each cycle, as well as the number of cycles, it is possible to modify significantly the electronic spectrum of the vertically coupled QDs. This allows the optimization of laser performance (Ledentsov, Shchukin, *et al.*, 1996; Ustinov *et al.*, 1997).

VI. MULTISHEET ARRAYS OF TWO-DIMENSIONAL ISLANDS

Submonolayer depositions of narrow-gap material on vicinal and singular surfaces were proposed for fabrica-

tion of quantum dots (Brandt *et al.*, 1992; Bressler–Hill *et al.*, 1994; Wang *et al.*, 1994). Scanning tunneling microscopy studies of InAs growth on GaAs(001) (Bressler-Hill *et al.*, 1994) revealed the formation of arrays of uniform-size two-dimensional islands having a width of 4 nm and elongated in the $[\bar{1}10]$ direction. InAs submonolayer insertions in a GaAs matrix were proven to exhibit a remarkably high exciton oscillator strength even for ultrathin coverage (Belousov *et al.*, 1995).

In contrast to the case for three-dimensional quantum dots, in the 2D case the volume of the potential well is rather small, resulting in relatively small QD exciton localization energies with respect to the matrix band-gap energy. Thus a very important task is to find a way of increasing the localization energy for these QDs and, more generally, to achieve a higher degree of wave-function control. This might be done by stacking sheets of 2D islands and thus creating a submonolayer superlattice.

The principal advantage of a submonolayer superlattice composed of dense arrays of 2D nanometer-scale islands is the possibility of achieving ultrahigh absorption or gain values and realizing an intrinsic resonant waveguiding effect without using thick cladding layers having a lower refractive index (Ledentsov, Krestnikov, *et al.*, 1996, 1997). This effect is based on resonant enhancement of the refractive index in the vicinity of the exciton resonance according to the Kramers-Kronig equations. Since the studied structures are grown on a thin buffer layer placed directly on strongly absorbing GaAs substrates, the resonant modulation of the refractive index must be remarkably strong to reduce absorption losses related to the substrate. Such strength is possible because of the ultrahigh material absorption/gain in QDs and the significantly high density of 2D islands for stacked submonolayer superlattices.

The basic physics governing spontaneous formation of multisheet arrays of 2D islands is to a large extent understood. In contrast to 3D islands, for which the thermodynamic versus kinetic nature of single-sheet arrays is a point of intense debate (see Sec. IV), 2D islands in single-sheet equilibrium arrays are a well-established universal phenomenon, which should occur at submonolayer coverage in any heteroepitaxial system that grows according to the Stranski-Krastanow growth mode. These arrays were described in detail in Sec. III. Two distinct possibilities for the structure of islands in a single sheet have been recognized (Vanderbilt, 1992; Ng and Vanderbilt, 1995), namely, a 1D array of stripes (potential quantum wires) and a 2D array of compact islands, say, disks (potential quantum dots), in which the phase transition between these two types of structures is driven by the areal coverage. Due to the high anisotropy of real crystal surfaces, compact islands will differ in shape from round disks.

For multisheet structures, the islands of every other sheet are formed in a strain field created by the buried islands of the previous sheet. The structure of the surface islands reaches equilibrium, upon growth interruption, under the constraint of the fixed structure of the buried islands.

It seems natural to expect that the general properties of multisheet arrays of 2D islands are similar to the properties of multisheet arrays of 3D islands discussed in Sec. V and that 2D islands will exhibit the same type of vertical correlations as 3D islands, i.e., surface islands will grow above buried islands.

However, very recent experiments on multisheet arrays of 2D islands of CdSe in a ZnSe matrix (Straßburg *et al.*, 1998) are in seeming contradiction with this expectation and with the theoretical explanations of Xie *et al.* (1995) and Tersoff *et al.* (1996). High-resolution electron microscopy studies of CdSe islands in a ZnSe matrix (Straßburg *et al.*, 1998) have unambiguously and surprisingly revealed vertical *anticorrelation* between islands in successive sheets, as shown schematically in Fig. 1(e). Surface islands are formed above the spacings in the sheet of buried islands.

As concerns the theory developed by Xie *et al.* (1994, 1995) and by Tersoff *et al.* (1996), buried islands were approximated in these papers by elastic point defects, and the crystal was treated as an elastically isotropic medium.

Motivated by the observations of Straßburg *et al.* (1998), Shchukin, Bimberg, *et al.* (1998) examined in detail the energetics of multisheet arrays of 2D islands and looked for an equilibrium configuration of surface islands under the constraint of a fixed array of buried islands. In this section, we follow the paper of Shchukin, Bimberg, *et al.* (1998). The two key factors which make our approach different from those of Xie *et al.* (1995) and of Tersoff *et al.* (1996) are as follows.

First, we consider 2D islands having a height of 1–2 monolayers where the separation between successive sheets is comparable to or even less than the lateral size of the islands in the (xy) plane. We take into account the exact shape of the islands.

Second, the elastic anisotropy of cubic crystals is known to favor ordering of nanostructures in elastically soft directions (Khachaturyan, 1974, 1983; Ipatova *et al.*, 1993; Shchukin, Ledentsov, *et al.*, 1995; Tersoff *et al.*, 1996; see also subsection IV.F), and one can expect a significant effect of elastic anisotropy on vertical correlations between islands.

A. Interaction of an array of surface islands and an array of buried islands

The key mechanism responsible for the relative arrangement of islands in successive sheets is the formation of an equilibrium array of surface islands in the strain field of buried islands. To extract the essential physics governing the anticorrelation, it suffices to examine a double-sheet array comprising one sheet of buried islands and one sheet of surface islands. Extension to an arbitrary number of sheets is then straightforward.

Let material 2 be deposited on the (001) surface of the cubic substrate 1. Upon submonolayer deposition, a pe-

riodic array of monolayer high islands is formed (Marchenko, 1981b; Alerhand *et al.*, 1988; Vanderbilt, 1992; Ng and Vanderbilt, 1995). Then let the structure be capped by the substrate material 1, and the second cycle of deposition of material 2 be introduced. The total energy of the surface array of islands in the strain field of the buried islands is

$$E_{\text{total}}=E_{\text{surf}}+E_{\text{boundaries}}+\Delta E_{\text{elastic}}^{(\text{SS})}+E_{\text{elastic}}^{(\text{SB})}. \tag{6.1}$$

Here E_{surf} is the sum of the surface energies of surface islands and of uncovered parts of material 1, $E_{\text{boundaries}}$ is the energy of island boundaries, $\Delta E_{\text{elastic}}^{(\text{SS})}$ is the elastic relaxation energy of surface (S) islands due to discontinuity of the intrinsic surface stress tensor on island boundaries (Marchenko, 1981b; Alerhand *et al.*, 1988). $E_{\text{elastic}}^{(\text{SB})}$ is the elastic energy of the interaction between surface islands (S) and buried islands (B). Since we address the effects of the finite lateral size of islands and of elastic anisotropy and avoid other complications, we focus on the typical experimental situation, in which there is an equal amount of material deposited in each deposition cycle. Then each sheet tends to form the same periodic structure, which corresponds to the minimum of the sum of the first three terms on the right-hand side of Eq. (6.1). If the interaction between surface islands and buried islands is neglected, the surface array of islands *as a whole* can be subject to an arbitrary shift in the xy plane. The strain field created by buried islands has the same periodicity as the array of surface islands alone. Therefore the fourth term in Eq. (6.1) does not change the periodicity of the surface structure and just defines its relative position with respect to the array of buried islands (Fig. 25). Since the interaction energy $E_{\text{elastic}}^{(\text{SB})}$ is the only term in Eq. (6.1) that depends on the shift of the surface array as a whole with respect to the buried array, we shall focus on this energy term only. Below, we consider the dependence of $E_{\text{elastic}}^{(\text{SB})}$ on the shift X_0 for a 1D array of stripes [Fig. 25(a)] and on the shifts X_0 and Y_0 for a 2D array of compact islands. For simplicity, we focus on the extreme case of compact islands distinct from infinitely elongated stripes, that is, on square-shaped islands [Fig. 25(b)].

To evaluate the strain due to buried islands, we refer, first, to the strain due to point defects (Eshelby, 1956). A point defect located at $\tilde{\mathbf{r}}$ is represented by the superposition of three mutually perpendicular double forces (by an elastic dipole), and the effective body force density is

$$f_i(\mathbf{r})=a_{ij}\nabla_j\delta(\mathbf{r}-\tilde{\mathbf{r}}). \tag{6.2}$$

A monolayer-thick inclusion in the plane $z=\tilde{z}$ with macroscopic lateral dimensions is a 2D array of point defects occupying every atomic site within a certain area. The island can be described by a 2D shape function $\Theta^B(\mathbf{r}_\parallel)$, which equals 1 inside the inclusion and 0 otherwise. The body force density associated with a given inclusion can be obtained by adding the contributions of single point defects from Eq. (6.2). In the macroscopic approach, this summation can be replaced by integration,

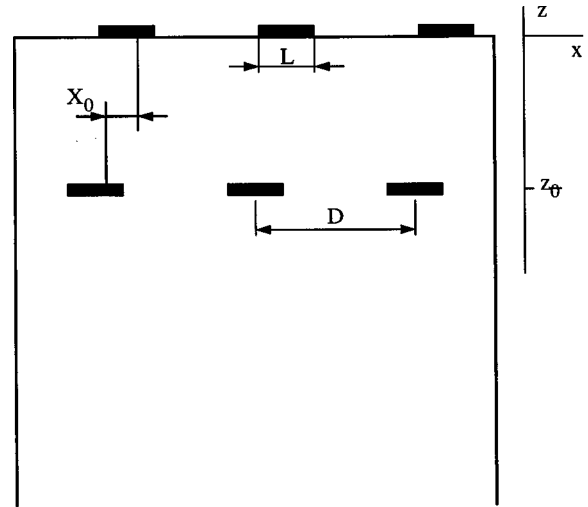

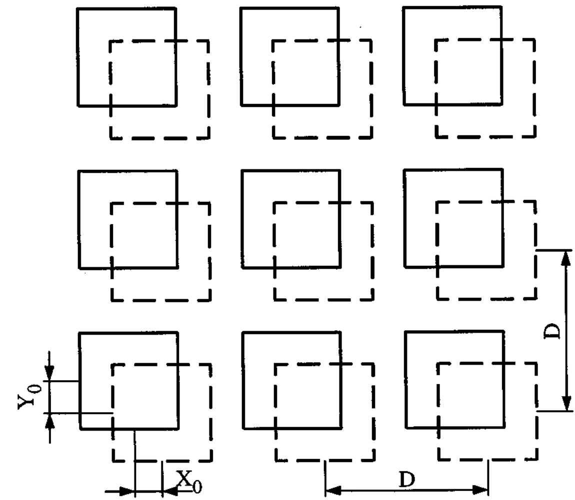

FIG. 25. Geometry of double-sheet arrays of two-dimensional islands. The array of surface islands has the same structure as the array of buried islands but is shifted as a whole. (a) Each sheet of islands forms a one-dimensional array of stripes. The cross section of a two-sheet structure is shown. (b) Each sheet of islands forms a two-dimensional array of square-shaped islands. The plan view of the double-sheet structure is plotted. Buried islands are depicted by dashed lines and surface islands by solid lines.

$$f_i(\mathbf{r})=\frac{1}{A_0}\int d^2\tilde{\mathbf{r}}_\parallel a_{ij}\nabla_j[\delta(\mathbf{r}_\parallel-\tilde{\mathbf{r}}_\parallel)\delta(z-\tilde{z})]\Theta^B(\tilde{\mathbf{r}}_\parallel), \tag{6.3}$$

where A_0 is the unit cell area in the xy plane. Equation (6.3) is derived under the assumption of no mutual influence among the point defects comprising the inclusion. Generally speaking, the tensor a_{ij} characterizing the double force density is different for a single point defect and for a monolayer-thick inclusion. A substitutional impurity atom in a zinc-blende crystal of a III-V or II-VI semiconductor has T_d site symmetry, and the corresponding double force tensor a_{ij} has cubic symmetry. On the other hand, if the inclusion of equal substi-

tutional impurity atoms is oriented in the (001) plane of the zinc blende crystal, has monolayer thickness and infinite lateral dimensions, each atom of the inclusion has D_{2d} symmetry. Therefore the tensor a_{ij} characterizing a monolayer-thick buried island has *uniaxial symmetry*, where $a_{xx}=a_{yy}$, $a_{zz}=P^B a_{xx}$, and P^B is the parameter of the uniaxial anisotropy of the double forces created by the buried islands. For an inclusion having all three macroscopic dimensions, the double force density is related to the lattice mismatch between the inclusion and the matrix and, for a cubic inclusion in a cubic matrix, has cubic symmetry again, $a_{ij}=v^{-1}(c_{11}+2c_{12})\times(\Delta a/a)\delta_{ij}$, where v is the unit cell volume, and c_{11} and c_{12} are elastic moduli in the Voigt notation.

The elastic properties of the surface islands are described by the difference between the two-dimensional intrinsic surface stress tensors $(\Delta\tau_{\alpha\beta})$ of the two materials. The energy of the elastic interaction between a periodic array of buried islands and a similar periodic array of surface islands is obtained in the form of a sum over the reciprocal lattice vectors (Shchukin, Bimberg, *et al.*, 1998),

$$E_{\text{elastic}}^{(\text{SB})}=\frac{h^B}{A_0}\sum_{\mathbf{k}_\parallel}\left|\tilde{\Theta}(\mathbf{k}_\parallel)\right|^2\exp(i\mathbf{k}_\parallel\mathbf{R}_0)(\Delta\tau_{\alpha\beta})a_{lm}\times\nabla'_m[\nabla_\alpha\widetilde{G_{\beta l}}(\mathbf{k}_\parallel;z,z')+\nabla_\beta\widetilde{G_{\alpha l}}(\mathbf{k}_\parallel;z,z')]\Big|_{\substack{z=0\\ z'=-z_0}}, \tag{6.4}$$

where $\mathbf{R}_0$ is the relative sheet of the two arrays, h^B is the thickness of the buried islands, $\nabla_x\equiv ik_x$, $\nabla'_x\equiv -ik_x$, $\nabla_y\equiv ik_y$, $\nabla'_y\equiv -ik_y$, $\alpha,\beta=1,2$, and l, $m=1,2,3$. Since we focus on III-V and II-VI semiconductors with the zinc-blende structure, we treat the crystal as an elastically anisotropic cubic medium and use the static Green's tensor $\widetilde{G_{il}}(\mathbf{k}_\parallel;z,z')$ from Portz and Maradudin (1977). The dependence of $E_{\text{elastic}}^{(\text{SB})}$ on the separation between the two sheets is determined by the behavior of $\widetilde{G_{il}}(\mathbf{k}_\parallel;z,z')$ as a function of z_0. $\widetilde{G_{il}}(\mathbf{k}_\parallel;z,z')$ is a linear combination of three exponentials, $\exp(-\alpha_s k_\parallel z_0)$, where the three attenuation coefficients α_s are functions of the direction $\mathbf{k}_\parallel$ in the surface plane. The key point is that, in a cubic crystal with a negative elastic anisotropy, $\Delta=(c_{11}-c_{12}-2c_{44})/c_{44}<0$, which is the case for all III-V and II-VI cubic semiconductors, two of the three α_s are complex conjugates (Portz and Maradudin, 1977). Complex attenuation coefficients α imply that the static analogs of Rayleigh waves exhibit not a purely exponential decay, but an oscillatory one. This phenomenon is known for surface acoustic waves which are generalized Rayleigh waves in elastically anisotropic crystals (Farnell, 1970; Kosevich *et al.*, 1985). The complex attenuation coefficients lead to the conclusion that the elastic strain created by the buried islands exhibits an oscillatory decay with distance from the sheet of islands (Fig. 26). As a consequence, the interaction between successive sheets of islands exhibits an oscillatory decay with the separation between sheets.

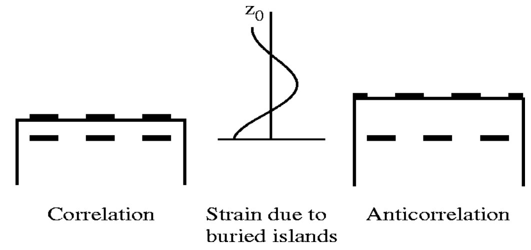

FIG. 26. The strain field at the surface created by a sheet of buried islands. Schematic plot shows an oscillatory decay of the strain with spacer thickness z_0. Dependent on the spacer thickness, the two sheets of islands exhibit a correlated (left) or an anticorrelated (right) arrangement.

The interaction energy (6.4) has been evaluated for double-sheet arrays of stripes and for double-sheet arrays of square islands. For the separation between the two sheets, $z_0\leq 0.5D_0$ where D_0 is the lateral period, the difference between the two values of $E_{\text{elastic}}^{(\text{SB})}$, the one for the most favorable relative arrangement, and the other for the most unfavorable arrangement, is of the order of $0.1\ \text{meV/Å}^2$. This is the same order of magnitude as the typical energy of a single sheet of surface islands. This comparison confirms that the elastic interaction between two sheets of islands can indeed result in vertical correlation or anticorrelation between the two sheets.

The phase diagram of Fig. 27(b) shows the favorable arrangement of the two sheets of islands. The most important regions of the phase diagram of Fig. 27(b) are 1a, which corresponds to vertical correlation, and 1b, which corresponds to vertical anticorrelation in both the (110) and ($\bar{1}10$) planes. The favorable arrangement of the two sheets of islands alternates from vertical correlation to anticorrelation, some intermediate arrangements being possible for small spacing between the two sheets. The separation corresponding to a transition from correlation to anticorrelation depends dramatically on the anisotropy parameter $P^B\equiv a_{zz}/a_{xx}$ of the double force density characterizing the buried islands.

B. Experiments on multisheets of 2D islands

The most complete structural characterizations and optical studies of multisheet arrays of 2D islands performed so far are of CdSe submonolayer superlattices in a ZnSe matrix (Straßburg *et al.*, 1998; Krestnikov, Straßburg *et al.*, 1998). The structures were grown on a GaAs substrate by molecular beam epitaxy. All structures consisted of a 360-nm buffer layer of ZnSSe and a 60-nm cap layer of ZnSSe lattice matched to a GaAs substrate. Between these layers a CdSe/ZnSe submonolayer was inserted. The average thickness of a single CdSe insertion was estimated as 0.7 monolayer. ZnSe barriers separated the sheets of CdSe submonolayer insertions and had thicknesses of 15 Å, 30 Å, 50 Å, and 80 Å.

The structures of two samples, one with a 15-Å spacer, and the other with a 30-Å spacer, were measured by high-resolution transmission microscopy (HREM).

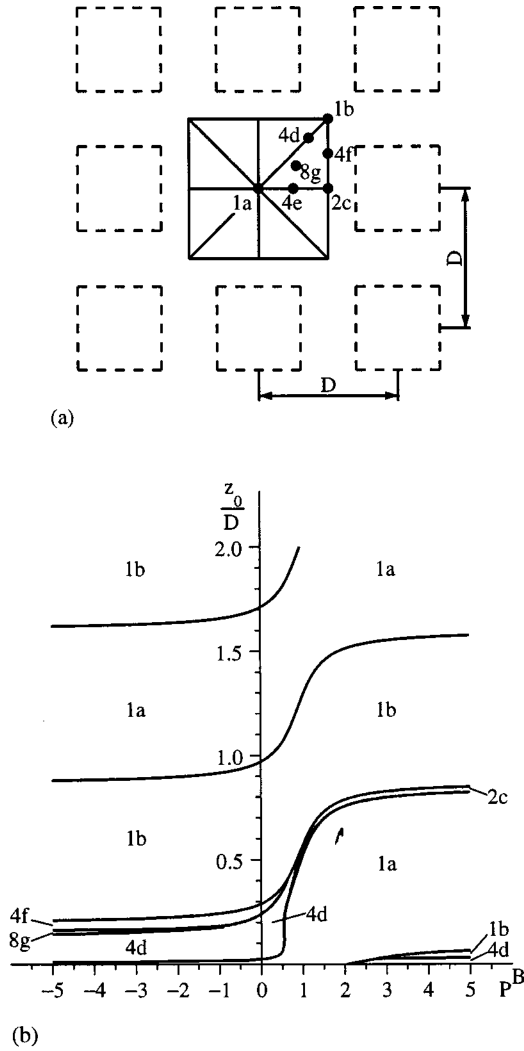

FIG. 27. Phase diagrams of a double-sheet array of square-shaped islands: (a) The relative shift (X_0, Y_0) is defined by the projection of the center of a surface island onto the superlattice formed by the buried islands. This projection is characterized by one of seven types of symmetry depicted in the figure; (b) phase diagram constructed in variables z_0/D vs P^B. P^B is the anisotropy of the double force density of the buried islands, z_0 is the separation between the surface and the sheet of buried islands, and D is the period. Domains of the phase diagram are labeled according to the symmetry of the projection of the center of a surface island onto the superlattice of buried islands, as defined in Fig. 27(a).

Cross-section HREM was performed in the ⟨110⟩ direction. To reveal the distribution of strained CdSe insertions, digitized HREM images were processed by the evaluation program DALI (Rosenauer *et al.*, 1996), which allowed Straßburg *et al.* and Krestnikov *et al.* to determine the local lattice parameter in the vertical direction. Figure 28 depicts two processed HREM images, one for a 30-Å-thick spacer from Straßburg *et al.* (1998) and the other for a 15-Å-thick spacer from Krestnikov *et al.* (1999). The structure with the 15-Å-thick spacer reveals vertical correlation between islands, whereas the structure with the 30-Å-thick spacer shows vertical anticorrelation.

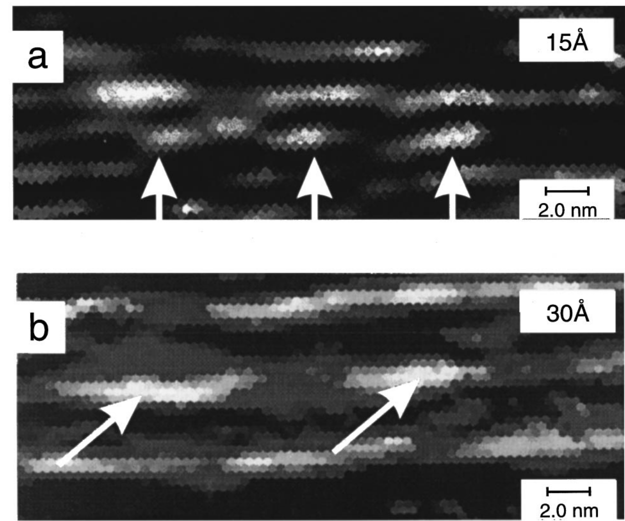

FIG. 28. Processed cross-section HREM image of a multisheet array of CdSe 2D islands embedded in a ZnSe matrix. The image has been processed by the DALI evaluation program. In the figure the local lattice parameter in the z direction is plotted. Black corresponds to the lattice parameter of ZnSe, white corresponds to the lattice parameter of CdSe, and the grey scale reproduces intermediate values. (a) An array with spacer thickness 15 Å reveals preferred vertical correlation of islands. (b) An array with spacer thickness 30 Å reveals preferred vertical anticorrelation of islands.

Different vertical arrangements of islands must result in different electronic spectra of the structures. To confirm this prediction, photoluminescence spectra of all the samples were measured. For spacer thicknesses 80 Å and 50 Å, only one line was observed. However, if the spacer thickness equalled 30 Å, a second photoluminescence line at a lower energy evolved. Although the lower energy line dominated the photoluminescence spectrum, the optical reflectance data indicated that the concentration of the corresponding states was relatively low and the optical reflectance resonance corresponded to the remaining high-energy line. Finally, for the spacer thickness 15 Å, the low-energy line dominated both photoluminescence and optical reflectance spectra. On the basis of the theoretical predictions and the HREM data discussed above, one may conclude that the appearance of the second line is related to the vertically correlated growth of 2D islands. The vertical correlation of the islands results in an efficient coupling of electronic states of vertically neighboring QDs.

For a more detailed comparison of experimental data and theoretical prediction, we note that HREM images are basically the same in the ⟨110⟩ and ⟨$\bar{1}$10⟩ directions. This indicates that a single sheet forms a 2D array of compact islands rather than a 1D array of stripes. The images of Fig. 28 reveal CdSe islands having mostly a thickness of two monolayers. Since in each deposition cycle, the amount of deposited CdSe is 0.7 ML, we shall model each single sheet of CdSe as an array of 2-ML-high islands, the areal coverage being 0.35. This value has been used in the phase diagram of Fig. 27(b).

Since in the sample having 30-Å spacer thickness there exist both vertically anticorrelated islands dominating the HREM image and optical reflectance spectrum and vertically correlated islands dominating the photoluminescence spectrum, we argue that this spacer thickness corresponds to a boundary between two regions of the phase diagram of Fig. 27(b). From the HREM images of Fig. 28, it is possible to estimate the in-plane period $D\approx 100$ Å. Then, since the spacer thickness 30 Å corresponds to the transition point from correlation to anticorrelation, we can extract the parameter of the uniaxial anisotropy P^B of the double force density created by the buried islands, $P^B\approx 0.6-0.7$.

The studies of the optical gain and of the stimulated emission from the submonolayer CdSe:ZnSe superlattice (Krestnikov, Straßburg, *et al.*, 1998) have confirmed the existence of the resonant waveguiding effect which governs stimulated emission from these structures up to room temperature.

Very recently, multisheet arrays of InAs submonolayer insertions embedded in a GaAlAs matrix have been fabricated (Volovik *et al.*, 1998), and resonant waveguiding and lasing have been demonstrated. We expect such submonolayer superlattices to be attractive for improvement of optical confinement in lasers, for creation of resonant waveguides, and, also for vertical cavity lasers with self-adjusted gain spectra and cavity modes.

VII. SUMMARY

To conclude, we have reviewed the theory of spontaneous formation of periodic nanometer-scale structures on crystal surfaces. We emphasize that, for all classes of nanostructures in question, the long-range elastic interaction is the driving force of ordering. A general approach is used in which three different classes of nanostructures, namely, periodically faceted surfaces, periodic structures of planar domains, and ordered arrays of 3D coherently strained islands, are considered as equilibrium structures of elastic domains.

We have focused particularly on arrays of 3D coherently strained islands (quantum dots), discussing the debate concerning the thermodynamic versus kinetic nature of these arrays. The thermodynamic theory is presented in detail, and a brief description of kinetic theories is given. Experimental data are discussed which confirm the existence in InAs/GaAs and GaInAs/GaAs systems of arrays of 3D islands whose formation is governed by thermodynamics rather than by kinetics. Key experiments are proposed which should determine, for any particular materials system, whether an array of 3D islands is thermodynamic or kinetic in nature.

Multisheet arrays of islands in a matrix are considered, in which the formation mechanism includes both equilibrium ordering of the islands in the first sheet and kinetic-controlled ordering of the islands of the succeeding sheets. The structure of surface islands is formed in the strain field created by the buried islands. Therefore the structure of surface islands corresponds to a partial equilibrium, i.e., to equilibrium under the constraint of a given structure of the buried islands.

We have shown two ways in which the elastic anisotropy of crystals affects on the formation of surface nanostructures. First, for a single-sheet array of 3D islands, the arrangement into a square lattice with primitive lattice vectors along the elastically soft directions [100] and [010] is the most favorable one. Second, for a multisheet array, the elastic interaction between successive sheets exhibits an oscillatory decay with increasing separation between the two sheets, thus leading to transitions from vertical correlation to vertical anticorrelation.

We have demonstrated that in a single-sheet array of 3D coherently strained islands, both the regime of the ordering of islands by size and the regime of Ostwald ripening are possible, and the transition from the first regime to the second can be driven externally, e.g., by varying arsenic pressure for an InAs/GaAs system.

Some questions remain open. First, the role of configuration entropy in spontaneous ordering phenomena has been studied so far only for planar domains on surfaces vicinal to Si(001) (see, for example, Mukherjee *et al.*, 1994, and references therein). The extension of this approach to other classes of spontaneously ordered nanostructures is needed to treat the temperature dependence of the ordering phenomena.

Second, an array of 3D coherently strained islands composed of an alloy (e.g., $Ga_{1-x}In_xAs$) is a system having both a nonplanar surface and an inhomogeneous alloy composition. The extension of the existing theory to alloy-based islands (quantum dots) will allow us to describe a considerably larger variety of experimental systems.

Third, the enhancement of ordering in multisheet arrays of (3D or 2D) islands over ordering for a single-sheet array is not well understood, although some modeling has been done by Tersoff *et al.* (1996). A more comprehensive theory is needed to elucidate this phenomenon.

ACKNOWLEDGMENTS

We are indebted to M. Grundmann, F. Heinrichsdorff, I. P. Ipatova, N. N. Ledentsov, and J. Villain for stimulating discussions. We are grateful to N. Moll, E. Pehlke, and M. Sheffler for fruitful comments and for providing results of their papers prior to publication. We thank I. Daruka and A.-L. Barabási, who made us aware of their paper prior to publication. We acknowledge support by the Russian Foundation for Basic Research, Grant No. 98-02-18304, by a Joint Grant of the Deutsche Forschungsgemeinschaft (Sfb 296) and the Russian Foundation for Basic Research (99-02-04009), and by the Volkswagen Stiftung.

APPENDIX

The dependence of the elastic relaxation energy of a 3D island on its volume is related to scaling properties in the equilibrium equations of the elasticity theory (see,

for example, Shchukin *et al.*, 1995a). Briefly, the idea is as follows. Let us consider a single island on a semi-infinite substrate. The material of the island is lattice-mismatched to the substrate, but coherent conjugation is maintained. Let all dimensions of the island scale isotropically, $\mathbf{r}' = \beta\mathbf{r}$. Then, if the elastic displacement field also scales similarly, $u_i(\mathbf{r}') = \beta u_i(\mathbf{r})$, the strain field $\varepsilon_{ij} = (1/2)[\partial u_i/\partial r_j + \partial u_j/\partial r_i]$ remains invariant. Since the lattice mismatch between the two materials is invariant, the invariant strain field satisfies the boundary conditions at the interface. Now, since the elastic energy density is proportional to the square of the strain [see also Eq. (4.6)], it does not change by the above scaling. Therefore the elastic energy of a coherently strained (and partially relaxed) island scales proportionally to the volume. The elastic relaxation energy, $\Delta E_{\mathrm{elastic}} = E_{\mathrm{elastic}} - \lambda\varepsilon_0^2 V$, is proportional to the island volume, too.

REFERENCES

Alerhand, O. L., D. Vanderbilt, R. D. Meade, and J. D. Joannopoulos, 1988, Phys. Rev. Lett. **61**, 1973.

Alferov, Zh. I., 1996, *Proceedings of the Nobel Symposium 99*, Arild, Sweden, 1996, Phys. Scr. **68**, 32.

Alferov, Zh. I., A. Yu. Egorov, A. E. Zhukov, S. V. Ivanov, P. S. Kop'ev, N. N. Ledentsov, B. Ya. Mel'tser, and V. M. Ustinov, 1992, Fiz. Tekh. Poluprovodn. **26**, 1715 [Sov. Phys. Semicond. **26**, 959 (1992)].

Andreev, A. F., 1980a, Pis'ma Zh. Éksp. Teor. Fiz. **32**, 654 [JETP Lett. **32**, 640 (1980)].

Andreev, A. F., 1980b, Zh. Éksp. Teor. Fiz. **80**, 2042 [Sov. Phys. JETP **53**, 1063 (1981)].

Andreev, A. F., and Yu. A. Kosevich, 1981, Zh. Éksp. Teor. Fiz. **81**, 1435 [Sov. Phys. JETP **54**, 761 (1981)].

Apetz, R., L. Vescan, A. Hartmann, C. Dieker, and H. Lüth, 1995, Appl. Phys. Lett. **66**, 445.

Asaro, R. J., and W. A. Tiller, 1972, Metall. Trans. A **3**, 1789.

Aspnes, D. E., 1985, J. Vac. Sci. Technol. B **3**, 1498.

Barabási, A.-L., 1997, Appl. Phys. Lett. **70**, 2565.

Bartels, W. J., and W. Nijman, 1978, J. Cryst. Growth **44**, 518.

Baski, A. A., and L. J. Whitman, 1995, Phys. Rev. Lett. **74**, 956.

Bauer, E., 1958, Z. Kristallogr. **110**, 372.

Belousov, M. V., N. N. Ledentsov, M. V. Maximov, P. D. Wang, I. N. Yassievich, N. N. Faleev, I. A. Kozin, V. M. Ustinov, P. S. Kop'ev, and C. M. Sotomayor Torres, 1995, Phys. Rev. B **51**, 14 346.

Berti, M., A. V. Drigo, G. Rossetto, and G. Torzo, 1997, J. Vac. Sci. Technol. B **15**, 1794.

Bimberg D., M. Grundmann, and N. N. Ledentsov, 1998, *Quantum Dot Heterostructures* (Wiley, Chichester, U.K.).

Bimberg, D., M. Grundmann, N. N. Ledentsov, S. S. Ruvimov, P. Werner, U. Richter, J. Heydenreich, V. M. Ustinov, P. S. Kop'ev, and Zh. I. Alferov, 1995, Thin Solid Films **267**, 32.

Bimberg, D., F. Heinrichsdorff, R. K. Bauer, D. Gerthsen, D. Stenkamp, D. E. Mars, and J. N. Miller, 1992, J. Vac. Sci. Technol. B **10**, 1793.

Bimberg, D., I. P. Ipatova, P. S. Kop'ev, N. N. Ledentsov, V. G. Malyshkin, and V. A. Shchukin, 1997, Uspekhi Fiz. Nauk **167**, 552 [Phys. Usp. **40**, 529 (1997)].

Bimberg, D., N. Kirstaedter, N. N. Ledentsov, Zh. I. Alferov, P. S. Kop'ev, and V. M. Ustinov, 1997, IEEE J. Sel. Top. Quantum Electron. **3**, 196.

Bimberg, D., N. N. Ledentsov, M. Grundmann, N. Kirstaedter, O. G. Schmidt, M.-H. Mao, V. M. Ustinov, A. Yu. Egorov, A. E. Zhukov, P. S. Kop'ev, Zh. I. Alferov, S. S. Ruvimov, U. Gösele, and J. Heydenreich, 1996, Phys. Status Solidi B **194**, 159.

Brandt, O., G. C. La Rocca, A. Heberle, A. Ruiz, and K. Ploog, 1992, Phys. Rev. B **45**, 3803.

Bressler-Hill, V., A. Lorke, S. Varma, K. Pond, P. M. Petroff, and W. H. Weinberg, 1994, Phys. Rev. B **50**, 8479.

Bressler-Hill, V., S. Varma, A. Lorke, B. Z. Nosho, P. M. Petroff, and W. H. Weinberg, 1995, Phys. Rev. Lett. **74**, 3209.

Cerva, H., and H. Oppolzer, 1990, Prog. Cryst. Growth Charact. Mater. **20**, 231.

Chakraverty, B. K., 1967, J. Phys. Chem. Solids **28**, 2401.

Chen, K. M., D. E. Jesson, S. J. Pennycook, T. Thundat, and R. J. Warmack, 1995, Mater. Res. Soc. Symp. Proc. **399**, 271.

Chen, K. M., D. E. Jesson, S. J. Pennycook, T. Thundat, and R. J. Warmack, 1997, Phys. Rev. B **56**, R1700.

Chen, M., and W. Porod, 1995, J. Appl. Phys. **78**, 1050.

Chen, Y., and J. Washburn, 1996, Phys. Rev. Lett. **77**, 4046.

Chernov, A. A., 1961, Uspekhi Fiz. Nauk **73**, 277 [Sov. Phys. Usp. **4**, 116 (1961)].

Chernov, A. A., 1984, *Modern Crystallography III* (Springer, Berlin).

Cirlin, G. E., V. G. Dubrovskii, V. N. Petroff, N. K. Polyakov, N. P. Korneeva, V. N. Demidov, A. O. Golubok, S. A. Masalov, D. V. Kurochkin, O. M. Gorbenko, N. I. Komyak, N. N. Ledentsov, Zh. I. Alferov, and D. Bimberg, 1998, in *Proceedings of the 6th International Symposium* "*Nanostructures: Physics and Technology*," St. Petersburg, Russia, 1998 (A.F. Ioffe Physical Technical Institute, St. Petersburg, Russia), p. 249.

Cirlin, G., G. M. Guryanov, A. O. Golubok, S. Ya. Tipissev, N. N. Ledentsov, P. S. Kop'ev, M. Grundmann, and D. Bimberg, 1995, Appl. Phys. Lett. **67**, 97. .

Dabrowski, J., E. Pehlke, and M. Scheffler, 1994, Phys. Rev. B **49**, 4790.

Darhuber, A. A., V. Holy, J. Stangl, G. Bauer, A. Krost, F. Heinrichsdorff, M. Grundmann, D. Bimberg, V. M. Ustinov, P. S. Kop'ev, A. O. Kosogov, and P. Werner, 1997, Appl. Phys. Lett. **70**, 955.

Darhuber, A. A., P. Schittenhelm, V. Holy, J. Stangl, G. Bauer, and G. Abstreiter, 1997, Phys. Rev. B **55**, 15 652.

Daruka, I., and A.-L. Barabási, 1997, Phys. Rev. Lett. **79**, 3708.

Dobbs, H. T., D. D. Vvedensky, A. Zangwill, J. Johansson, N. Carlsson, and W. Seifert, 1997, Phys. Rev. Lett. **79**, 897.

Drucker, J., 1993, Phys. Rev. B **48**, 18 203.

Duport, C., C. Priester, and J. Villain, 1997, in *Morphological Organization in Epitaxial Growth and Removal*, edited by Z. Zhang and M. Lagally (World Scientific, Singapore).

Eaglesham, D. J., and M. Cerullo, 1990, Phys. Rev. Lett. **64**, 1943.

Eaglesham, D. J., A. E. White, L. C. Feldman, N. Moriya, and D. C. Jacobson, 1993, Phys. Rev. Lett. **70**, 1643.

Eshelby, J. D., 1956, in *Solid State Physics*, Vol. 3, edited by F. Seitz and D. Turnbull (Academic, New York), p. 79.

Farnell, G. W., 1970, in *Properties of Elastic Surface Waves. Vol. 6. Physical Acoustic*, edited by W. P. Mason and R. N. Thurston (Academic, New York).

Fiorentini, V., M. Methfessel, and M. Scheffler, 1993, Phys. Rev. Lett. **71**, 1051.

Floro, J. A., G. A. Lucadamo, E. Chason, L. B. Freund, M. Sinclair, R. D. Twesten, and R. Q. Hwang, 1998, Phys. Rev. Lett. **80**, 4717.

Frank, F. C., and J. H. van der Merwe, 1949, Proc. R. Soc. London, Ser. A **198**, 205.

Garcia, A., and J. E. Northrup, 1993, Phys. Rev. B **48**, 17 350.

Garcia, J. M., G. Medeiros-Ribeiro, K. Schmidt, T. Ngo, J. L. Feng, A. Lorke, J. Kotthaus, and P. M. Petroff, 1997, Appl. Phys. Lett. **71**, 2014.

Georgsson, K., N. Carlsson, L. Samuelson, W. Seifert, and L. R. Wallenberg, 1995, Appl. Phys. Lett. **67**, 2981.

Gibbs, J. W., 1928, *Collected Works, Vol. 1, Thermodynamics* (Longmans, London).

Glas, F., C. Guille, P. Hénoc, and F. Housay, 1987, Inst. Phys. Conf. Ser. **87**, 71.

Goldstein, L., F. Glas, J. Y. Marzin, M. N. Charasse, and G. Le Roux, 1985, Appl. Phys. Lett. **47**, 1099.

Golubok, A. O., G. M. Gur'yanov, V. N. Petrov, Yu. B. Samsonenko, S. Ya. Tipisev, G. E. Tsyrlin, and N. N. Ledentsov, 1994, Fiz. Tekh. Poluprovodn. **28**, 516 [Semiconductors **28**, 317 (1994)].

Grinfel'd, M. A., 1986, Dokl. Akad. Nauk SSSR **290**, 1358 [Sov. Phys. Dokl. **31**, 831 (1986)].

Grossmann, A., W. Erley, J. B. Hannon, and H. Ibach, 1996, Phys. Rev. Lett. **77**, 127.

Grundmann, M., J. Christen, N. N. Ledentsov, J. Böhrer, D. Bimberg, S. S. Ruvimov, P. Werner, U. Richter, U. Gösele, J. Heydenreich, V. M. Ustinov, A. Yu. Egorov, A. E. Zhukov, P. S. Kop'ev, and Zh. I. Alferov, 1995a, Phys. Rev. Lett. **74**, 4043.

Grundmann, M., N. N. Ledentsov, R. Heitz, L. Eckey, J. Christen, J. Böhrer, D. Bimberg, S. S. Ruvimov, P. Werner, U. Richter, U. Gösele, J. Heydenreich, V. M. Ustinov, A. Yu. Egorov, A. E. Zhukov, P. S. Kop'ev, and Zh. I. Alferov, 1995b, Phys. Status Solidi B **188**, 249.

Grundmann, M., O. Stier, and D. Bimberg, 1995c, Phys. Rev. B **52**, 11 969.

Guha, S., A. Madhukar, and K. C. Rajkumar, 1990, Appl. Phys. Lett. **57**, 2110.

Güntherodt, H.-J., and R. Wiesendanger, editors, 1994, *Scanning Tunneling Microscopy I*, Springer Series in Surface Sciences No. 20 (Springer, Berlin).

Gurianov, G. M., G. E. Tsyrlin, V. N. Petrov, Yu. B. Samsonenko, V. B. Gubanov, N. K. Polyakov, A. O. Golubok, S. Ya. Tipisev, E. P. Musikhina, and N. N. Ledentsov, 1995, Fiz. Tekh. Poluprovodn. **29**, 1642 [Semiconductors **29**, 854 (1995)].

Guryanov, G. M., G. E. Cirlin, A. O. Golubok, S. Ya. Tipisev, N. N. Ledentsov, V. A. Shchukin, M. Grundmann, D. Bimberg, and Zh. I. Alferov, 1996, Surf. Sci. **352-354**, 646.

Guyer, J. E., and P. W. Voorhees, 1995, Phys. Rev. Lett. **74**, 4031.

Guyer, J. E., and P. W. Voorhees, 1996, Phys. Rev. B **54**, 11710.

Hahn, T., 1983, Editor, *International Tables for Crystallography*, Vol. A, *Space Group Symmetry* (Reidel, Dordrecht, The Netherlands).

Hatami, F., N. N. Ledentsov, M. Grundmann, J. Böhrer, F. Heinrichsdorff, M. Beer, D. Bimberg, S. S. Ruvimov, P. Werner, U. Gösele, J. Heydenreich, U. Richter, S. V. Ivanov, B. Ya. Meltser, P. S. Kop'ev, and Zh. I. Alferov, 1995, Appl. Phys. Lett. **67**, 656.

Häusler, K., K. Eberl, F. Noll, and A. Trampert, 1996, Phys. Rev. B **54**, 4913.

Heinrichsdorff, F., A. Krost, D. Bimberg, A. O. Kosogov, and P. Werner, 1998, Appl. Surf. Sci. **123/124**, 725.

Heinrichsdorff, F., A. Krost, M. Grundmann, D. Bimberg, F. Bertram, J. Christen, A. Kosogov, P. Werner, J. Heydenreich, and U. Gösele, 1997, J. Cryst. Growth **170**, 568.

Heinrichsdorff, F., A. Krost, M. Grundmann, D. Bimberg, A. Kosogov, P. Werner, F. Bertram, and J. Christen, 1996, in *Proceedings of the 23rd International Conference on Physics of Semiconductors*, Berlin, Germany, 1996, edited by M. Scheffler and R. Zimmermann (World Scientific, Singapore), Vol. 2, p. 1321.

Herring, C., 1951a, Phys. Rev. **82**, 87.

Herring, C., 1951b, in *The Physics of Powder Metallurgy, a symposium held at Bayside, New York*, August 1949, edited by W. E. Kingston (McGraw-Hill, New York).

Hibino, H., T. Fukuda, M. Suzuki, Y. Hommo, T. Sato, M. Iwatsuki, K. Miki, and H. Tokumoto, 1993, Phys. Rev. B **47**, 13 027.

Ipatova I. P., 1990, in *Proceedings of the 20th International Conference on Physics of Semiconductors*, Thessaloniki, Greece, 1990, edited by E. M. Anastassakis and J. D. Joannopoulos (World Scientific, Singapore), Vol. 2, p. 913.

Ipatova, I. P., V. G. Malyshkin, A. A. Maradudin, V. A. Shchukin, and R. F. Wallis, 1997, in *Proceedings of the 23rd International Symposium on Compound Semiconductors*, St. Petersburg, Russia, 1996, Inst. Phys. Conf. Ser. **155**, 323.

Ipatova, I. P., V. G. Malyshkin, A. A. Maradudin, V. A. Shchukin, and R. F. Wallis, 1998, Phys. Rev. B **57**, 12 969.

Ipatova, I. P., V. G. Malyshkin, A. Yu. Maslov, and V. A. Shchukin, 1993, Fiz. Tekh. Poluprovodn. **27**, 285 [Semiconductors **27**, 158 (1993)].

Ipatova, I. P., V. G. Malyshkin, and V. A. Shchukin, 1993, J. Appl. Phys. **74**, 7198.

Ipatova, I. P., V. G. Malyshkin, and V. A. Shchukin, 1994, Philos. Mag. B **70**, 557.

Ipatova, I. P., V. A. Shchukin, V. G. Malyshkin, A. Yu. Maslov, and E. Anastassakis, 1991, Solid State Commun. **78**, 19.

Jeppesen, S., M. S. Miller, D. Hessman, B. Kowalski, I. Maximov, and L. Samuelson, 1996, Appl. Phys. Lett. **68**, 2228.

Jesson, D. E., G. Chen, K. M. Chen, and S. J. Pennycook, 1998, Phys. Rev. Lett. **80**, 5156.

Jesson, D. E., K. M. Chen, and S. J. Pennycook, 1996, MRS Bull. **21**, 31.

Jesson, D. E., K. M. Chen, S. J. Pennycook, T. Thundat, and R. J. Warmack, 1996, Phys. Rev. Lett. **77**, 1330.

Jesson, D. E., S. J. Pennycook, J.-M. Baribeau, and D. C. Houghton, 1993, Phys. Rev. Lett. **71**, 1744.

Joós, B., T. L. Einstein, and N. C. Bartelt, 1991, Phys. Rev. B **43**, 8153.

Joyce, B. A., J. H. Neave, P. J. Dobson, and P. K. Larsen, 1984, Phys. Rev. B **29**, 814.

Kamins, T. I., E. C. Carr, R. S. Williams, and S. J. Rosner, 1997, J. Appl. Phys. **81**, 211.

Kamins, T. I., G. Medeiros-Ribeiro, D. A. A. Ohlberg, and R. Stanley Williams, 1998, Appl. Phys. A: Mater. Sci. Process. **67**, 1.

Kaminski, A. Yu., and R. A. Suris, 1996, in *Proceedings of the 23rd International Conference on Physics of Semiconductors*, Berlin, Germany, 1996, edited by M. Scheffler and R. Zimmermann (World Scientific, Singapore), Vol. 2, p. 1337.

Kamiya, I., D. E. Aspnes, H. Tanaka, L. T. Florez, J. P. Harbison, and R. Bhat, 1992, Phys. Rev. Lett. **68**, 627.

Kastner, M. A., 1996, in *Proceedings of the 23rd International Conference on Physics of Semiconductors*, Berlin, Germany, 1996, edited by M. Scheffler and R. Zimmermann (World Scientific, Singapore), Vol. 1, p. 27.

Kasu, M., and N. Kobayashi, 1993, Appl. Phys. Lett. **62**, 1262.

Kern, K., H. Niehus, A. Schatz, P. Zeppenfeld, J. George, and G. Comsa, 1991, Phys. Rev. Lett. **67**, 855.

Khachaturyan, A. G., 1969, Phys. Status Solidi **35**, 119.

Khachaturyan, A. G., 1974, *Theory of Phase Transformations and the Structure of Solid Solution*, in Russian (Nauka, Moscow).

Khachaturyan, A. G., 1983, *Theory of Structural Transformations in Solids* (Wiley, New York).

Kirstaedter, N., N. N. Ledentsov, M. Grundmann, D. Bimberg, V. M. Ustinov, S. S. Ruvimov, M. V. Maximov, P. S. Kop'ev, Zh. I. Alferov, U. Richter, P. Werner, U. Gösele, and J. Heydenreich, 1994, Electron. Lett. **30**, 1416.

Kobayashi, N., T. R. Ramachandran, P. Chen, and A. Madhukar, 1996, Appl. Phys. Lett. **68**, 3299.

Koch, R., M. Borbonus, O. Haase, and K. H. Rieder, 1991, Phys. Rev. Lett. **67**, 3416.

Kosevich, Yu. A., 1997, Prog. Surf. Sci. **55**, 1.

Kosevich, A. M., Yu. A. Kosevich, and E. S. Syrkin, 1985, Zh. Éksp. Teor. Fiz. **88**, 1089 [Sov. Phys. JETP **61**, 639 (1985)].

Krestnikov, I. L., S. V. Ivanov, P. S. Kop'ev, N. N. Ledentsov, M. V. Maximov, A. V. Sakharov, S. V. Sorokin, C. M. Sotomayor Torres, D. Bimberg, and Zh. I. Alferov, 1998, J. Electron. Mater. **27**, 72.

Krestnikov, I. L., P. S. Kop'ev, Zh. I. Alferov, M. Straßburg, N. N. Ledentsov, A. Hoffmann, D. Bimberg, A. Rosenauer, U. Fischer, D. Gerthsen, and C. M. Sotomayor Torres, 1999, Phys. Rev. B, in press.

Krestnikov, I. L., M. Straßburg, M. Caesar, V. A. Shchukin, A. Hoffmann, U. W. Pohl, D. Bimberg, N. N. Ledentsov, V. G. Malyshkin, P. S. Kop'ev, Zh. I. Alferov, D. Litvinov, A. Rosenauer, and D. Gerthsen, 1998, in Proceedings of the 24th International Conference on Physics of Semiconductors, Jerusalem, Israel, 1998 (World Scientific, Singapore, in press).

Krost, A., F. Heinrichsdorff, D. Bimberg, A. Darhuber, and G. Bauer, 1996, Appl. Phys. Lett. **68**, 785.

Kuan, T., and S. S. Iyer, 1991, Appl. Phys. Lett. **59**, 2242.

Kurtenbach, A., K. Eberl, and T. Shitara, 1995, Appl. Phys. Lett. **66**, 361.

Landau, L. D., and E. M. Lifshits, 1959, *Theory of Elasticity* (Pergamon, New York).

Landau, L. D., and E. M. Lifshits, 1960, *Electrodynamics of Continuous Media* (Pergamon, New York).

Landolt-Börnstein, 1982, Vol. 17b, *Semiconductors. Physics of II-VI and I-VII Compounds, Semimagnetic Semiconductors*, edited by O. Madelung (Springer, Berlin).

Larsen, P. K., and P. J. Dobson, Eds., 1988, *Reflection High Energy Electron Diffraction and Electron Imaging of Surfaces*, NATO ASI Series B: Physics Vol. 188 (Plenum, New York, 1988).

Ledentsov, N. N., 1996, in *Proceedings of the 23rd International Conference on Physics of Semiconductors*, Berlin, Germany, 1996, edited by M. Scheffler and R. Zimmermann (World Scientific, Singapore), Vol. 1, p. 19.

Ledentsov, N. N., D. Bimberg, Yu. M. Shernyakov, V. Kochnev, M. V. Maximov, A. V. Sakharov, I. L. Krestnikov, A. Yu. Egorov, A. F. Tsatsul'nikov, B. V. Volovik, V. M. Ustinov, P. S. Kop'ev, Zh. I. Alferov, A. O. Kosogov, and P. Werner, 1997, Appl. Phys. Lett. **70**, 2888.

Ledentsov, N. N., J. Böhrer, D. Bimberg, I. V. Kochnev, M. V. Maximov, P. S. Kop'ev, Zh. I. Alferov, A. O. Kosogov, S. S. Ruvimov, P. Werner, and U. Gösele, 1996, Appl. Phys. Lett. **69**, 1095.

Ledentsov, N. N., M. Grundmann, N. Kirstaedter, J. Christen, R. Heitz, J. Böhrer, F. Heinrichsdorff, D. Bimberg, S. S. Ruvimov, P. Werner, U. Richter, U. Gösele, J. Heydenreich, V. M. Ustinov, A. Yu. Egorov, M. V. Maximov, P. S. Kop'ev, and Zh. I. Alferov, 1994, in *Proceedings of the 22nd International Conference on Physics of Semiconductors*, Vancouver, Canada, 1994, edited by D. J. Lockwood (World Scientific, Singapore), Vol. 3, p. 1855.

Ledentsov, N. N., M. Grundmann, N. Kirstaedter, O. Schmidt, R. Heitz, J. Böhrer, D. Bimberg, V. M. Ustinov, V. A. Shchukin, P. S. Kop'ev, Zh. I. Alferov, S. S. Ruvimov, A. O. Kosogov, P. Werner, U. Richter, U. Gösele, and J. Heydenreich, 1996, in *Proceedings of the 7th International Conference on Modulated Semiconductor Structures*, Madrid, Spain, 1995 [Solid-State Electron. **40**, 785].

Ledentsov, N. N., G. M. Gurianov, G. E. Tsyrlin, V. N. Petrov, Yu. B. Samsonenko, A. O. Golubok, and S. Ya. Tipisev, 1994, Fiz. Tekh. Poluprovodn. **28**, 903 [Semiconductors **28**, 526].

Ledentsov, N. N., I. L. Krestnikov, M. V. Maximov, S. V. Ivanov, S. L. Sorokin, P. S. Kop'ev, Zh. I. Alferov, D. Bimberg, and C. M. Sotomayor Torres, 1996, Appl. Phys. Lett. **69**, 1343.

Ledentsov, N. N., I. L. Krestnikov, M. V. Maximov, S. V. Ivanov, S. L. Sorokin, P. S. Kop'ev, Zh. I. Alferov, D. Bimberg, and C. M. Sotomayor Torres, 1997, Appl. Phys. Lett. **70**, 2776.

Ledentsov, N. N., V. A. Shchukin, M. Grundmann, N. Kirstaedter, J. Böhrer, O. Schmidt, D. Bimberg, V. M. Ustinov, A. Yu. Egorov, A. E. Zhukov, P. S. Kop'ev, S. V. Zaitsev, N. Yu. Gordeev, Zh. I. Alferov, A. I. Borovkov, A. O. Kosogov, S. S. Ruvimov, P. Werner, U. Gösele and J. Heydenreich, 1996, Phys. Rev. B **54**, 8743.

Ledentsov, N. N., V. M. Ustinov, V. A. Shchukin, P. S. Kop'ev, Zh. I. Alferov, and D. Bimberg, 1998, Fiz. Tekh. Poluprovodn. **32**, 385 [Semiconductors **32**, 343 (1998)].

Leon, R., S. Fafard, D. Leonard, J. L. Merz, and P. M. Petroff, 1995, Appl. Phys. Lett. **67**, 521.

Leonard, D., M. Krishnamurthy, C. M. Reaves, S. P. Denbaars, and P. M. Petroff, 1993, Appl. Phys. Lett. **63**, 3203.

Leonard, D., K. Pond, and P. M. Petroff, 1994, Phys. Rev. B **50**, 11 687.

Li, C., and C. Jagadish, 1996, Appl. Phys. Lett. **69**, 2551.

Lian, G. D., J. Yuan, L. M. Brown, G. H. Kim, and D. A. Ritchie, 1998, Appl. Phys. Lett. **73**, 49.

Lifshits, I. M., and V. V. Slyozov, 1958, Zh. Éksp. Teor. Fiz. **35**, 479.

Madhukar, A., P. Chen, Q. Xie, A. Konkar, T. R. Ramachandran, N. P. Kobayashi, and R. Viswanathan, 1995, in *Low Dimensional Structures prepared by Epitaxial Growth or Regrowth on Patterned Substrates* (Proceedings of the NATO Advanced Workshop, 1995, Ringberg Castle, Germany), edited by K. Eberl, P. Petroff, and P. Demeester (Kluwer, Dordrecht, the Netherlands), p. 19.

Madhukar, A., Q. Xie, P. Chen, and A. Koknar, 1994, Appl. Phys. Lett. **64**, 2727.

Malyshkin, V. G., and V. A. Shchukin, 1993, Fiz. Tekh. Poluprovodn. **27**, 1932 [Semiconductors **27**, 1062 (1993)].
Maradudin, A. A., X. Huang, and A. P. Mayer, 1991, J. Appl. Phys. **70**, 53.
Maradudin, A. A., and R. F. Wallis, 1980, Surf. Sci. **91**, 423.
Marchenko, V. I., 1981, Zh. Éksp. Teor. Fiz. **81**, 1141 [Sov. Phys. JETP **54**, 605 (1981)].
Marchenko, V. I., Pis'ma Zh. Éksp. Teor. Fiz. **33**, 397 [JETP Lett. **33**, 381 (1981)].
Marchenko,, I. V., and A. Ya. Parshin, 1980, Zh. Éksp. Teor. Fiz. **79**, 257 [Sov. Phys. JETP **52**, 129 (1980)].
Men, F. K., W. E. Packard, and M. B. Webb, 1988, Phys. Rev. Lett. **61**, 2469.
Mo, Y.-W., D. E. Savage, B. S. Swartzentruber, and M. G. Lagally, 1990, Phys. Rev. Lett. **65**, 1020.
Mo, Y.-W., B. S. Swartzentruber, R. Kariotis, M. B. Webb, and M. G. Lagally, 1989, Phys. Rev. Lett. **63**, 2393.
Moison, J. M., F. Houzay, F. Barthe, L. Leprince, E. André, and O. Vatel, 1994, Appl. Phys. Lett. **64**, 196.
Moll, N., A. Kley, E. Pehlke, and M. Scheffler, 1996, Phys. Rev. B **54**, 8844.
Moll, N., M. Scheffler, and E. Pehlke, 1998, Phys. Rev. B, in press.
Mukherjee, S., E. Pehlke, and J. Tersoff, 1994, Phys. Rev. B **49**, 1919.
Mullins, W. W., 1957, J. Appl. Phys. **28**, 333.
Mullins, W. W., 1963, in *Metal Surfaces: Structure, Energetics and Kinetics* (American Society for Metals, Metals Park), p. 17.
Nabetani, Y., T. Ishikawa, S. Noda, and A. Sakaki, 1994, J. Appl. Phys. **76**, 347.
Needs, R. J., 1987, Phys. Rev. Lett. **58**, 53.
Neumann, W., H. Hofmeister, D. Conrad, K. Scheerschmidt, and S. Ruvimov, 1996, Z. Kristallogr. **211**, 147.
Ng, Kwok-On and D. Vanderbilt, 1995, Phys. Rev. B **52**, 2177.
Ngo, T. T., P. M. Petroff, H. Sakaki, and J. L. Merz, 1996, Phys. Rev. **53**, 9618.
Nötzel, R., 1996, Semicond. Sci. Technol. **11**, 1365.
Nötzel, R., N. N. Ledentsov, L. Däweritz, M. Hohenstein, and K. Ploog, 1991, Phys. Rev. Lett. **67**, 3812.
Nötzel, R., J. Temmyo, and T. Tamamura, 1994, Nature (London) **369**, 131.
Nozières, P., and D. E. Wolf, 1988, Z. Phys. B **70**, 399 (Part I); 1988, Z. Phys. B **70**, 507 (Part II).
Olson, J. M., and A. Kibbler, 1986, J. Cryst. Growth **77**, 182.
Ourmazd, A., F. H. Baumann, M. Bode, and Y. Kim, 1990, Ultramicroscopy **34**, 237.
Ozasa, K., Y. Aoyagi, Y. J. Park, and L. Samuelson, 1997, Appl. Phys. Lett. **71**, 797.
Pehlke, E., N. Moll, A. Kley, and M. Scheffler, 1997, Appl. Phys. A: Solids Surf. **65**, 525.
Pehlke, E., N. Moll, and M. Scheffler, 1996, in *Proceedings of the 23rd International Conference on Physics of Semiconductors*, Berlin, Germany, 1996, edited by M. Scheffler and R. Zimmermann (World Scientific, Singapore), Vol. 2, p. 1301.
Ponchet, A., A. Le Corre, H. L'Haridon, B. Lambert, and S. Salaün, 1995, Appl. Phys. Lett. **67**, 1850.
Portz, K., and A. A. Maradudin, 1977, Phys. Rev. B **16**, 3535.
Qian, G.-X., R. M. Martin, and D. J. Chadi, 1988, Phys. Rev. B **38**, 7649.
Ratsch, C., and A. Zangwill, 1993, Surf. Sci. **293**, 123.
Reimer, L., 1984, *Transmission Electron Microscopy*, Springer Series in Optical Sciences, Vol. 36 (Springer, Berlin).
Reinhardt, F., W. Richter, A. B. Müller, D. Gursche, P. Kurpas, K. Ploska, K. C. Rose, M. Zorn, 1993, J. Vac. Sci. Technol. B **11**, 1427.
Richter, W., and D.R.T. Zahn, 1996, in *Optical Characterization of Epitaxial Semiconductor Layers*, edited by G. Bauer and W. Richter (Springer, Berlin), p. 12.
Roitburd, A. L., 1976, Phys. Status Solidi A **37**, 329.
Roland, C., and G. H. Gilmer, 1993, Phys. Rev. B **47**, 16 286.
Rosenauer, A., S. Kaiser, T. Reisinger, J. Zweck, W. Gebhardt, and D. Gerthsen, 1996, Optik (Stuttgart) **102**, 63.
Rottman, C., and M. Wortis, 1984, Phys. Rep. **103**, 59.
Ruvimov, S. S., and K. Scheerschmidt, 1995, Phys. Status Solidi A **150**, 471.
Ruvimov, S. S., P. Werner, K. Scheerschmidt, U. Richter, U. Gösele, J. Heydenreich, N. N. Ledentsov, M. Grundmann, D. Bimberg, V. M. Ustinov, A. Yu. Egorov, P. S. Kop'ev, and Zh. I. Alferov, 1995, Phys. Rev. B **51**, 14 766.
Schittenhelm, P., M. Gail, J. Brunner, J. F. Nützel, and G. Abstreiter, 1995, Appl. Phys. Lett. **67**, 1292.
Segmüller, A., I. C. Noyan, V. S. Speriosu, 1989, Prog. Cryst. Growth Charact. **18**, 21.
Seifert, W., N. Carlsson, M. Miller, M.-E. Pistol, L. Samuelson, and L. R. Wallenberg, 1996, Proc. Cryst. Growth Charact. Mater. **33**, 423.
Shchukin, V. A., 1996, in *Proceedings of the 23rd International Conference on Physics of Semiconductors* Berlin, Germany, 1996, edited by M. Scheffler and R. Zimmermann (World Scientific, Singapore), Vol. 2, p. 1261.
Shchukin, V. A., and D. Bimberg, 1998, Appl. Phys. A: Solids Surf. **67**, 687.
Shchukin, V. A., D. Bimberg, V. G. Malyshkin, and N. N. Ledentsov, 1998, Phys. Rev. B **57**, 12 262.
Shchukin, V. A., A. I. Borovkov, N. N. Ledentsov, and D. Bimberg, 1995a, Phys. Rev. B **51**, 10 104.
Shchukin, V. A., A. I. Borovkov, N. N. Ledentsov, and P. S. Kop'ev, 1995b, Phys. Rev. B **51**, 17 767.
Shchukin, V. A., N. N. Ledentsov, M. Grundmann, and D. Bimberg, 1997, in *Optical Properties of Low-Dimensional Semiconductors*,—NATO ASI Series, Series E: Applied Physics, edited by G. Abstreiter, A. Aydinli, and J.-P. Leburton (Kluwer, Dordrecht, the Netherlands), p. 257.
Shchukin, V. A., N. N. Ledentsov, M. Grundmann, P. S. Kop'ev, and D. Bimberg, 1996, Surf. Sci. **352-354**, 117.
Shchukin, V. A., N. N. Ledentsov, P. S. Kop'ev, and D. Bimberg, 1995, Phys. Rev. Lett. **75**, 2968.
Shuttleworth, R., 1950, Proc. R. Soc. London, Ser. A **63**, 444.
Snyder, C. W., B. G. Orr, D. Kessler, and L. M. Sander, 1991, Phys. Rev. Lett. **66**, 3032.
Solomon, G. S., J. A. Trezza, A. F. Marshall, and J. S. Harris, Jr., 1996, Phys. Rev. Lett. **76**, 952.
Spencer, B. J., P. W. Voorhees, and S. H. Davis, 1991, Phys. Rev. Lett. **67**, 3696.
Spencer, B. J., and J. Tersoff, 1997, Phys. Rev. Lett. **79**, 4858.
Srolovitz, D., 1989, Acta Metall. **37**, 621.
Steimetz, E., F. Scheinle, J.-T. Zettler, and W. Richter, 1997, J. Cryst. Growth **170**, 208.
Stranski, I. N., and L. Krastanow, 1937, Sitzungsber. Akad. Wiss. Wien, Math.-Naturwiss. Klasse **146**, 797.
Straßburg, M., V. Kutzer, U. W. Pohl, A. Hoffmann, I. Broser, N. N. Ledentsov, D. Bimberg, A. Rosenauer, U. Fischer, D. Gerthsen, I. L. Krestnikov, M. V. Maximov, P. S. Kop'ev, and Zh. I. Alferov, 1998, Appl. Phys. Lett. **72**, 942.

Tanaka, S., S. Iwai, and Y. Aoyagi, 1996, Appl. Phys. Lett. **62**, 1376.
Tapfer, L., and K. Ploog, 1986, Phys. Rev. B **33**, 5565.
Tersoff, J., 1991, Phys. Rev. B **43**, 9377.
Tersoff, J., 1996, Phys. Rev. Lett. **77**, 2017.
Tersoff, J., Y. H. Phang, Zh. Zhang, and M. G. Lagally, 1995, Phys. Rev. Lett. **75**, 2730.
Tersoff, J., C. Teichert, and M. G. Lagally, 1996, Phys. Rev. Lett. **76**, 1675.
Tersoff, J., and R. M. Tromp, 1993, Phys. Rev. Lett. **70**, 2782.
Tournié, E., A. Trampert, and K. Ploog, 1994, Europhys. Lett. **25**, 663.
Ustinov, V. M., A. Yu. Egorov, A. R. Kovsh, A. E. Zhukov, M. V. Maximov, A. F. Tsatsul'nikov, N. Yu. Gordeev, S. V. Zaitsev, Yu. M. Shernyakov, N. A. Bert, P. S. Kop'ev, Zh. I. Alferov, N. N. Ledentsov, J. Böhrer, D. Bimberg, A. O. Kosogov, P. Werner, U. Gösele, 1997, J. Cryst. Growth **175/176**, 689.
Ustinov, V. M., E. R. Weber, S. Ruvimov, Z. Liliental-Weber, A. E. Zhukov, A. Yu. Egorov, A. R. Kovsh, A. F. Tsatsul'nikov, and P. S. Kop'ev, 1998, Appl. Phys. Lett. **72**, 362.
Vanderbilt, D., 1992, Surf. Sci. **268**, L300.
Vanderbilt, D., and L. K. Wickham, 1991, in *Evolution of Thin-Film and Surface Microstructure*, edited by C. V. Thompson, J. Y. Tsao, and D. J. Srolovitz, MRS Proceedings, Vol. 202 (MRS, Pittsburgh), p. 555.
Volmer, M., and A. Weber, 1926, Z. Phys. Chem. (Munich) **119**, 277.
Volovik, B. V., A. Yu. Egorov, P. S. Kop'ev, A. R. Kovsh, I. E. Kozin, I. L. Krestnikov, M. V. Maximov, A. V. Sakharov, A. F. Tsatsul'nikov, V. M. Ustinov, A. E. Zhukov, Zh. I. Alferov, N. N. Ledentsov, M. Straßburg, A. Hoffmann, D. Bimberg, I. P. Soshnikov, and P. Werner, 1998, in Proceedings of the 24th International Conference on Physics of Semiconductors, Jerusalem, Israel, 1998 (World Scientific, Singapore, in press).
Wang, P. D., N. N. Ledentsov, C. M. Sotomayor Torres, P. S. Kop'ev, and V. M. Ustinov, 1994, Appl. Phys. Lett. **64**, 1526.
Wang, P. D., N. N. Ledentsov, C. M. Sotomayor Torres, P. S. Kop'ev, and V. M. Ustinov, 1995, Appl. Phys. Lett. **66**, 112.
Watson, G. M., D. Gibbs, D. M. Zehner, M. Yoon, and S. G. J. Mochrie, 1993, Phys. Rev. Lett. **71**, 3166.
Wiesendanger, R., 1994, *Scanning Probe Microscopy and Spectroscopy* (Cambridge University Press, Cambridge).
Williams, E. D., R. J. Phaneuf, J. Wei, N. C. Bartelt, and T. L. Einstein, 1993, Surf. Sci. **294**, 219.
Wolf, D. E., and P. Nozières, 1998, Z. Phs. B **70**, 507 (Part II of Noziéres and Wolf, 1988).
Wolf, D., 1993, Phys. Rev. Lett. **70**, 627.
Wu, W., J. R. Tucker, G. S. Solomon, and J. S. Harris, Jr., 1997, Appl. Phys. Lett. **71**, 1083.
Wulff, G., 1901, Z. Kristallogr. Mineral. **34**, 449.
Xie, Q., P. Chen, and A. Madhukar, 1994, Appl. Phys. Lett. **65**, 2051.
Xie, Q., A. Madhukar, P. Chen, and N. Kobayashi, 1995, Phys. Rev. Lett. **75**, 2542.
Xin, S. H., P. D. Wang, A. Yin, C. Kim, M. Dobrowolska, J. L. Merz, and J. K. Furdyna, 1996, Appl. Phys. Lett. **69**, 3884.
Yang, W. H., and D. J. Srolovitz, 1993, Phys. Rev. Lett. **71**, 1593.
Yao, J. Y., T. G. Andersson, and G. L. Dunlop, 1991, J. Appl. Phys. **69**, 2224.
Zeppenfeld, P., M. Krzyzowski, C. Romainczuk, G. Comsa, and M. G. Lagally, 1994, Phys. Rev. Lett. **72**, 2737.
Zuo, J.-K., R. J. Warmack, D. M. Zehner, and J. F. Wendelken, 1993, Phys. Rev. B **47**, 10 743.